Air Force Office of Scientific Research #AFOSR-91-0269
National Oceanic & Atmospheric Admin. #NA90RAH-00077
Colorado Agricultural Experiment Station #COL00692

# MESOSCALE NUMERICAL PREDICTION OF COLORADO SNOWFALL AND WINDS

by Capt. Brian A. Beitler



William R. Cotton, P.I.

Colorado State University

**DEPARTMENT OF ATMOSPHERIC SCIENCE**

PAPER NO. 556

# MESOSCALE NUMERICAL PREDICTION OF COLORADO SNOWFALL AND WINDS

by
**Capt. Brian A. Beitler**
Department of Atmospheric Science
Colorado State University
Fort Collins, CO 80523

Research Supported by

**Air Force Office of Scientific Research**
under contract #AFOSR-91-0269

**National Oceanic & Atmospheric Administration**
under contract #NA90RAH-00077

**Colorado Agricultural Experiment Station**
under grant #COL00692

May 24, 1994

Atmospheric Science Paper No. 556

# ABSTRACT

## MESOSCALE NUMERICAL PREDICTION OF COLORADO SNOWFALL AND WINDS

The prediction of spring snow run-off in the Colorado Rocky Mountains has lasting effects throughout the year. The climatology of the snowfall in the high terrain directly influences the water supply for Colorado and neighboring states and dictates any water restrictions for the remainder of the year. Existing methods of predicting snow amounts include using data from SNOTEL sites and interpolating these measurements for the entire region. The advantages of using a real-time mesocale model is the spatial regularity of information and expanded coverage a model can allow.

Using the Regional Atmospheric Modeling System (RAMS) developed at Colorado State University (CSU), calculations of seasonal precipitation were made, employing a precipitation efficiency scheme based on cloud top temperature. Overall, this scheme under-forecast precipitation; however, a correlation existed between this simple scheme and topography. It was found that the best results are obtained by using a bulk microphysics scheme. The trade-off of using this more physically-based approach is the extended computing time required to attain results. The accuracy in precipitation forecasting in individual events when using the bulk microphysics is seen when simulating the winter storm of 8 February 1994. Not only are the amounts of precipitation forecast at particular sites improved over the efficiency scheme results, but the regions of maximum snowfall are also better predicted.

The Colorado Front Range downslope windstorm of 3 July 1993 was also simulated using RAMS. The model was run using different levels of microphysical complexity. For this type of mesoscale phenomenon, increased resolution along the Front Range produced windstorm-scale velocities in the foothills. The use of the bulk microphysics scheme greatly increased the forecast skill of the simulations.

Brian A. Beitler
Department of Atmospheric Science
Colorado State University
Fort Collins, Colorado 80523
Summer 1994

# ACKNOWLEDGMENTS

I would like to thank my advisor, Dr. William Cotton, for his continued support and direction. His advise, know-how, and bad puns made him a pleasure to work with. Also, thanks to committee members Dr. Roger Pielke and statistician Dr. Paul Mielke. Your inputs and suggestions have enriched the quality (and spelling!) of this thesis.

Thanks to the National Meteorological Center in Washington DC for access to the gridded data used in this study. Also, thanks to the Soil Conservation Service's office in Portland, OR for the SNOTEL data needed for verification purposes. Finally, thanks to Steve Finley for the use of his workstations to retrieve the required surface and upper-air stations.

I would like to acknowledge the Air Force and extend my gratitude for being assigned to Colorado State over the last 21 months. Special thanks goes to Major Mary Smith and everyone else at the AFIT Civilian Institution Program at Wright-Patterson AFB in Ohio for their "long-distance" support. Closer to home, thanks goes out to all the staff at AFROTC Detachment 90 for serving all my administrative needs.

A heartfelt thanks to Gregory Thompson for teaching me the ways of RAMS. Not only did he pass on all the tricks of the trade but he also instilled in me his excitement for real-time forecasting. Without his continued help and suggestions (even from as far away as Boulder!), I'd still be trying to figure out how to log on. My success is your success, Greg!

My thanks go out to long-time friend Lawrence Carey for his moral support throughout my thesis. His words of assurance helped me along and his letting me (occasionally) beat him at racquetball did wonders for my ego.

Special thanks to David Mocko for being a great pal who helped me out of many a RAMS corner. The lunch chats, "funny" conversations, and convective field studies are considered some of my best moments here and will be missed. My three office mates (Sharon Nebuda, Brian Gaudet and Jerry Harrington) are to be commended for putting up with all my quirky ways, especially my attempts at being a rock-'n-roll DJ. Thanks to Brenda Thompson and Abby Hodges for their administrative assistance and office supplies. Also, everyone else in the Cotton and Pielke groups, especially Scot "Vis 5-D Man" Randell, Jeff "Civ" Copeland, Jason "Chasin'" Nachamkin, Bob "Try This" Walko, Craig "Works For Me" Tremback, Donna "Ensign Roe" Chester, and everyone else not mentioned is thanked for additional RAMS help and/or comic relief.

Finally I'd like to thank my wife, Laurie, for her unending support and willingness to move west of the Mississippi. Except for picking up the phone when I was connected to the workstations via modem, she has been helpful and understanding in all that I have done. I'll have to take a break before getting a Ph.D. so I can finally spend some time with her.

This research was supported by the Air Force Office of Scientific Research contract #AFOSR-91-0269, the National Oceanic and Atmospheric Administration under contract #NA90RAH-00077, and the Colorado Agricultural Experiment Station under grant #COL00692.

# TABLE OF CONTENTS

# LIST OF FIGURES

# LIST OF TABLES

# 1. INTRODUCTION

The ability to properly forecast the snowfall in the Rocky Mountains is the first step to understanding the climatology of the water supply in the western US. The primary source of water for Colorado and its neighboring states is the spring runoff of the winter snowpack of the inter-mountain region. Current methods of predicting this snowpack include measurements taken from Soil Conservation Service's SNOw TELemetry system (SNOTEL) at certain locations. SNOTEL sensors measure snow water equivalent, precipitation and temperature. This information is transmitted by reflecting its radio signals off ionized meteor trails in the upper atmosphere. A central computer at the Soil Conservation Service polls these different sites, files the site data, and produces special reports of site conditions. However, the placement of these sites is sporadic and much must be inferred in areas without SNOTEL measurements. Another tool available for prediction of seasonal snowfall is the utilization of a mesoscale numerical model.

Until recently, the use of mesoscale numerical models was limited due to available computer technology. The amount of time and computing power required to simulate a season's worth of data would take longer than the entire season itself. The high speed workstations of today compute at much higher rates, allowing daily prediction of snowfall and a running total of seasonal snowfall throughout the entire mountain region. Also, the grid spacing which can be used and still maintain real-time results is many times finer than any other operational numerical model.

The purpose of this paper is to use the Regional Atmospheric Modeling System (RAMS) developed at Colorado State University (CSU) to produce daily forecasts for

Colorado, including precipitation. These precipitation forecasts will be compared to data obtained from SNOTEL measuring sites in the mountains. Besides snowfall measurements, RAMS real-time forecasts are useful in other ways. The real-time forecast system will be examined (Chapter 3), along with its ability to forecast particular mesoscale events. The downslope windstorm of 3 July 1993 will be simulated (Chapter 4) with minor changes to the real-time setup. Also, the snow event of 8 February 1994 (Chapter 5) will show the accuracy of RAMS in forecasting the orographically produced precipitation required for the annual study. The seasonal snowfall results will be examined (Chapter 6) and some conclusions will be made along with possible directions for future research (Chapter 7).

# 2. BACKGROUND

Throughout the last century, farmers have learned firsthand how fickle the climatology of the water supply can be. Many years of plentiful water could easily be followed by many years of drought. Years of little water which could drive a farmer to starvation or bankruptcy could suddenly turn around and provide perfect conditions. The water supply for any given area directly influences the life and livelihood of the farmer.

## 2.1 Water Management

Within the last fifty years or so, federal, state and local governments have provided many forms of water management. A complex system of reservoirs was built to help buffer the effects of years of low water supply, extend water availability from early spring peak runoff to include the entire growing season, and save excesses in high water years. Strict laws dealing with water rights and distribution were enacted to provide equitable treatment to all farmers. Methods of irrigation which used less water and farming practices which yielded higher returns also cut down on water demand per acre. At this point, one or two years of drought would not necessarily devastate a region's agriculture.

Over the last thirty years, a new problem has arisen for the water supply- increased population. The Rocky Mountain region and surrounding states have grown faster than any other part of the country. At the same time, the average annual water supply has remained nearly the same. Figure 2.1 shows the twelve fastest-growing states from 1980 to 1990. Five of these states (Nevada, Arizona, California, Utah and New Mexico) get part

of their water supply from the spring run-off from the Colorado Rockies. One of the most easily seen result of this increased demand on the water supply is the new extent of the Colorado River, the main water supplier to the Southwest US. Until recently, the Colorado emptied into the Gulf of California in Mexico. Now, this river dries up a few miles short of its original destination (Tyler, 1992). This is just one reason why it became important to monitor the water supply more closely so proper actions in water distributions could be planned for. Since 85% of the area's total streamflow is derived from snowpack annually (Grant and Kahan, 1974), snowpack measurements were made. Correlations between the snow depths and water amounts were calculated, and an estimate of water supply for the spring and summer months could be made. Most years, proper estimates were made using these correlation methods (Doesken, 1987). However, if the snowpack measurements are not indicative of the entire snowpack, these estimates may be off. Adding many more measuring sites would help to alleviate this problem; however, the cost involved to double the number of existing sites is well beyond the careful budgeting of the 90's. A more cost-effective approach is employing the use of a mesoscale numerical model.

## 2.2 Mesoscale Numerical Models

### 2.2.1 History of real-time simulations

The use of mesoscale models in a forecasting role is still in its infancy. Primarily used for pure research (i.e.: changing an individual parameter in an idealized environment

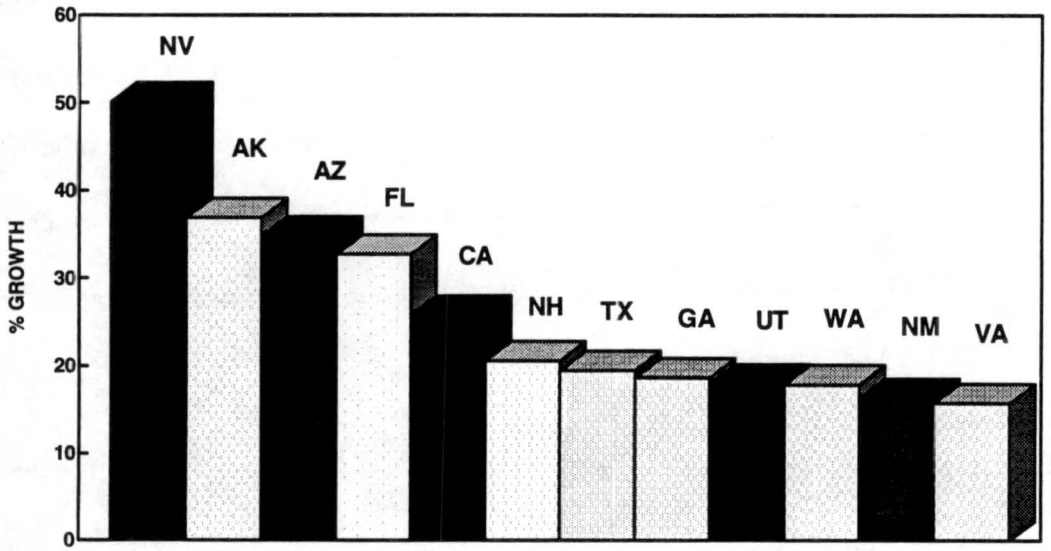


**Figure 2.1 Fastest growing states by percentage increase between 1980 and 1990. Solid columns indicate states which are dependent on Colorado for water**

and seeing how this will effect the results), mesoscale models are now complex enough and computers are fast enough to allow for real-time forecasting applications.

In a university setting, RAMS is only the second mesoscale numerical model to be used in real-time forecasting. The Pennsylvania State University adapted their mesoscale model, the PSU/NCAR MM4, to run in real-time, and it has been quasi-operational since 1989 (Warner and Seaman, 1990). More recently, the newer MM5 has also produced results for lake effect storms (Sousounis, 1993) and coastal cyclogenesis (Doyle and Warner, 1993).

RAMS use as a real-time forecast system began in 1991. Thompson (1993) used RAMS in two different scenarios. First, he used RAMS to predict orographically produced precipitation and mesoscale weather patterns throughout the winter of 1991-92 and again in 1992-93 in the Colorado region. He investigated in detail the Colorado Front

Range blizzard of 9 March 1992 in various real-time and sensitivity study configurations. Secondly, real-time forecasts of cirrus-level clouds were produced for use by investigators involved in the FIRE II field program in Kansas from 13 November to 6 December 1991. These simulations which included concentrations and mixing ratios of pristine ice crystals, snow, and rain were available in real-time only because they were produced by the faster NCAR CRAY YM-P computer.

### 2.2.2 Fundamentals

All numerical weather models have three common stages- input, model execution, and output. The input stage sets the atmospheric variables, such as winds, temperature and moisture, for the first time step of the model execution. Numerical models require an initial state of the atmosphere in order to begin. One assumption available for initialization is a horizontally homogeneous state. The data used for each of the individual levels are usually obtained from rawinsonde output or an idealized sounding, such as the US Standard Atmosphere. The assumption of horizontal homogeneity is normally only valid over a small domain and for non-baroclinic large-scale environments; therefore, a second method of initializing with inhomogeneous conditions is also available. The variable initialization used in RAMS has been described by Tremback (1990), Cram (1990), and Heckman (1991) with a variety of data sources. Further details of variable initialization of RAMS will be described in Section 3.3.

The second step of modeling, the model execution stage, is the heart of any numerical model. This is where the equations of motion and thermodynamics along with conservation of mass, momentum, and water are integrated with respect to time in order

to find a future state of the atmosphere. Just as initial conditions are required to begin the model execution, boundary conditions are necessary for the model to continue running. Boundary conditions are used to communicate conditions from outside the model's domain into the execution stage. Analogous to homogeneous initial states, constant boundary conditions imply that the atmosphere is in steady-state just outside the model domain. Beyond this simple assumption is the slightly more complex cyclical boundary conditions. A cyclical boundary can be used if the phenomenon being simulated is symmetric- such as mountain waves along a series of ridges- or statistically horizontally homogeneous such as boundary layer eddies. The most realistic boundary conditions are those which vary with time. The use of time-dependent boundary conditions in RAMS will be discussed in detail in Section 3.3.1.

The final stage of numerical modeling is the output stage. The solution obtained from the execution stage is displayed in a way which is useful to the end user. The form of the output can be as simple as a numerical table listing results of a particular field (see Section 6.3 for an example of precipitation tables) or as complex as a three-dimensional display in full color of many different atmospheric variables. Another part of the output stage is the diagnosis of useful quantities. For example, a model which prognoses equivalent potential temperature and dry air density is able to calculate temperature from basic equations. In many early numerical models, the output stage was often the weakest link in the process, producing hard to understand maps, paper printouts, or cryptic tables. With recent advancement of computer graphics capabilities, output data can be displayed and manipulated in virtually any way the end user prefers.

# 3. REAL-TIME FORECASTING

## 3.1 Model description

The numerical model used throughout this research is the RAMS model. RAMS is a merger of features from a non-hydrostatic cloud model (Tripoli and Cotton, 1982) and a hydrostatic mesoscale model (Mahrer and Pielke, 1977) rewritten into new code. For this research, the non-hydrostatic version of RAMS was used. Some features of this version included a leapfrog time differencing which integrates acoustic terms on a short time step (for this research, 30 seconds was used) and all other terms on a long timestep (90 seconds in this research) (Klemp and Wilhelmson, 1978). The predicted variables include three-dimensional wind components (u, v, w), the Exner function ($\pi$), the ice-liquid potential temperature ($\theta_{il}$), dry air density ($\rho$), and mixing ratios of various water species, such as rain, pristine ice crystals, graupel, aggregates, snow, and total water. From these prognostic variables, quantities such as potential temperature, pressure, temperature, cloud mixing ratio and vapor mixing ratio can be diagnosed (Tripoli and Cotton, 1982). Further descriptions of RAMS can be found in Cotton et al. (1982), Tremback et al. (1985), Tripoli (1986), Tremback (1990), Pielke et al. (1992), Nicholls et al. (1993), Thompson (1993) and Cotton et al. (1994).

## 3.2 Setup

The real-time setup was developed with two criteria in mind; produce forecasts in Colorado with grid spacing much smaller than any synoptic scale model and do it in a

length of time that would make these forecasts operationally useable. This implies that a 36-hour forecast should be completed in six to nine hours. In operational terms, this would allow a forecaster working the midnight to 8 a.m. shift use of the RAMS forecast initialized at 0000 UTC for his morning forecast at any weather service office or Air Force base weather station in the continental US.

To maintain this real-time criteria, a modest number of vertical levels were used. The levels were stretched in such a way to allow highest resolution near the surface and lowest resolution near the model's top. Spacing between the levels begins at 250 meters at the surface and tapers off to 1 kilometer at the model top of approximately 17 km (Figure 3.1).

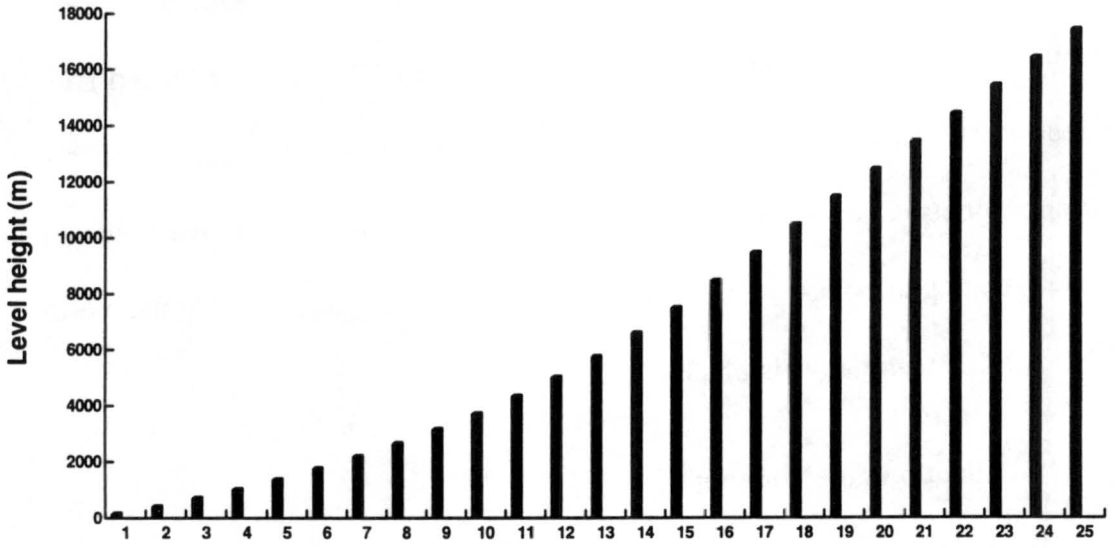


**Figure 3.1 Grid level heights for real-time setup**

The grid spacing and domain used in the horizontal was also chosen with the real-time limitations in mind. To allow high resolution forecasts in the state of Colorado, a two-grid setup was selected. The courser grid (Grid #1) extends over the western two-

thirds of the US (Figure 3.2). The grid spacing chosen was 80 km. The choice of Grid #1 grid spacing affects the finest grid spacing allowable for the nested grid because it is recommended that a maximum of 5-to-1 ratio between the course and fine grid spacing be used (Walko et. al, 1993). The large extent of the domain allows RAMS to develop synoptic-scale patterns versus a pure translation of conditions from the horizontal boundaries into the fine grid. It is also contained within the domain of the initialization data sets. (see Section 3.3).

The location of the fine grid (Grid #2) was dependent on the season. In the summer mode (15 April-1 October), Grid #2 extends into western Kansas and Nebraska. This location was chosen because this is a preferred region of storm and mesoscale convective complex development (Maddox, 1980). This is the grid location used in the downslope windstorm case study (Chapter 4). For the remainder of the year, the second grid is centered over the Colorado Rocky Mountains to obtain information about mountain precipitation amounts (Chapters 5 and 6). Grid #2 grid spacing of 16 km allowed approximately 726 separate grid points over Colorado compared to 12 grid points for the Nested Grid Model (NGM) normally distributed data set.

### 3.3 Initialization and Nudging

The first stage of the RAMS forecasting process is the initialization stage. This is where observations at the time the model is to begin are interpolated into a form useable by RAMS. The form which RAMS uses is a $\sigma_z$ terrain-following coordinate system. The input observations are converted into this form by the isentropic analysis (ISAN) package described by Tremback (1990) and Cram (1990).

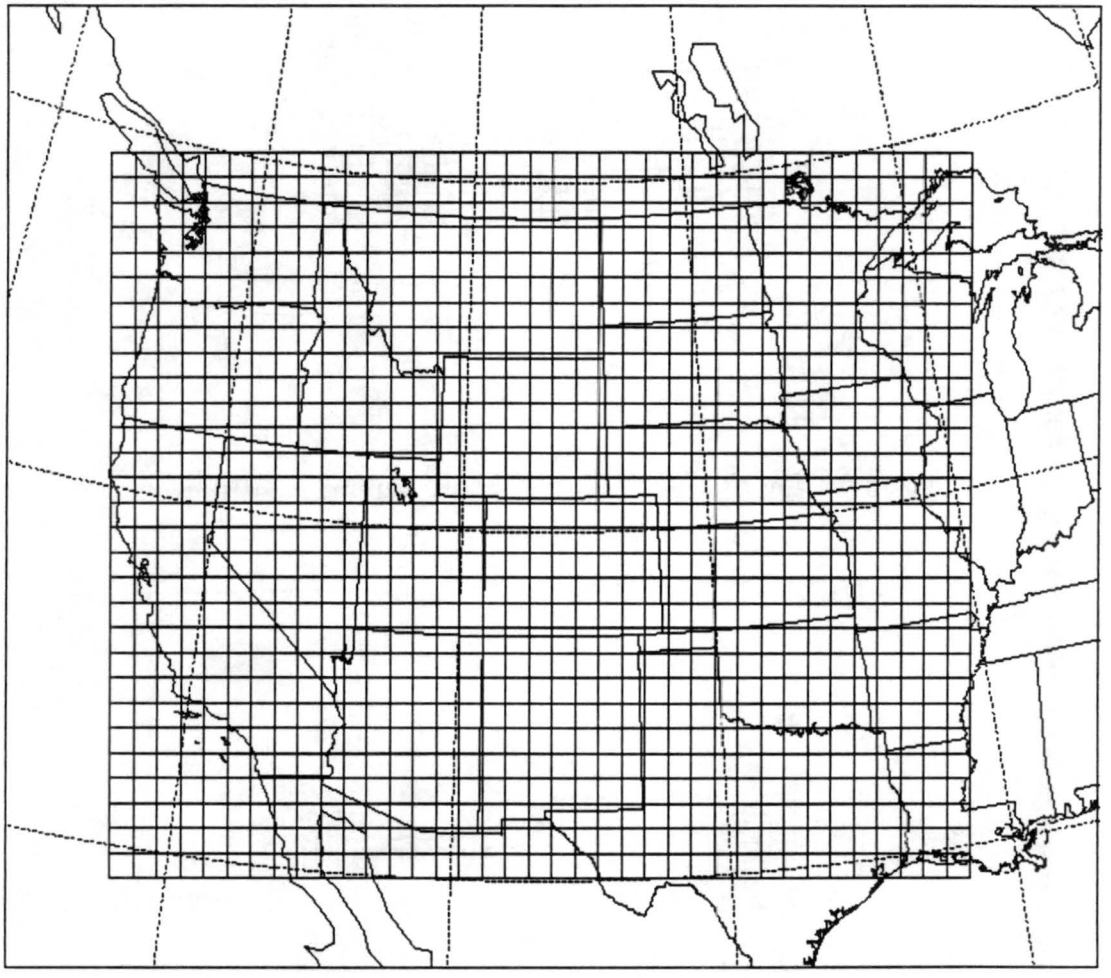

**Figure 3.2- Real-time Grid #1 setup**

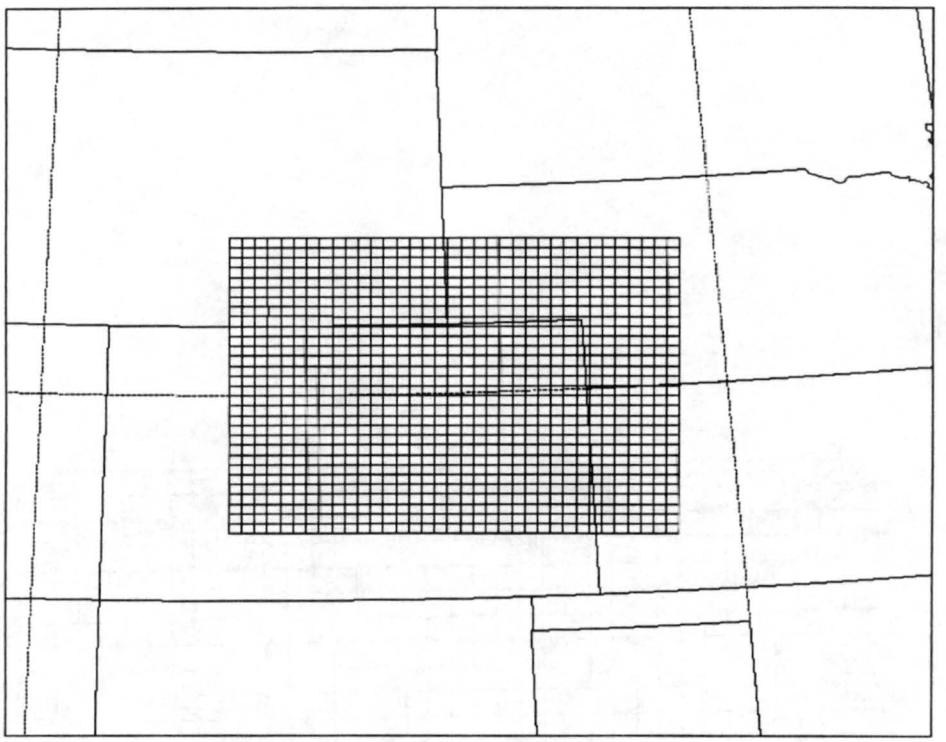

**Figure 3.3- Real-time Grid #2 setup (summer position)**

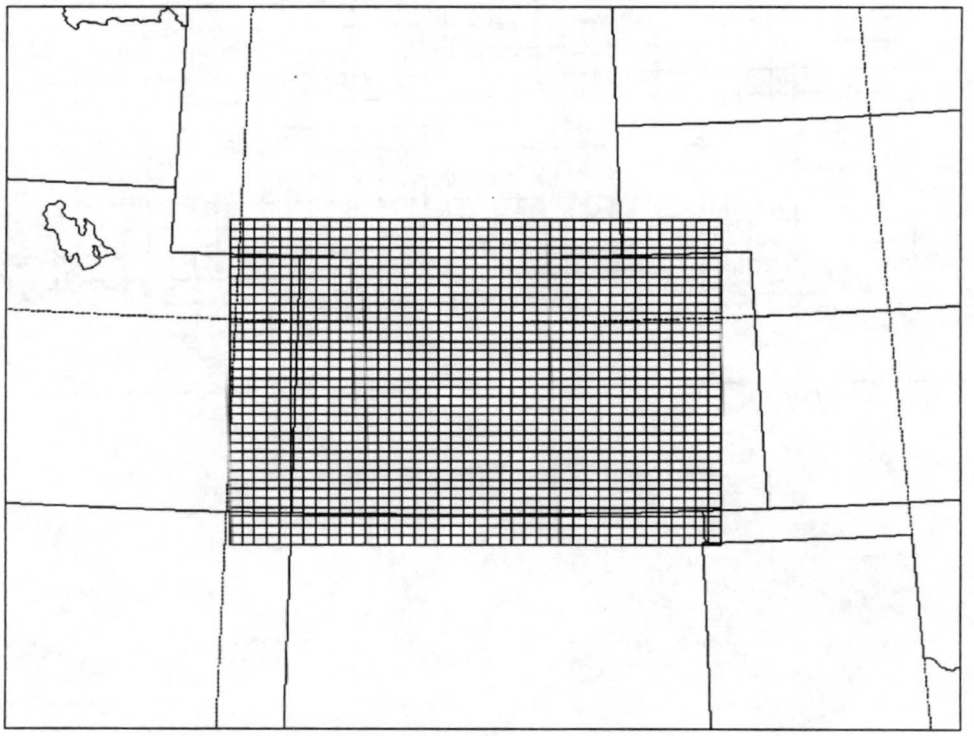

**Figure 3.4- Real-time Grid #2 setup (winter position)**

The observations used by RAMS fall under two categories: gridded and non-gridded data. The two types of non-gridded data used were surface airways observations (SAOs) and upper air data reported by rawinsondes. On average, over 700 SAOs and over 60 rawinsonde reports are used to initialize RAMS each day. The ISAN package uses Barnes (1983) objective analysis to interpolate the data to the RAMS grid setup. Since non-gridded data can be sparse in certain regions of the domain (especially in the upper levels), gridded data supplements this information. The two sources of gridded data used are the ETA and MAPS data sets.

The procedure to produce nudging files was similar to the initialization files; however, no observations could be used. As in initialization, the gridded data was interpolated to the RAMS grid. Nudging files were produced for the 12-, 18-, 24-, 30-, and 36-hour point of the simulations. Only Grid #1 was nudged along its boundaries. The borders of Grid #1 were forced to the values provided by the nudging files only within 5 gridpoint of the borders by using a tendency at these points during the normal model execution (Cram, 1990). Therefore, within 5 gridpoint of the boundaries, the RAMS forecast would approximately match the nudging dataset's forecast at the times of the nudging files. This utilization of time-vary boundary conditions did not directly effect Grid #2- it was only used for the boundary conditions provided by Grid #1. Throughout the simulations, the ETA dataset was used exclusively to produce the nudging files.

### 3.3.1 ETA Initialization and Nudging

The newest gridded product to be released by the National Meteorological Center (NMC) is the ETA dataset. ETA has an advantage over the older NGM dataset by virtue

of its fine grid spacing. Figure 3.5 shows the domain and grid spacing of the ETA model. Not only is the horizontal grid spacing finer for ETA versus NGM but the vertical resolution is also much better. Table 3.1 compares the vertical and horizontal grid spacing of ETA to other datasets and the RAMS setup. A comparison between the ETA setup and the Grid 1 RAMS setup shows many similarities in both the horizontal and vertical. Therefore, the amount of calculations required to convert the ETA grid to the RAMS course grid is minimal. This cuts down on the time required to run the objective analysis of the initialization stage and speeds up the forecasting process.

### 3.3.2 MAPS Initialization

The other dataset RAMS is able to initialize with is the Mesoscale Analysis and Prediction System (MAPS) dataset. Developed at NOAA's Forecast System Laboratories, MAPS is unique in that it uses aircraft reports, wind profiler data and surface mesonetwork data besides the normal SAOs and rawinsonde soundings. From this wide variety of data sources, a gridded dataset with 60 km square horizontal grid spacing is produced (see Figure 3.6). Table 3.1 compares the vertical and horizontal grid spacing of MAPS to other datasets and the RAMS setup. MAPS also produces limited forecasts; however, only its use as an initialization source was utilized. Another unique feature of MAPS is its two types of vertical levels. Throughout the different levels of the atmosphere above the boundary layer, MAPS uses an isentropic coordinate system split into 19 levels. This is fortuitous because synoptic-scale flow tends to be adiabatic, and in regions of discontinuities - such as baroclinic zones and fronts - higher resolution is obtained (Tremback 1990). The disadvantage to isentropic coordinates is resolving features in the

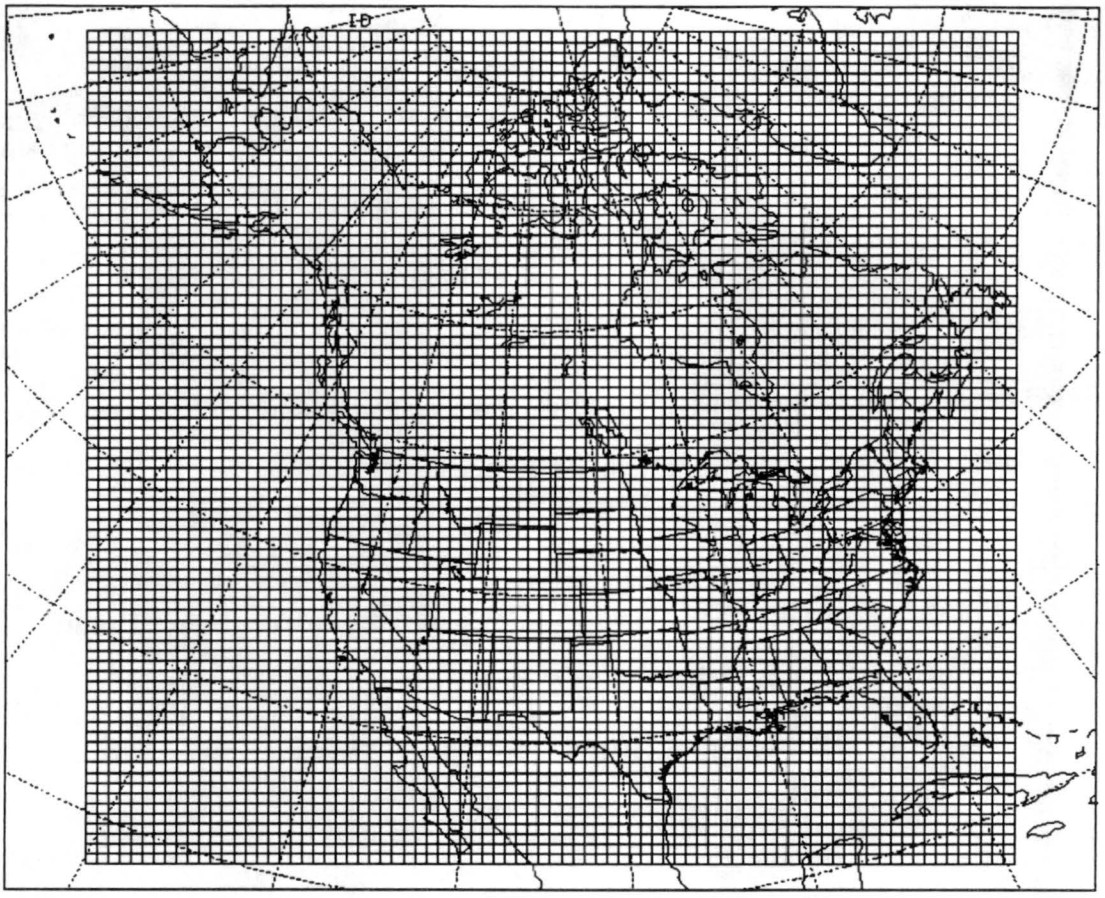

**Figure 3.5- Grid spacing and domain of ETA dataset**

well-mixed boundary layer. MAPS compensates for this shortcoming by including six hybrid-σ (terrain-following) levels in the lowest 150 mb of the model. Figure 3.7 shows an example of an east-west cross section of MAPS' vertical levels using the combined hybrid-σ and isentropic vertical coordinates. A full description of the MAPS dataset can be found in Benjamin et al. (1991). Unfortunately, the availability of MAPS was too inconsistent to use on a regular basis. Also, the format of MAPS has changed a few times over the last year. Only a scattering of days containing useable MAPS files were available.

| DATASET | DOMAIN SIZE | VERTICAL GRID SPACING | HORIZONTAL GRID SPACING |
|---|---|---|---|
| ETA | 83 x 83 gridpoints | 19 pressure levels | 80 km square |
| MAPS | 81 x 62 gridpoints | 6 $\sigma_z$ levels in lowest 150 mb / 19 preset $\theta$ levels | 60 km square |
| NGM | 36 x 33 gridpoints | 10 pressure levels | 1.25° Lat x 2.5° Long |
| RAMS Setup (Grid #1) | 39 x 31 gridpoints | 26 levels stretched from 250m near the surface to 1000m at the top of model | 80 km square |

**Table 3.1- Description of various datasets and the RAMS Grid #1 setup**

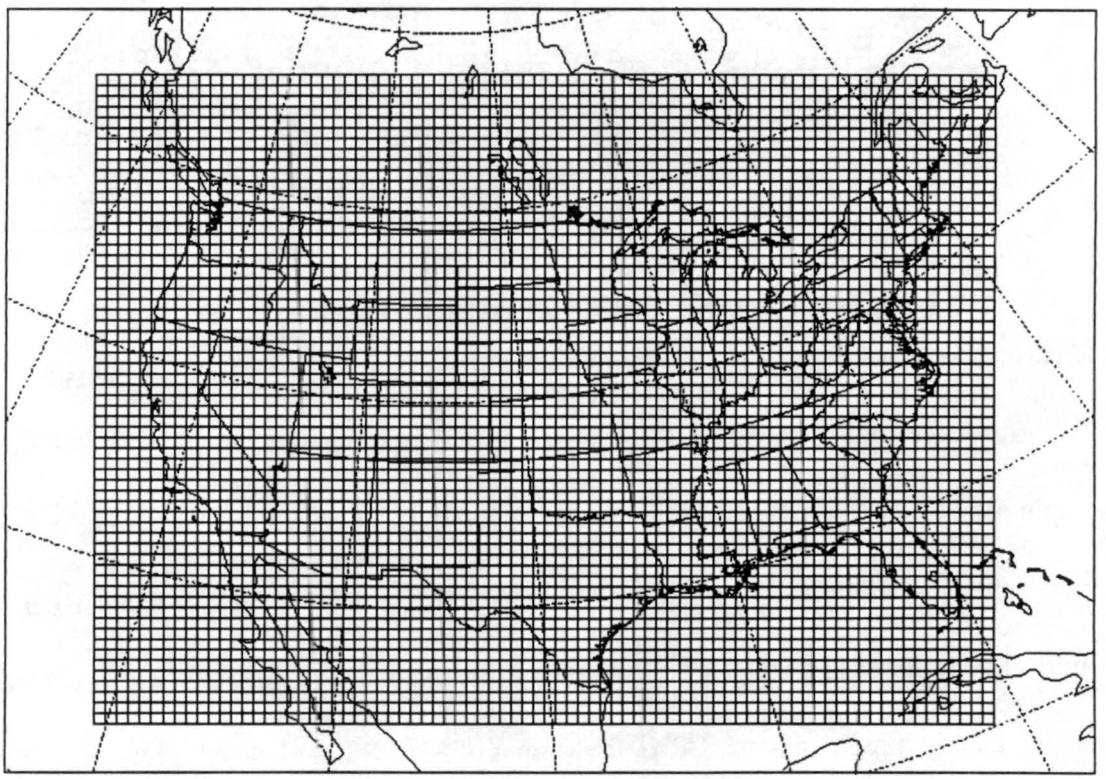

**Figure 3.6- Grid spacing and domain of MAPS dataset**

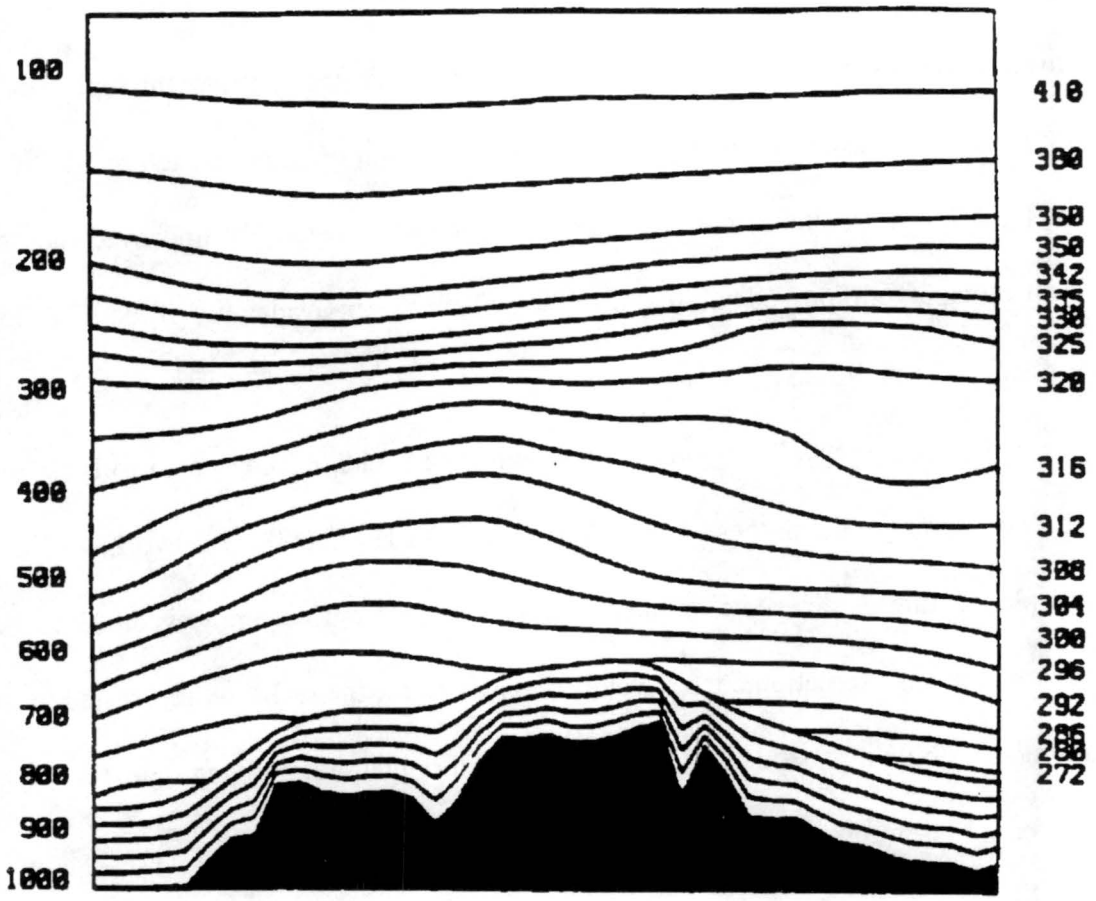


**Figure 3.7- Cross-section of MAPS illustrating the 6 hybrid-σ levels(lowest levels) and the 19 isentropic levels (from Benjamin et al., 1991)**

### 3.4 Results

The real-time setup of RAMS has been producing daily forecasts with relative consistency over the last three years. Over the past 9 months, these results have become even more consistent. Figure 3.8 shows the frequency of 24-hour forecasts- the minimum amount of output to consider that day as a "successful run." A vast majority (over 95%) of these successful runs completed the full 36 hours of simulations. The gap in successful runs in August is due to moving the real-time simulation to a new computer. In Novem-

ber, attempts were made to compile a version of the real-time model using a new microphysics. Unfortunately, tests run during this time indicated the new microphysics could not be run in real-time. The gap in December is a result of using the full microphysics to run the 3 July 1993 downslope windstorm (Chapter 4). Overall, the improved success rate is attributable to improved automation code and consistent availability of the ETA dataset, surface observations, and upper-air soundings.

Figure 3.9 details a typical daily schedule of events leading up to forecast results. The computer used for these simulations is a IBM RISC/6000 375 workstation. The completion time is delayed if initialization and nudging data are not available at the expected times. Automation code developed expressly for the real-time forecasts repeatedly attempts to obtain these datasets. Once obtained, initial and nudging datasets are transformed into isentropic gridded data (as described in Section 3.3).

Once the model run has completed, printouts of different meteorological fields can be produced. The following figures shows the four basic types of displays which can be produced- map view (Figure 3.10), cross section (Figure 3.11), time series (Figure 3.12), and Skew-T (Figure 3.13). A map view can be produced for any pressure level. The cross section view is available for either a west-east or north-south perspective. The time series is defined at a point and pressure level for a given amount of time. The Skew-T sounding is chosen for individual locations.

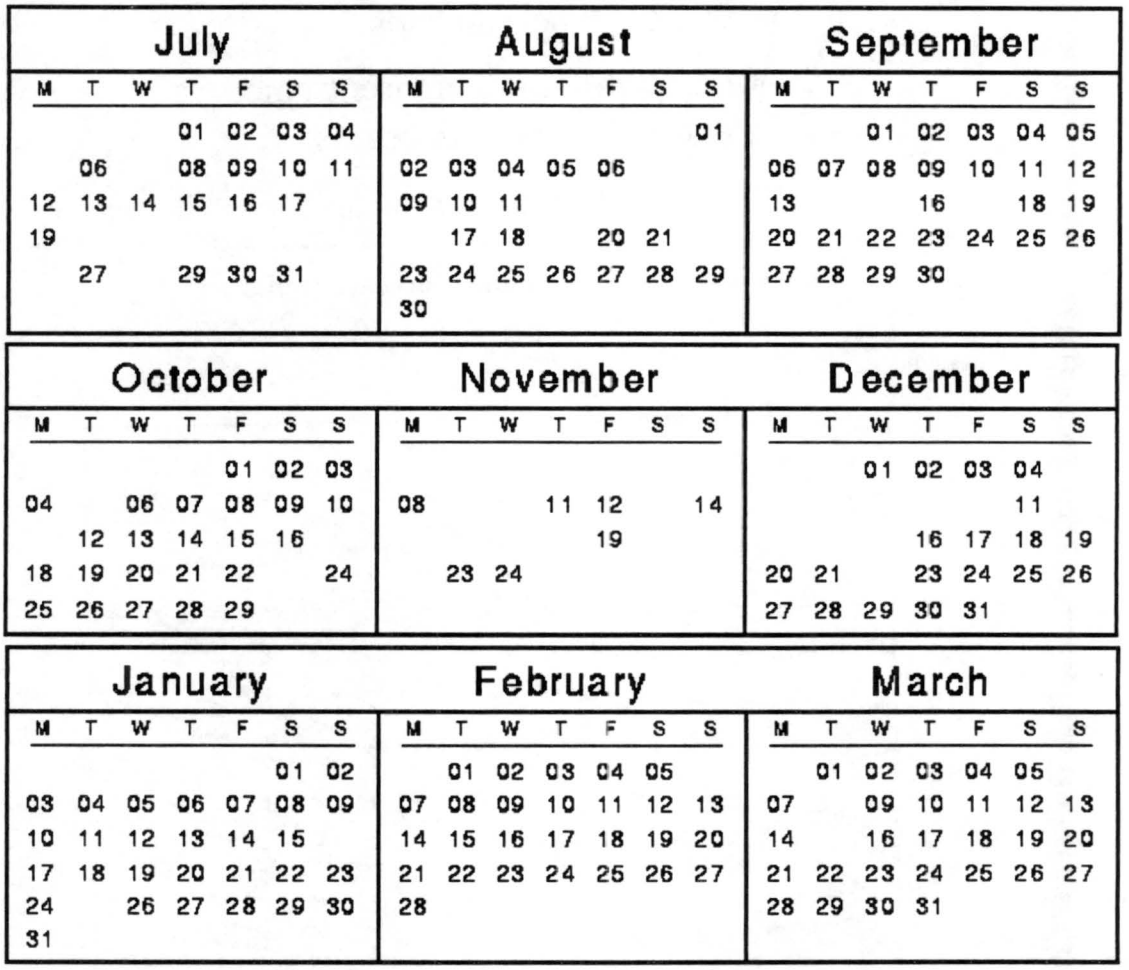

| July | | | | | | |
|---|---|---|---|---|---|---|
| M | T | W | T | F | S | S |
| | | | 01 | 02 | 03 | 04 |
| | 06 | | 08 | 09 | 10 | 11 |
| 12 | 13 | 14 | 15 | 16 | 17 | |
| 19 | | | | | | |
| | 27 | | 29 | 30 | 31 | |

| August | | | | | | |
|---|---|---|---|---|---|---|
| M | T | W | T | F | S | S |
| | | | | | | 01 |
| 02 | 03 | 04 | 05 | 06 | | |
| 09 | 10 | 11 | | | | |
| | 17 | 18 | | 20 | 21 | |
| 23 | 24 | 25 | 26 | 27 | 28 | 29 |
| 30 | | | | | | |

| September | | | | | | |
|---|---|---|---|---|---|---|
| M | T | W | T | F | S | S |
| | | 01 | 02 | 03 | 04 | 05 |
| 06 | 07 | 08 | 09 | 10 | 11 | 12 |
| 13 | | | 16 | | 18 | 19 |
| 20 | 21 | 22 | 23 | 24 | 25 | 26 |
| 27 | 28 | 29 | 30 | | | |

| October | | | | | | |
|---|---|---|---|---|---|---|
| M | T | W | T | F | S | S |
| | | | | 01 | 02 | 03 |
| 04 | | 06 | 07 | 08 | 09 | 10 |
| | 12 | 13 | 14 | 15 | 16 | |
| 18 | 19 | 20 | 21 | 22 | | 24 |
| 25 | 26 | 27 | 28 | 29 | | |

| November | | | | | | |
|---|---|---|---|---|---|---|
| M | T | W | T | F | S | S |
| | | | | | | |
| 08 | | | 11 | 12 | | 14 |
| | | | | 19 | | |
| | 23 | 24 | | | | |
| | | | | | | |

| December | | | | | | |
|---|---|---|---|---|---|---|
| M | T | W | T | F | S | S |
| | | 01 | 02 | 03 | 04 | |
| | | | | | 11 | |
| | | | 16 | 17 | 18 | 19 |
| 20 | 21 | | 23 | 24 | 25 | 26 |
| 27 | 28 | 29 | 30 | 31 | | |

| January | | | | | | |
|---|---|---|---|---|---|---|
| M | T | W | T | F | S | S |
| | | | | | 01 | 02 |
| 03 | 04 | 05 | 06 | 07 | 08 | 09 |
| 10 | 11 | 12 | 13 | 14 | 15 | |
| 17 | 18 | 19 | 20 | 21 | 22 | 23 |
| 24 | | 26 | 27 | 28 | 29 | 30 |
| 31 | | | | | | |

| February | | | | | | |
|---|---|---|---|---|---|---|
| M | T | W | T | F | S | S |
| | 01 | 02 | 03 | 04 | 05 | |
| 07 | 08 | 09 | 10 | 11 | 12 | 13 |
| 14 | 15 | 16 | 17 | 18 | 19 | 20 |
| 21 | 22 | 23 | 24 | 25 | 26 | 27 |
| 28 | | | | | | |

| March | | | | | | |
|---|---|---|---|---|---|---|
| M | T | W | T | F | S | S |
| | 01 | 02 | 03 | 04 | 05 | |
| 07 | | 09 | 10 | 11 | 12 | 13 |
| 14 | | 16 | 17 | 18 | 19 | 20 |
| 21 | 22 | 23 | 24 | 25 | 26 | 27 |
| 28 | 29 | 30 | 31 | | | |

**Figure 3.8- RAMS "successful days" from 1 July 1993 to 31 March 1994**

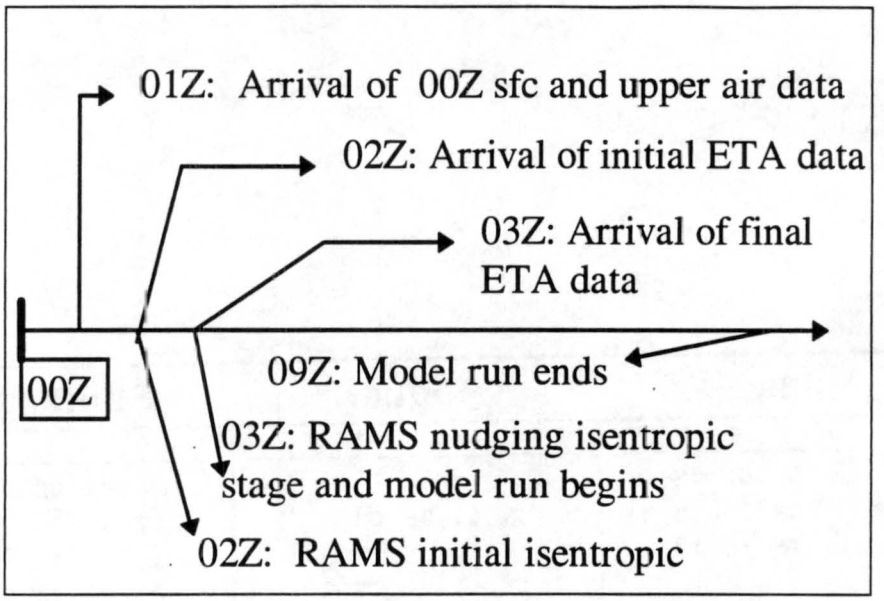


**Figure 3.9- Timeline of daily forecast events**

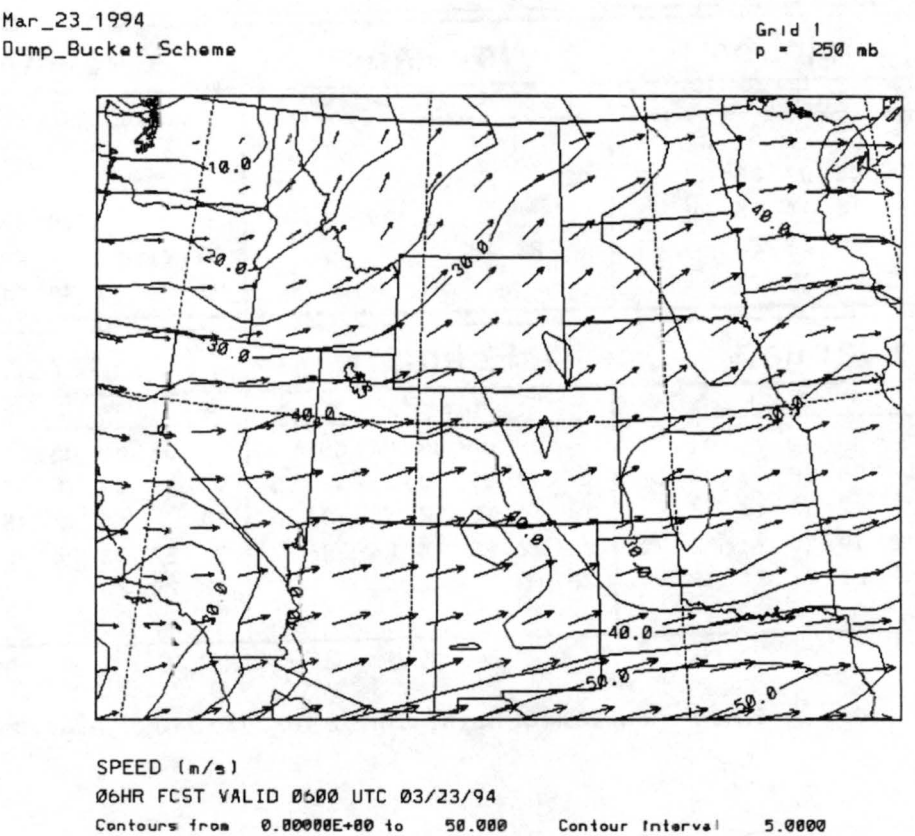


**Figure 3.10- Example of map-view display**

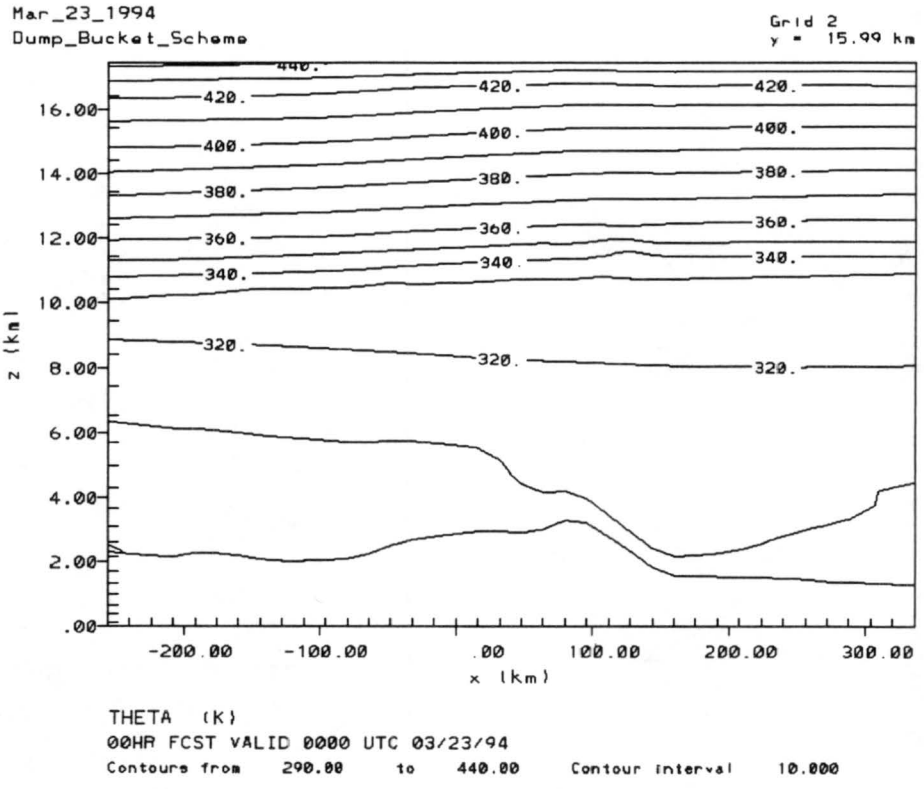


**Figure 3.11- Example of cross section display**

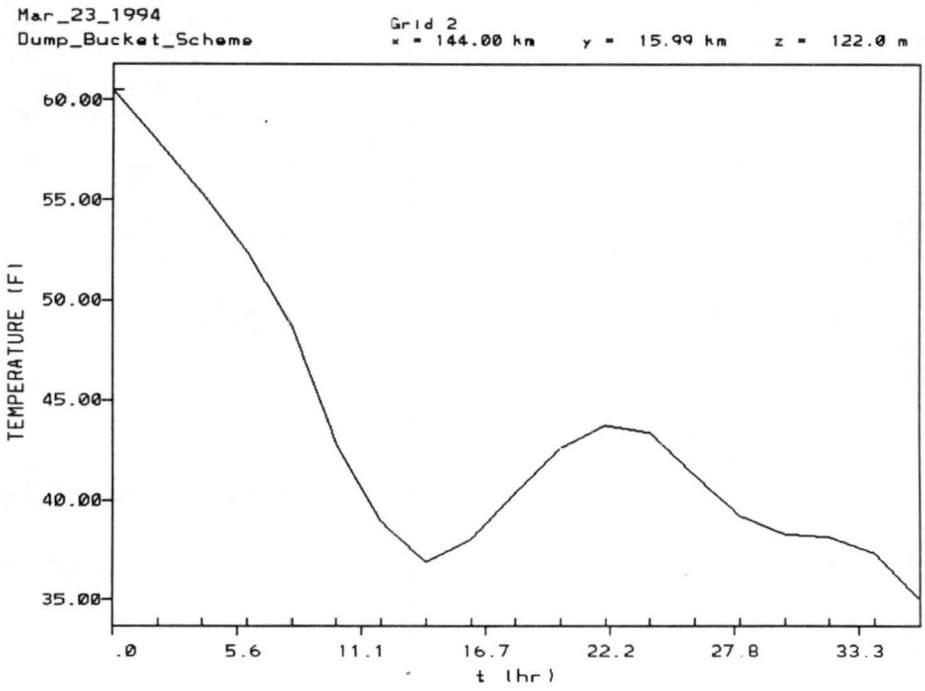


**Figure 3.12- Example of time-series display**

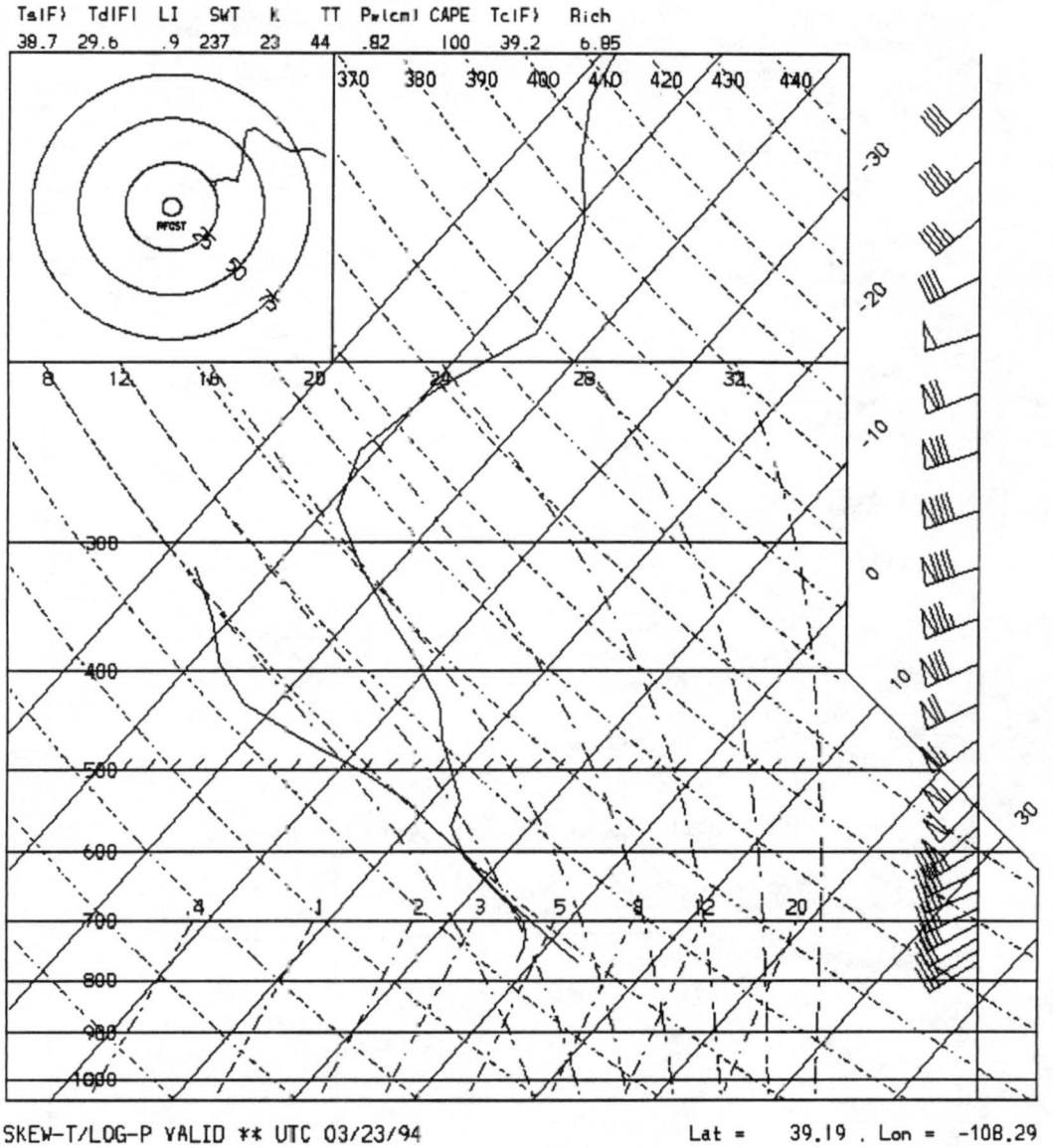


**Figure 3.13- Example of Skew-T display**

## 3.5 Summary

At this time, the model has reached a level of consistent execution, allowing it to be used for daily mesoscale forecasting. The variety of output options assures the end-user that the data will be displayed for his specific purposes. The ability to initialize using different types of data prevents the model from being dependent on one source of information.

The variety of forecast areas which can be explored with a real-time mesoscale model are virtually endless. In the next two chapters, two specific cases will be examined, along with results from the bulk-microphysics version of RAMS, allowing comparison of results. In Chapter 4, a Colorado downslope windstorm will be examined, including some of the variations in results between a simple version of cloud microphysics and details microphysics. In Chapter 5, a winter storm over the high terrain of Colorado will be examined in detail using a variety of model configurations.

# 4. DOWNSLOPE WINDSTORM CASE STUDY

## 4.1 Introduction

During normal daily forecasting in the summer of 1993, RAMS had the opportunity to model a unique event. On 3 July, the Colorado Front Range experienced an unseasonable windstorm. These events can produce winds in excess of 100 kts and can cause thousands of dollars in damage for each event. The downslope windstorm of 3 July 1993 was extraordinary due to the time of the year it occurred (Figure 4.1). Since downslope windstorms are primarily confined to the Front Range, large scale models such as the NGM have had limited success in forecasting these events. The ability to forecast this particular windstorm using a mesoscale model running with real initial conditions was tested under a variety of model configurations.

## 4.2 Synoptic situation

The 1200 UTC analysis on 3 July 93 showed some very "un-July"-like features. At 300 mb, a strong jet was analyzed to be just entering western Colorado (see Figure 4.2). At 500 mb, a short wave trough (shown in Figure 4.3) associated with an upper level low was centered over western Utah. The surface low was measured at 992 mb and located on the Wyoming-Nebraska border (Figure 4.4). The 1200 UTC synoptic situation was more typical of late November than that of early July! According to Lee, et al. (1989), this pattern matched the most favorable synoptic scale pressure pattern, with high pressure

to the southwest and low pressure to the northeast. The stage was set for downslope winds in the Fort Collins area.

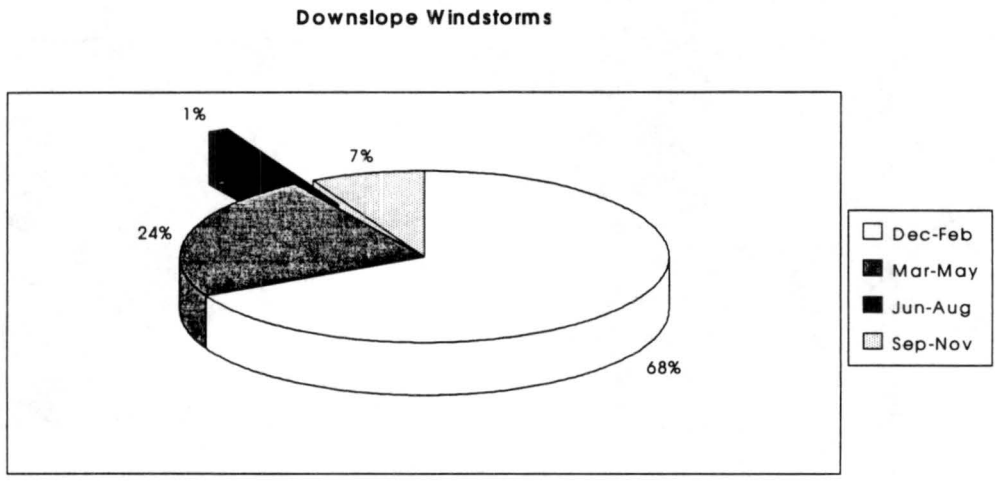


**Figure 4.1- Normal occurrences of downslope windstorm throughout the year (adapted from Lee et al. (1989) )**

## 4.3 Results (Setup 1)

Because the conditions looked favorable for strong winds, the real-time model was run an additional time on 3 July 1993. Using the ETA 00h initialization dataset along with surface and upper air observations, the model's initial state was produced for 1200 UTC. Figure 4.5 and Figure 4.6 shows the initial vertical cross sections for zonal wind and potential temperature ($\theta$) through a west-to-east cross section running through Fort Collins. Figure 4.5 shows the strongest winds measured below the jet stream were only about 25 m/s over the mountains at an elevation of $\cong$ 8 km. Figure 4.6 shows a dip in the 320 °K $\theta$-line as it crosses over the mountain crest. Figure 4.5, however, does not indicate any acceleration in this area.

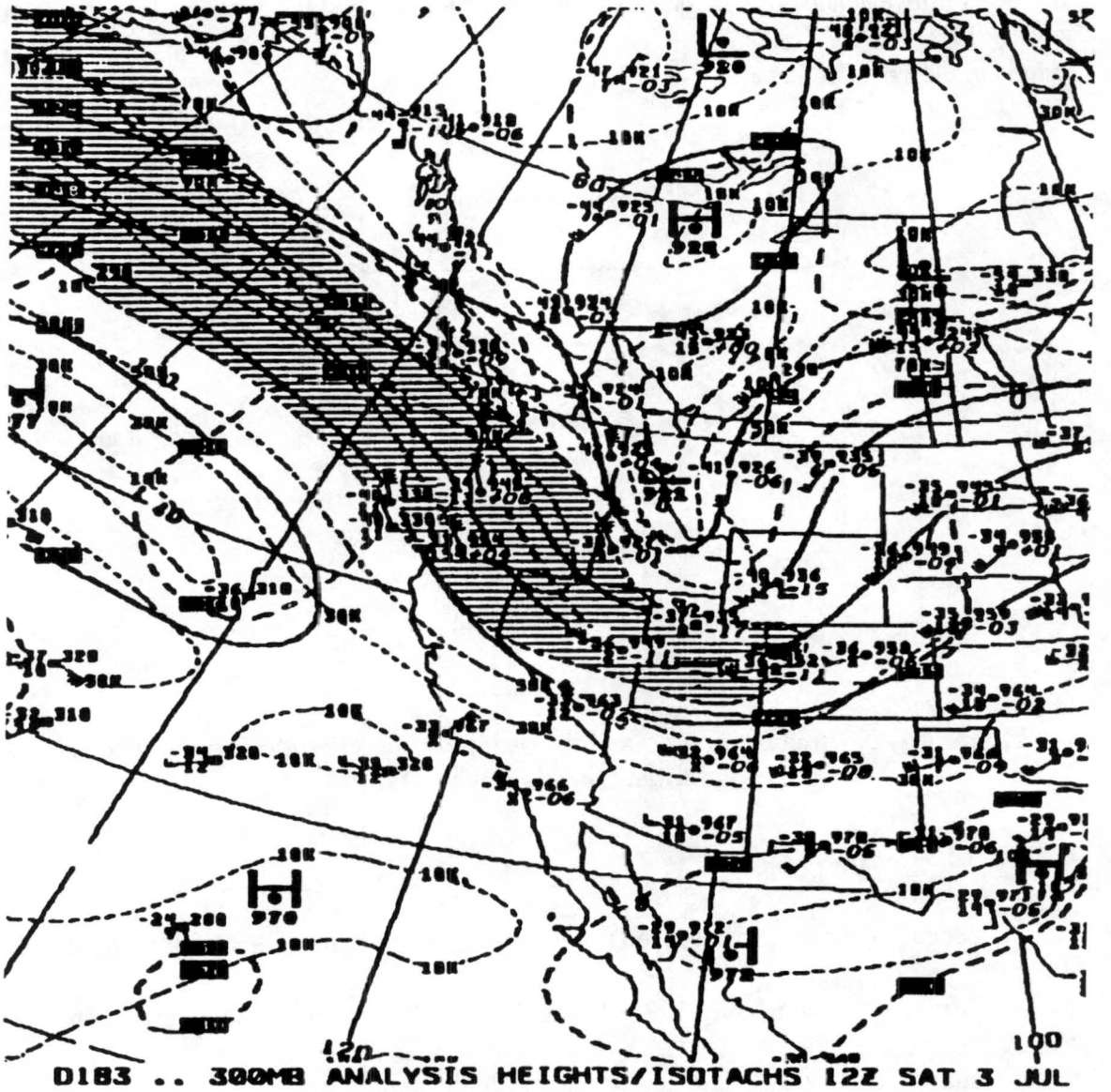


**Figure 4.2- Location of 300 mb jet max, 1200 UTC 3 July 1993**

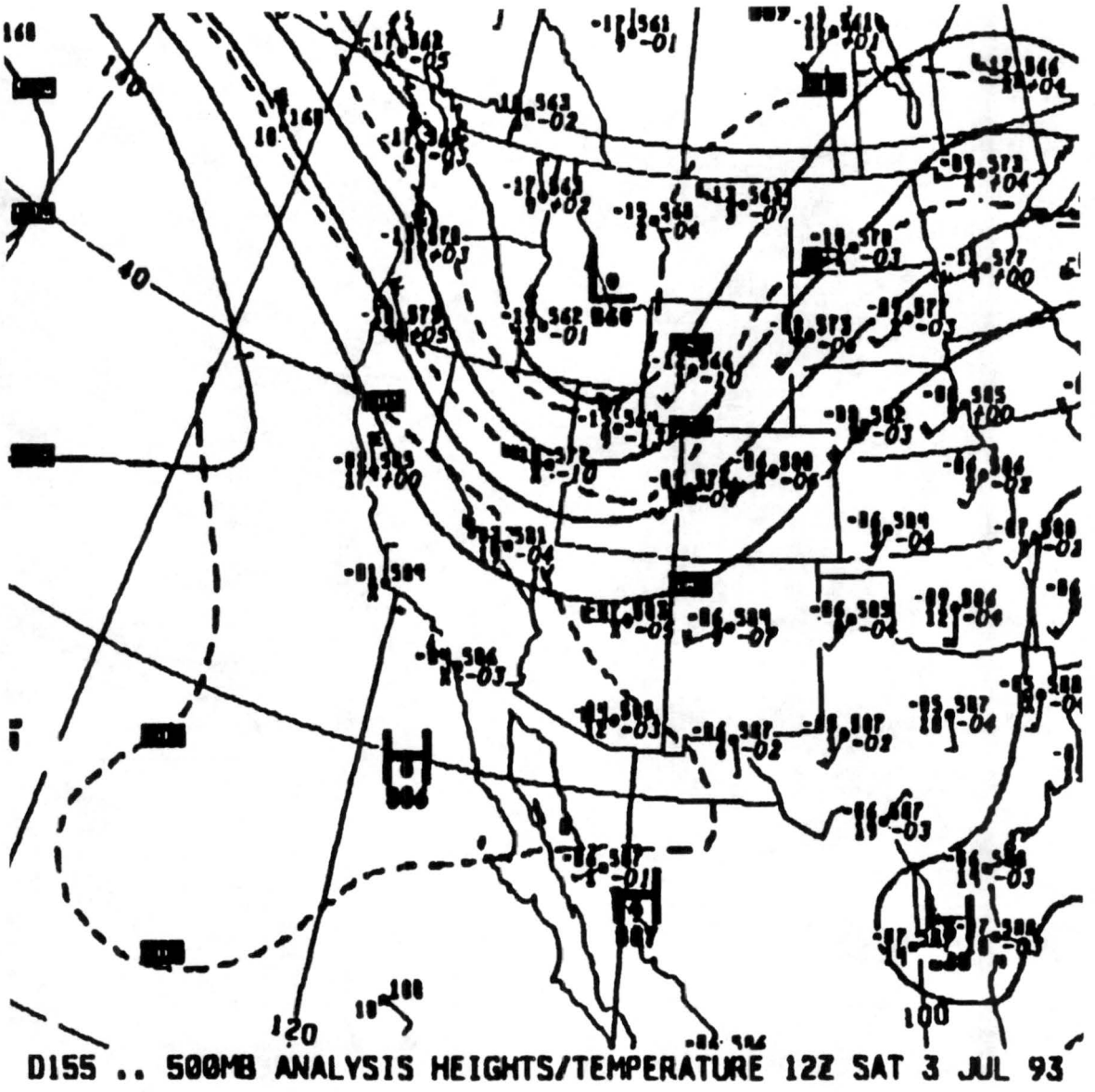


**Figure 4.3- Location of 500 mb short wave, 1200 UTC 3 July 1993**

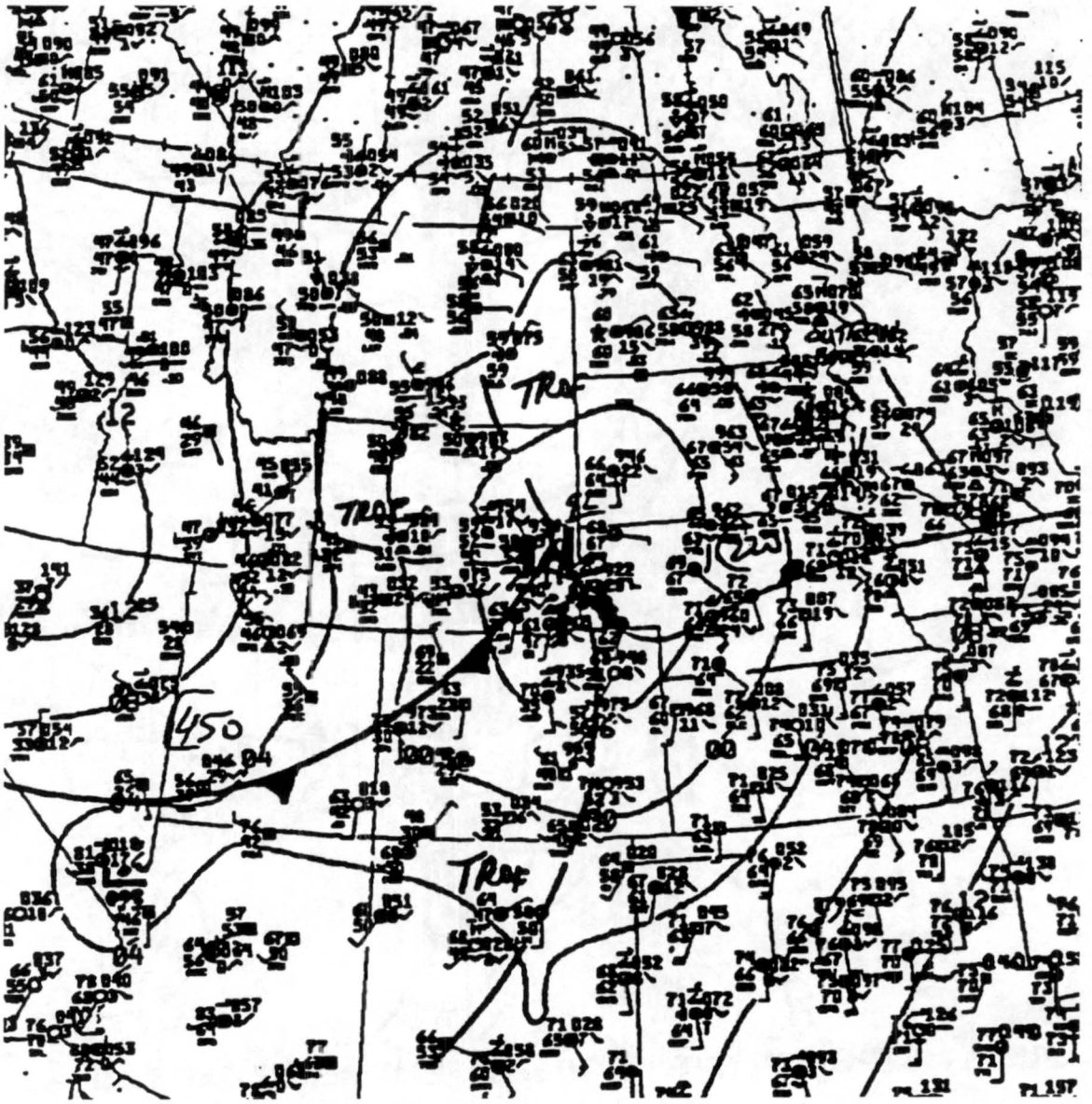


**Figure 4.4- Surface analysis, 1200 UTC 3 July 1993**

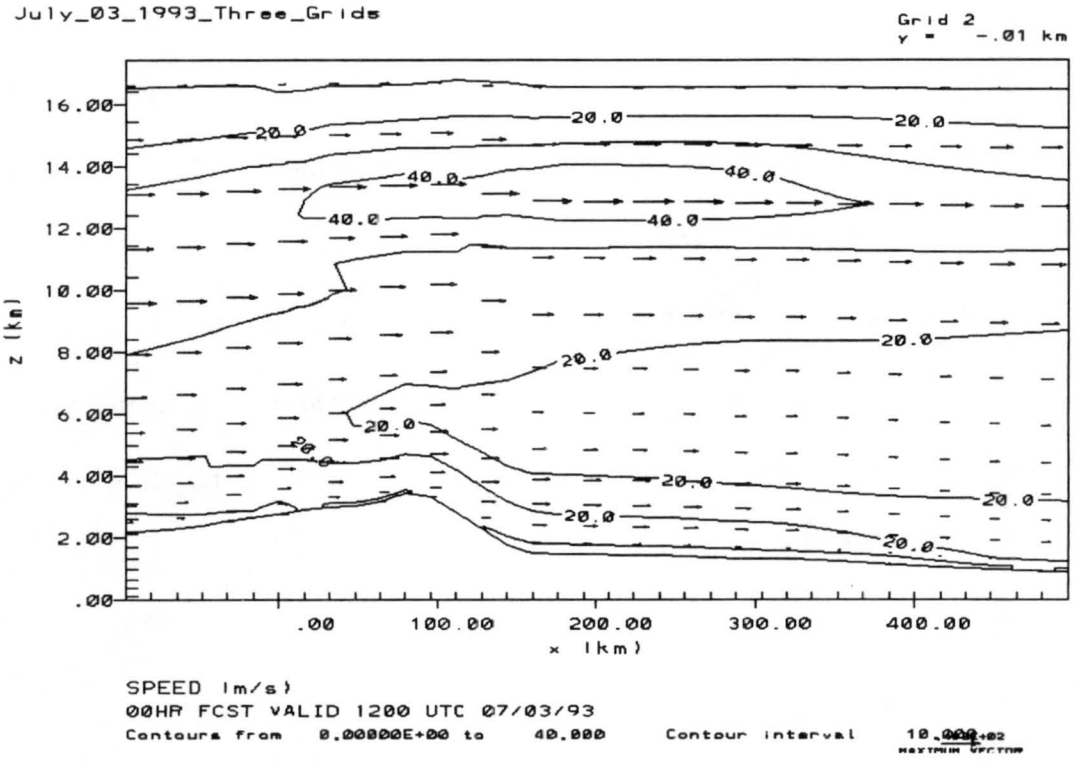


**Figure 4.5- Initial 1200 UTC wind field**

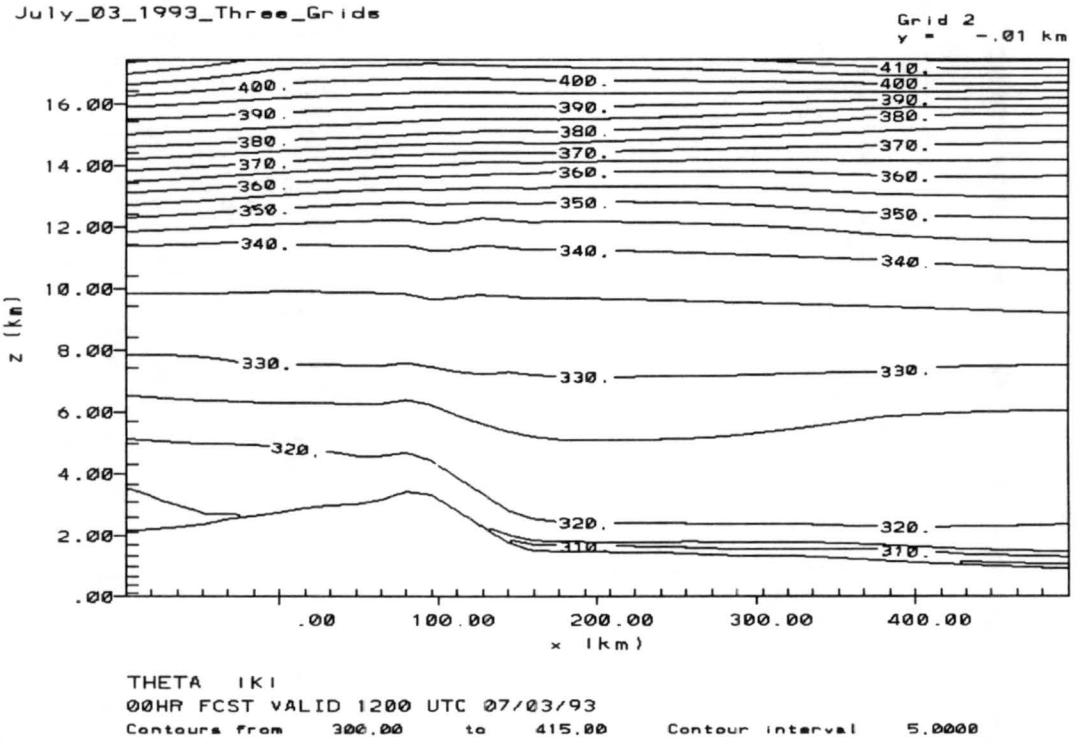


**Figure 4.6- Initial 1200 UTC θ field**

At two hours into the simulation, stronger winds develop along the Front Range. Figure 4.7 shows winds in excess of 30 m/s at mountain level, dipping down along the Front Range. Figure 4.8 shows a vertical circulation along the Front Range, where solid contours are upward motion, and dashed contours are downward motion. Figure 4.9 shows a continued drop in higher θ air along the Front Range. By the 8-hour point in the simulation, the winds in excess of 30 m/s are no longer in contact with the mountain top (Figure 4.10), and the vertical circulation has weakened near the surface (Figure 4.11). Also, the θ field no longer dips drastically down to the surface (Figure 4.12).

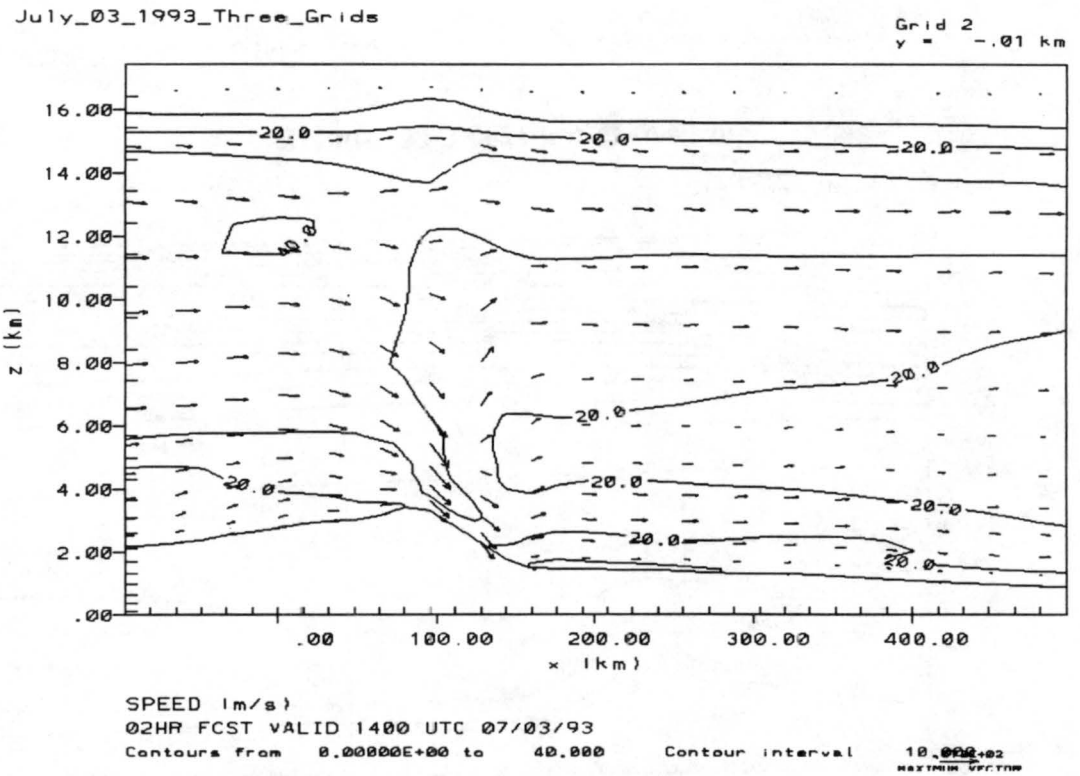


**Figure 4.7- 02 hour zonal wind speed (in m/s)**

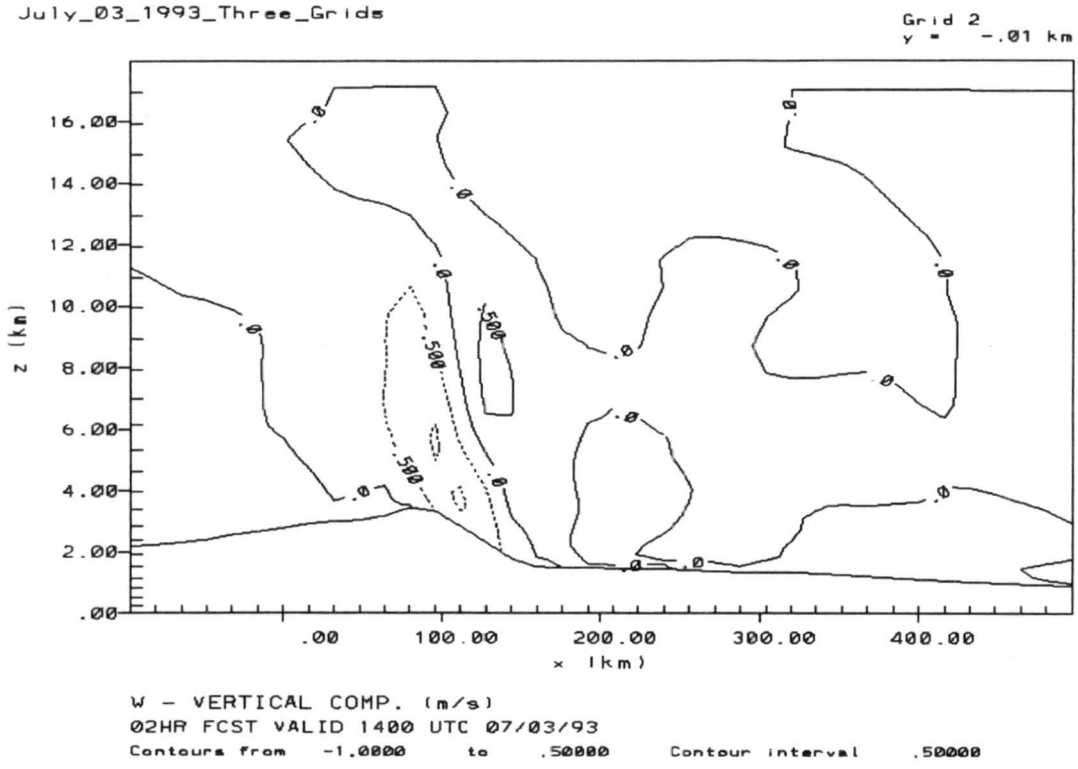


**Figure 4.8- 02 hour vertical velocity (in m/s)**

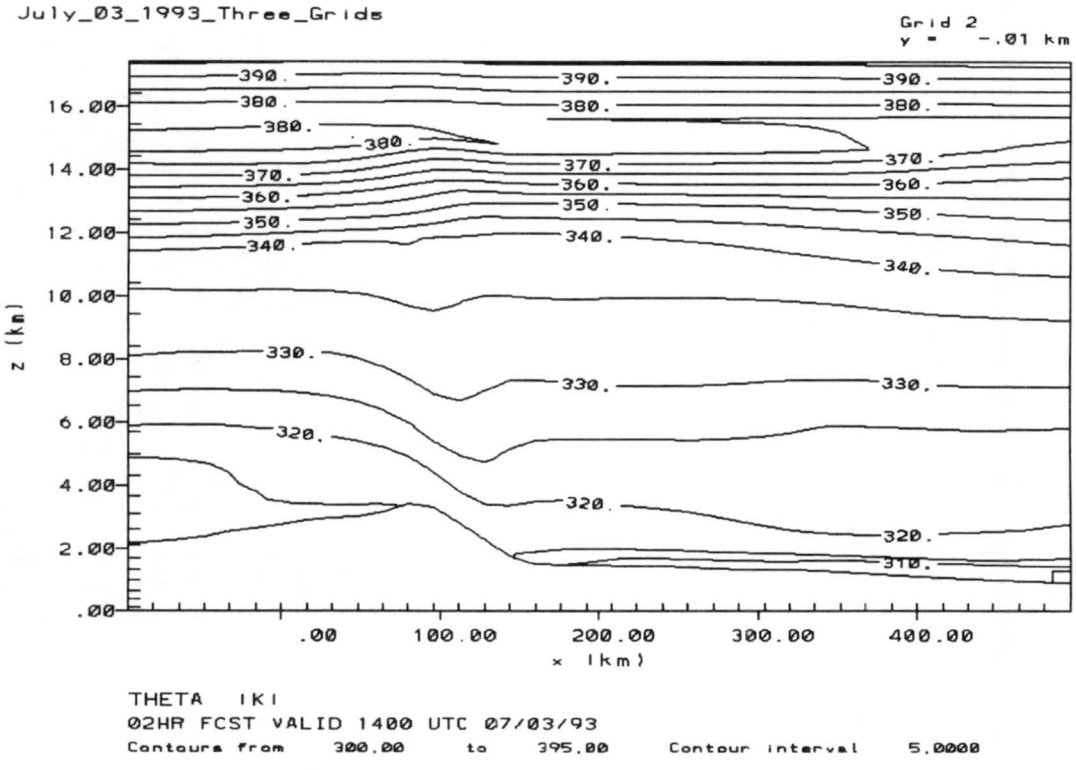


**Figure 4.9- 02 hour θ field (in °K)**

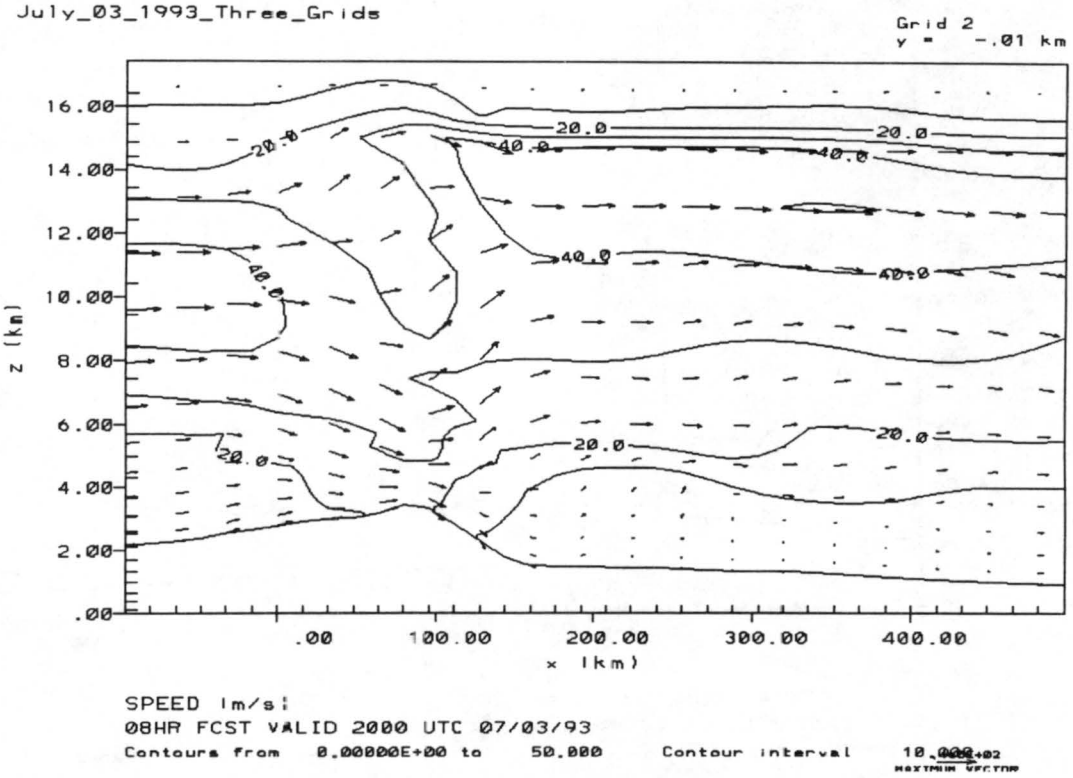


**Figure 4.10- 08 hour zonal wind speed (in m/s)**

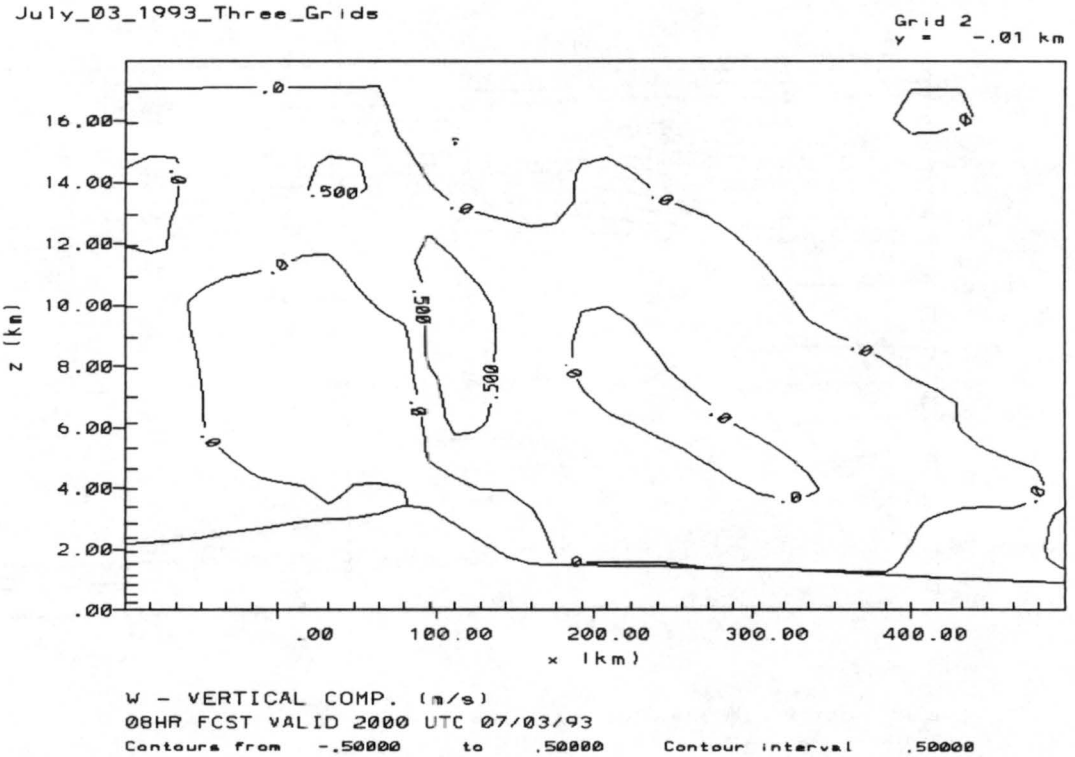


**Figure 4.11- 08 hour vertical velocity field (in m/s)**

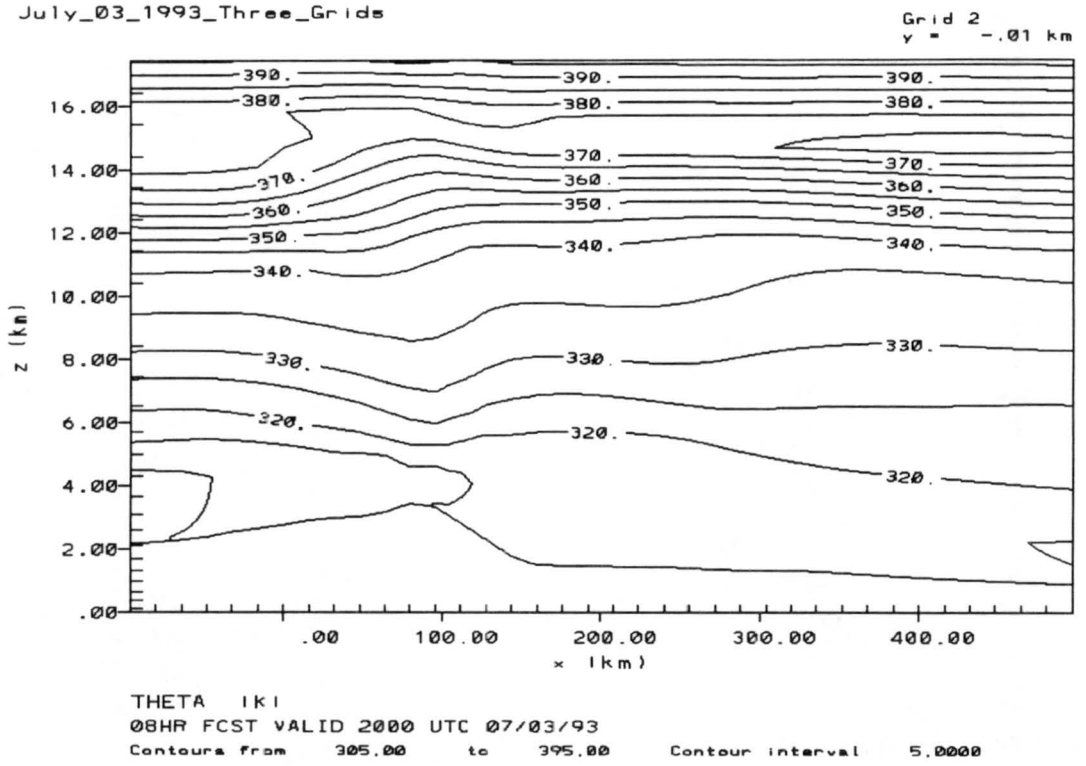


**Figure 4.12- 08 hour θ field (in °K)**

Figure 4.13 shows a time series comparison between what was observed at the NOAA Mesonet site in Fort Collins (hourly average) and what the model predicted. Although there is initial indications of stronger winds developing, the model fails to produce any significant winds during its entire run. To add more realism to the simulation, the moisture complexity was changed from Level 1 to Level 2 and run again (see Table 4.1 for a description of the various moisture complexities). This change had no effect on surface wind speed. The model was also run a third time at a moisture complexity of Level 3, but this also had no effect on surface winds. The model's inability to forecast the windstorm in its normal real-time forecasting configuration was immediately obvious.

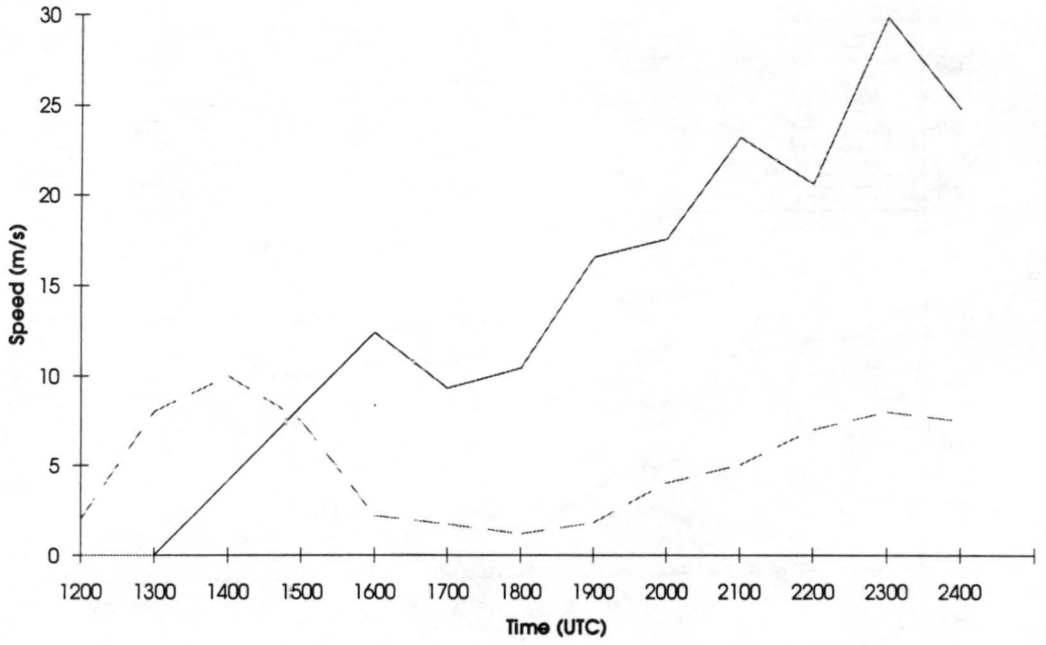


**Figure 4.13- Observed (solid) vs. two-grid forecast winds (dashed) at Fort Collins. Speed in m/s**

| Level | Description |
|---|---|
| 0 | Dry |
| 1 | Vapor used as passive tracer |
| 2 | All supersaturation condensed into liquid |
| 3 | Full microphysics |

**Table 4.1- Moisture complexities of RAMS (from Flatau et al, 1989)**

## 4.4 New setup

According to Durran (1986), the two theories that describe the development of strong lee slope winds are the linear theory and the hydraulic theory. Both these theories (and Durran's theory which links these two theories), along with previous modeling results, show strong interactions in the region of the leeward slope. In the original RAMS grid setup, this region was only represented by 3 grid points; therefore, a third, finer grid was added in this area for the entire simulation (Figure 4.14). Grid #3 has a grid spacing

of 4 km square, which extends along the Front Range from the Colorado-Wyoming border to Denver and has the same vertical dimensions as the other two grids.

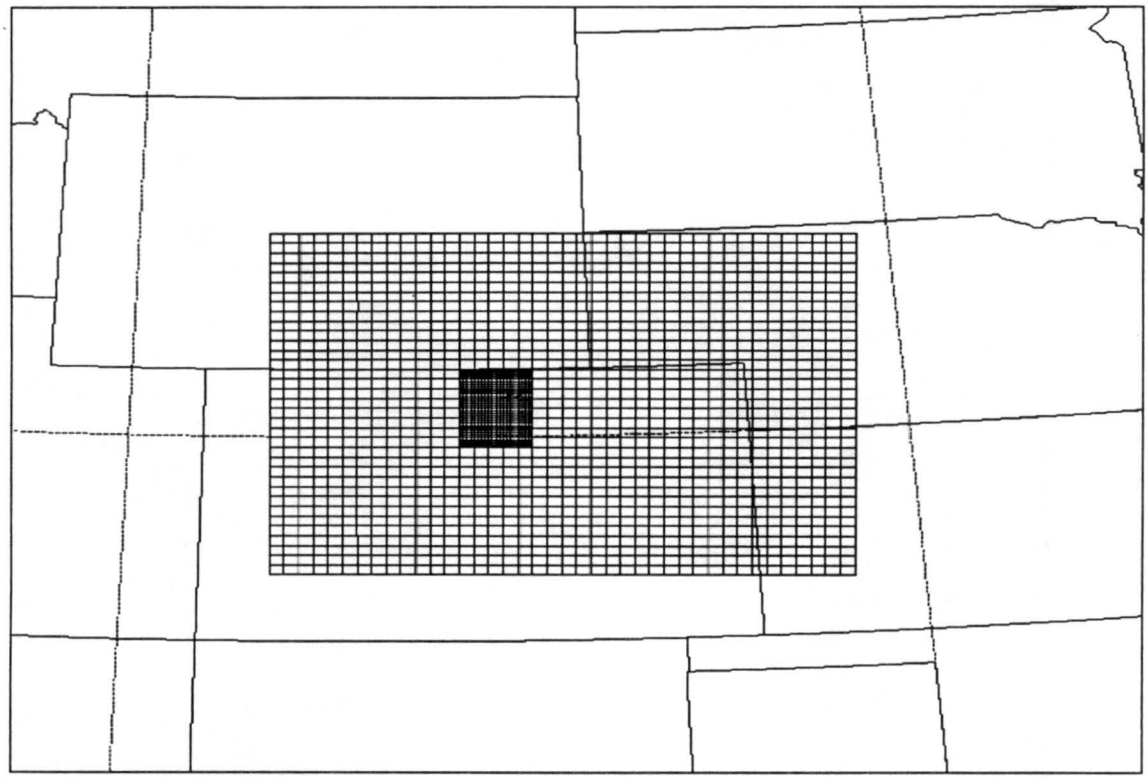

**Figure 4.14- Three- grid setup**

## 4.5 Results (Setup 2)

Within the first two hours of the simulation, the effects of the third grid can be plainly seen. Figure 4.15 shows the strong winds coming down the lee slope of the mountains. Figure 4.16 shows a vertical circulation with a strength of ≈ 2.5 m/s. The field most dramatically changed is the θ cross-section. Figure 4.17 shows a wave pattern developing just east of the mountain crest. The 340 °K θ-line drops down from 11.5 km to 6 km directly above the mountain top.

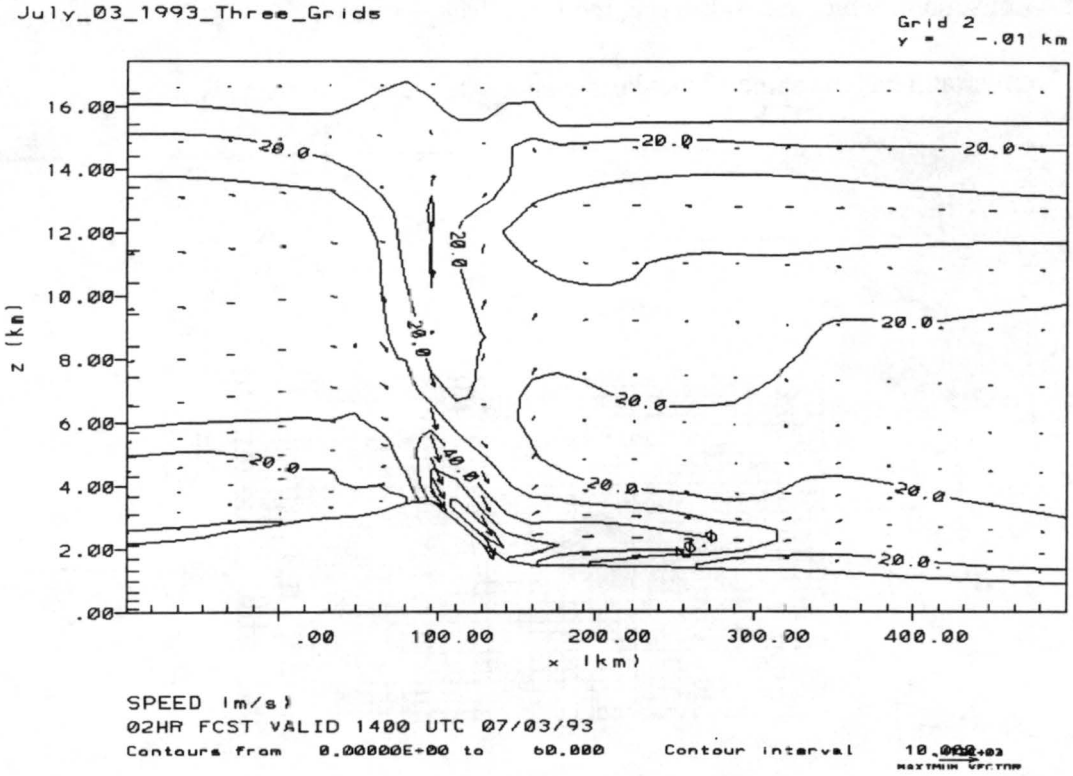


**Figure 4.15- Three grid 02 hour wind speed (in m/s)**

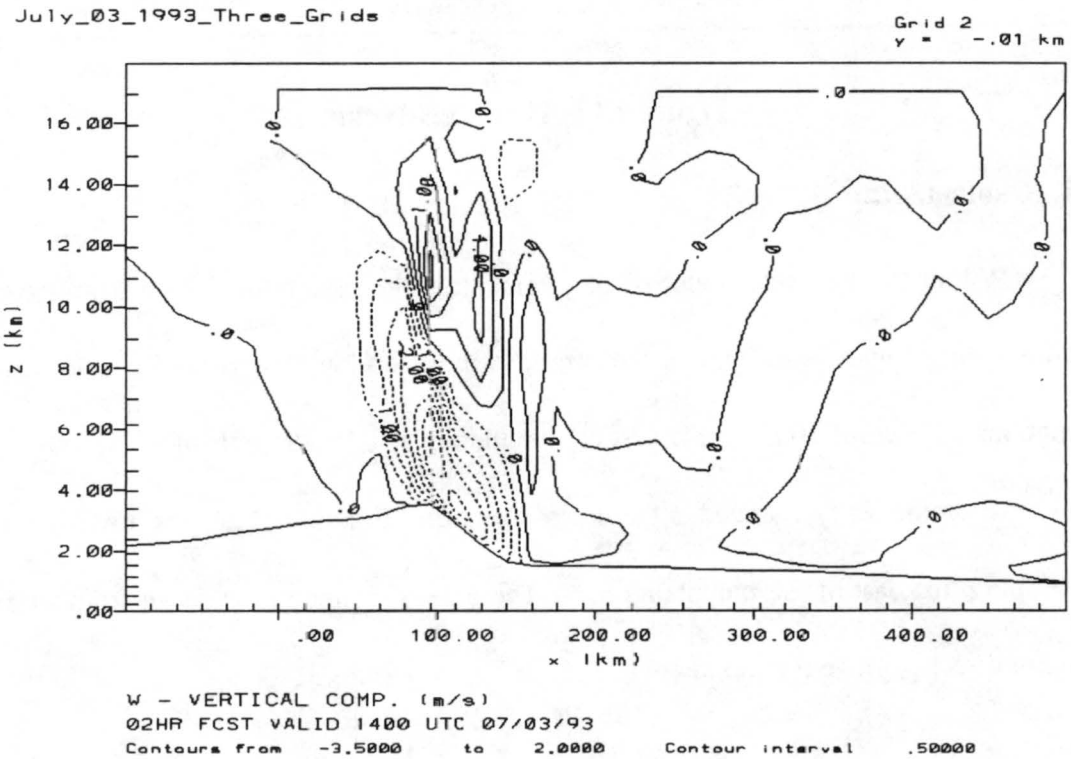


**Figure 4.16- Three grid 02 hour vertical velocity (in m/s)**

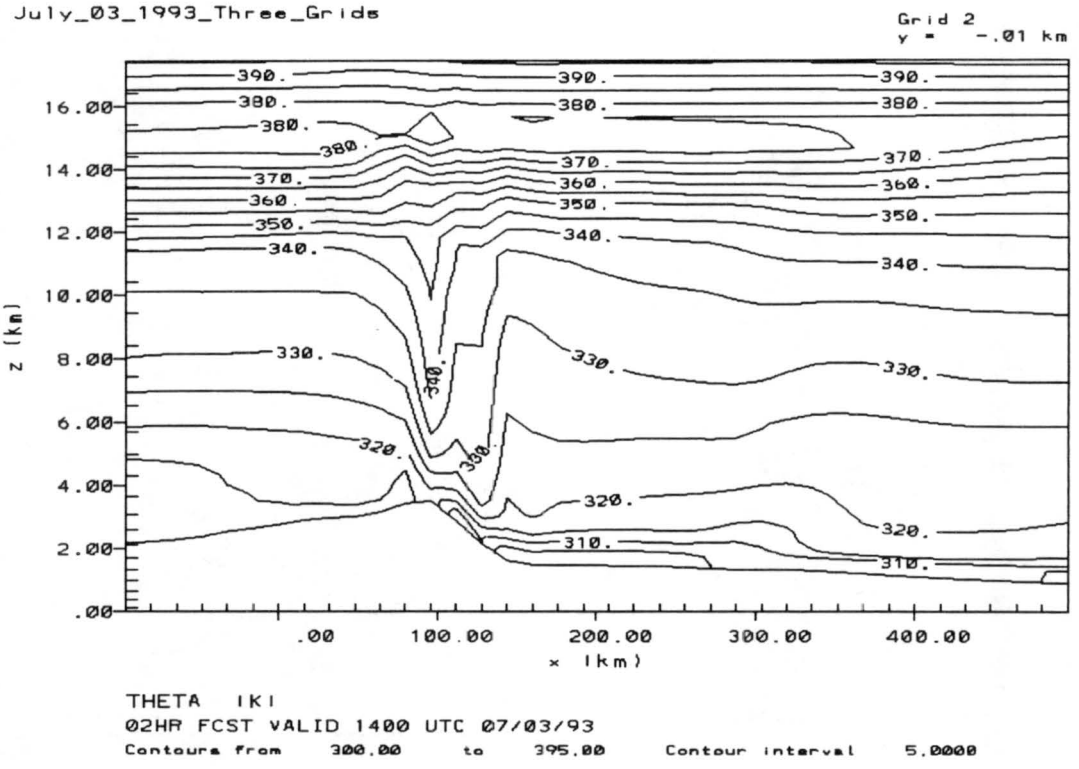


**Figure 4.17- Three grid 02 hour θ field (in °K)**

As the simulation continues, stronger winds develop. A comparison can be made between the 10h (2200 UTC) wind field and that observed by Lilly and Zipser in the 11 January 1972 windstorm. Figure 4.18 shows the observed θ field cross section through Boulder as recorded by the NCAR Sabreliner on 11 January 1972 during the windstorm. Figure 4.19 shows RAMS θ field cross section through Fort Collins. The most striking similarity between the two fields is the injection of high θ stratospheric air into the lower troposphere in the vicinity of the mountain top. A wave pattern in the θ field can also be seen on the east side of the ridge. Figure 4.20 and Figure 4.21 compare observed wind fields and the simulated wind fields. Similarities in these fields include a wind maximum of 60 m/s just to the east of the lee slope and a wind minimum in the mid- and upper- troposphere of 10 m/s in a narrow area directly above mountain top.

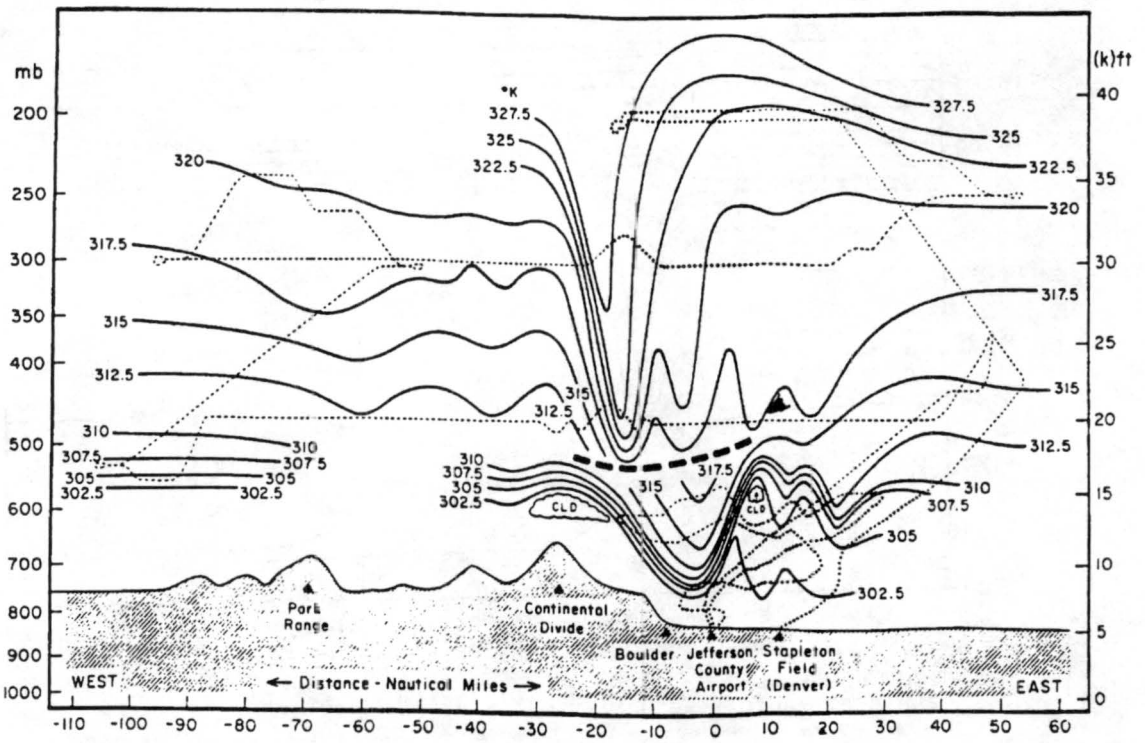


**Figure 4.18- Observed θ field from 11 Jan 72 windstorm (Lilly and Zipser 1972)**

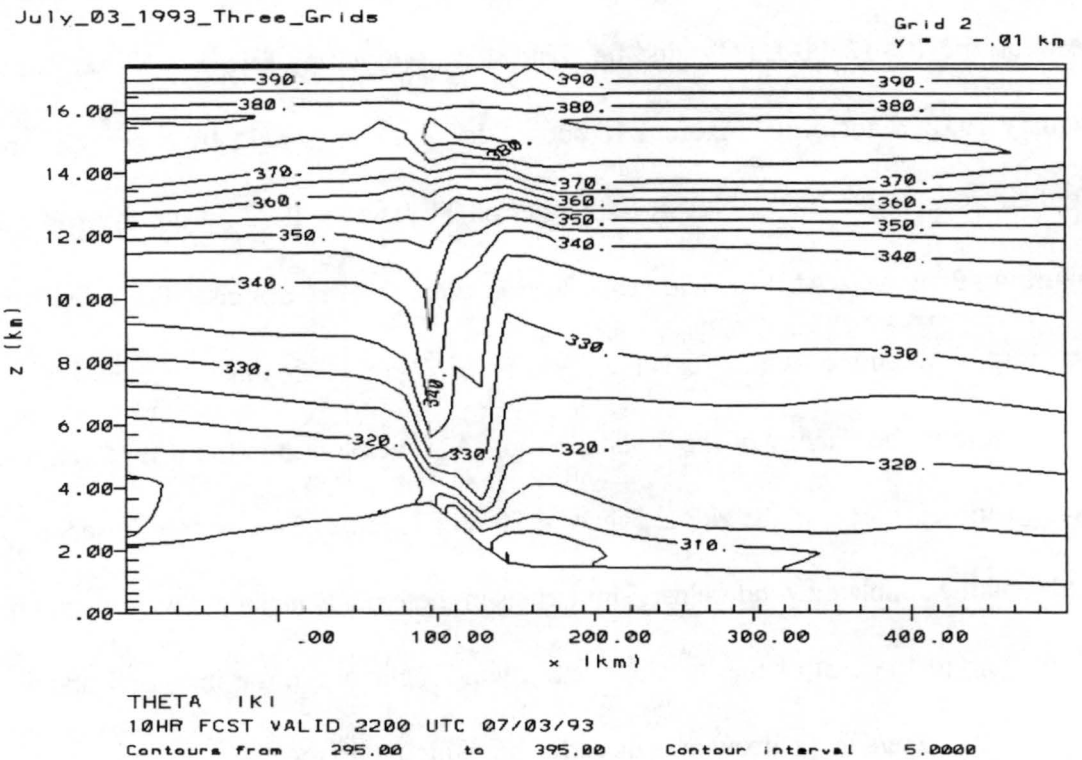


**Figure 4.19- RAMS generated θ field for 3 July 1993 windstorm**

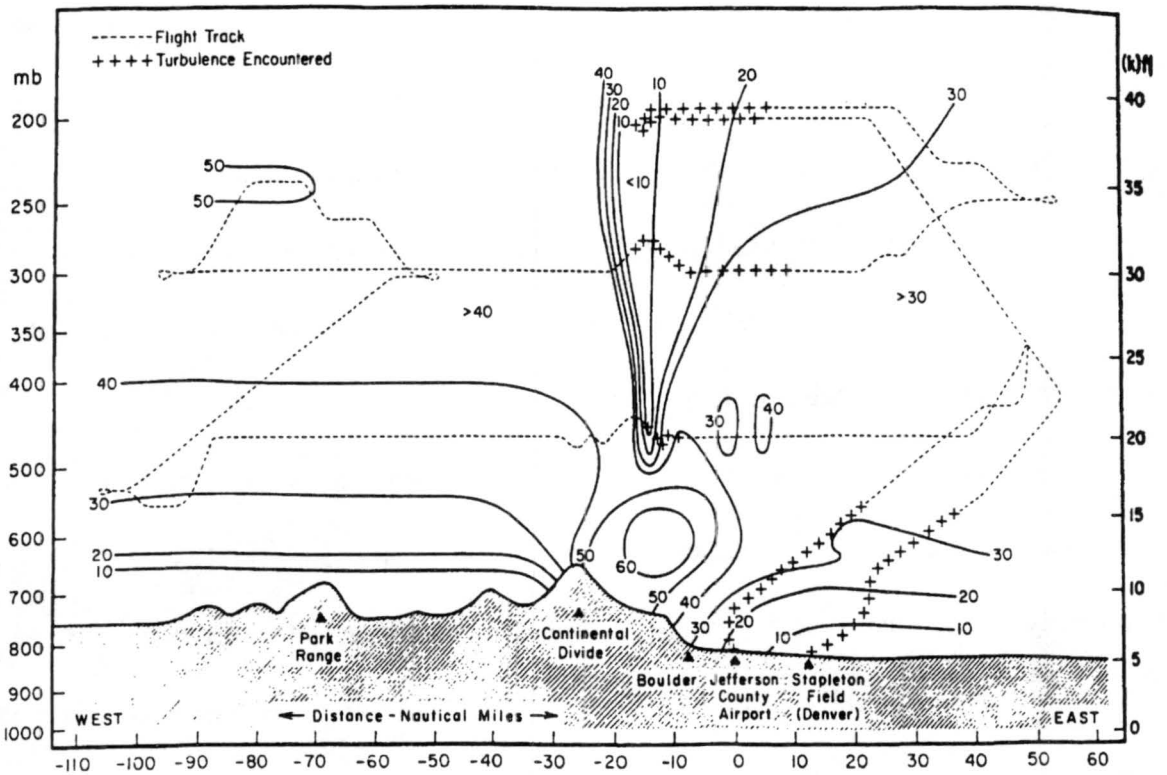


**Figure 4.20- Observed wind field from 11 Jan 72 windstorm (Lilly and Zipser 1972)**

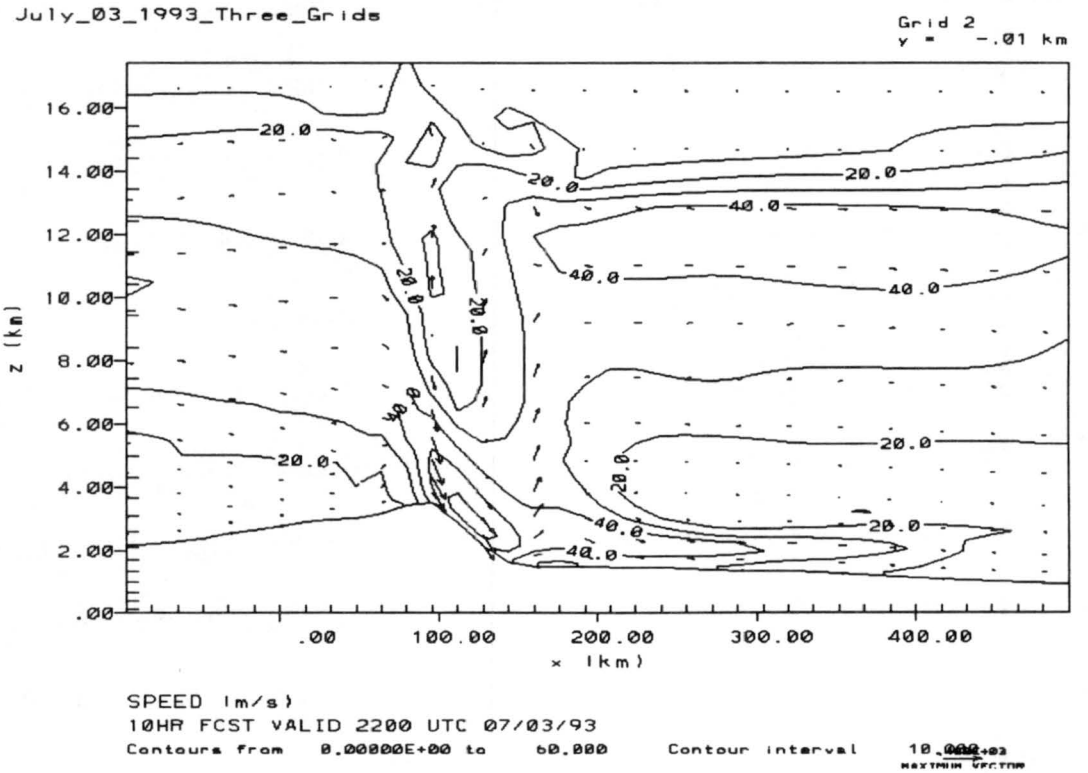


**Figure 4.21- RAMS generated wind field for 3 July 1993 windstorm**

Figure 4.22 shows a time series comparison between observed and forecast winds for all model runs. As with the two-grid simulations, the three-grid simulations were run at Level 1 through Level 3 moisture complexity. Unlike the two-grid simulations, the three-grid full microphysics run (Level 3) differed considerably from the Level 2 run. Although both three-grid simulations exhibited high initial winds due to spin-up, the Level 3 run matched observations fairly well after 6 hours.

One possible reason for these results is the existence of hydrometeors in the Level 3 run and only cloud water in Level 2. In the spin-up of the model, it takes a few hours to properly develop hydrometeors to their proper concentrations. At a given time, there is equal water mass in the Level 2 and Level 3 runs. The main difference, however, is the form this water takes. The Level 2 runs have many very small cloud droplets, while the Level 3 runs have fewer, large rain drops and ice particles. Because the full microphysics option is in use, the thermodynamics of the hydrometeors must be considered. As the flow moves over the mountains, the heating and cooling will cause the isotherms to have a bit less of a dip on the leeward side. Therefore, the winds will not be as strong as the cases which do not consider the thermodynamics of the precipitation physics.

The one remaining problem in these simulations is the spin-up effects. There is virtually no accuracy in the wind forecasts within the first six hours of the simulation. One way to counter these effects is start the model twelve hours earlier. Figure 4.23 compares the observed wind and gusts and the original three-grid Level 3 forecast to a Level 3 forecast using 0000 UTC initial conditions. Starting the model 12 hours earlier removes the spin up effects and produces better results 12 hours earlier.

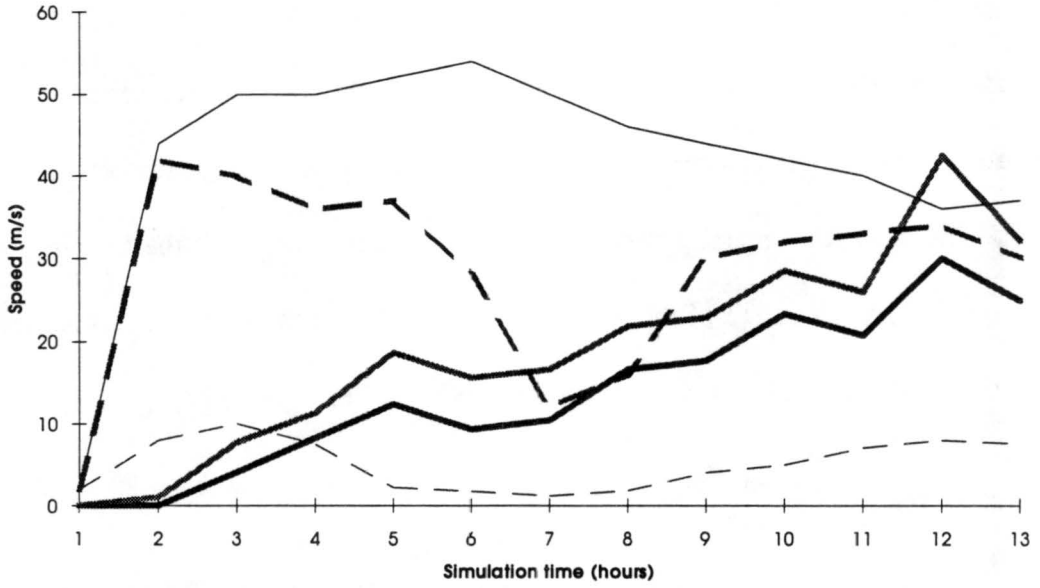


**Figure 4.22- Observed wind speed (dark thick solid) and gusts (light thick solid) for Fort Collins versus RAMS forecast winds for two grid simulations (thin dashed) and three grid simulations at Level 2 (thin solid) and Level 3 (thick dashed) microphysics options. Speed in m/s**

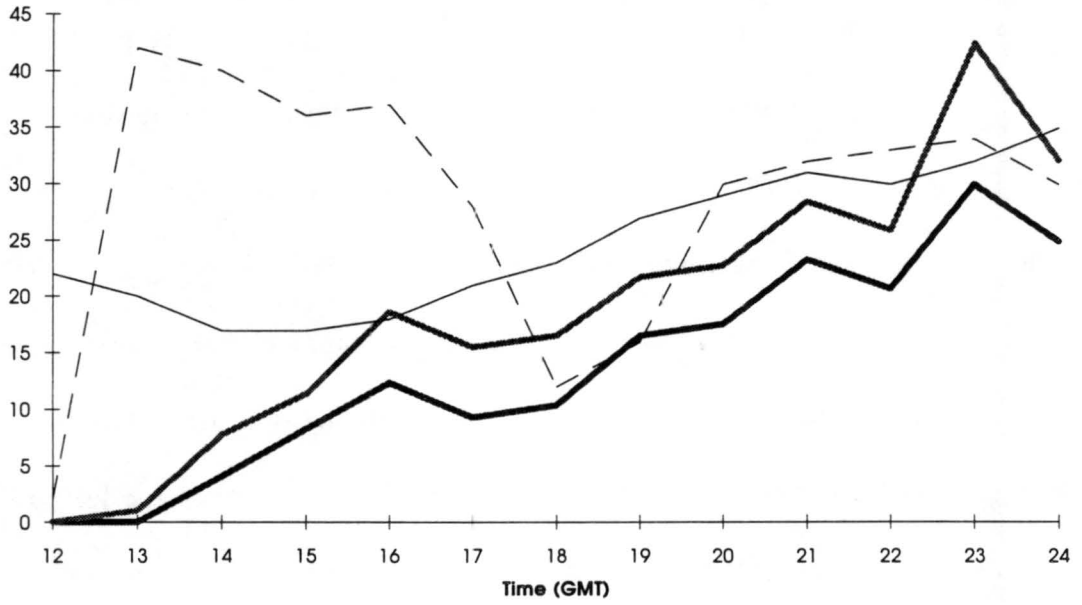


**Figure 4.23- Observed wind speed and gusts (thick solid) for Fort Collins versus RAMS forecast winds for three grid simulations at Level 3 complexity for 0000 UTC initialization (thin solid) and 1200 UTC initialization (thin dashed). Speed in m/s**

Another method of data assimilation which reduces spin-up problems is the adjoint method. The adjoint method is a procedure in which the model is repeatedly integrated forward and backward in time with observations being constantly introduced into the model. Therefore, the model will predict values that most closely fit the known observational data. The advantage of this method over nudging is the dynamical consistency of the initial conditions(Talagrand and Courtier, 1987; Pielke, et. al, 1992).

### 4.6 Summary

From the results of simulating the 3 July windstorm, the most important factor in getting good results is the grid spacing along the leeward slope. To resolve a particular feature in a numerical model, the grid spacing must be at least 4 times smaller than the characteristic length of the feature. In this case, the spacing must be smaller than a quarter wavelength of the high $\theta$ air injected from the lower stratosphere. If the grid spacing is bigger, the model cannot resolve this feature and the strong winds won't develop. A secondary factor is the use of full microphysics to model the moisture. As moist air is blown up and over the Front Range, the Level 3 microphysics will allow precipitation to form and fall out. Level 2 will not allow this, and all the moisture will make it over the Front Range and that which evaporates will enhance the kink in the isotherms. The thermodynamics simulated using full microphysics will reduce the magnitude of the leeward isotherm kink, thus properly reducing the upper limits of wind speed. However, if the grid spacing criterion is not met, the level of moisture complexity has little effect on wind speed.

Some of the shortcomings of these simulations include the required spin-up time until accurate results can be achieved. Initializing the simulation at least six hours before the onset of strong winds is one way to reduce this error. Other changes in the model setup which could improve results include reducing the size of the vertical grid spacing and increasing the number of levels, reducing the length of the timestep from 90 seconds, and increasing the domain size of the finer grids. Increasing the number of gridpoints, however, also slows down the model. Table 4.2 compares the amount of time required to run each 90 second timestep for each of the different setups in this study on an IBM 375 running this model exclusively.

| Moisture Level | Two Grids | Three Grids |
|---|---|---|
| Level 1 | 12 seconds | 22 seconds |
| Level 2 | 13 seconds | 28 seconds |
| Level 3 | 36 seconds | 70 seconds |

**Table 4.2- Time requirements for a 90 second timestep**

It is difficult to use the three grid, Level 3 setup to forecast because simulated weather is occurring almost as fast as observed weather! Therefore, to accurately use RAMS as a forecaster of downslope windstorms, the finest grid must be used sparingly but in a large enough area to capture all of the important features. With the advent of even faster computers or use of clusters of workstations (see Cotton et al., 1994), the hardware requirements needed to forecast this type of mesoscale phenomenon will become more commonplace.

# 5. CASE STUDY: 8 - 9 FEBRUARY 1994 WINTER STORM AND COLD-AIR OUTBREAK

## 5.1 Introduction

During the 1993-1994 winter season, RAMS had the opportunity to simulate a variety of winter storms throughout Colorado. Although no major storms occurred along the highly populated Front Range, a major storm did occur starting on 8 February 1994 over the western mountains of Colorado. This one storm contributed more to the total snowpack throughout the state than any other single event during this season. This was also a good choice to examine because a cold-air outbreak was occurring in the eastern part of the state.

## 5.2 Synoptic situation

At 0000 UTC on 8 February 1994, a 996 mb low was centered over the southern border of Idaho. At the same time, a 1034 mb arctic high was dropping out of Canada near the Minnesota-North Dakota border, bringing record low temperatures to the central US. By 0600 UTC, the low had intensified and moved over the Great Salt Lake in Utah and the ridge associated with the arctic high had become better defined. A stationary front was analyzed between these air masses and ran north-south through Colorado over the Eastern Plains (Figure 5.1). Contrasts in temperatures on either side of the stationary fronts were dramatic. For example, at 0600 UTC Denver reported a temperature of 43 °F, while 100 miles to the east in Akron, CO, the temperature was 8 °F! This cold air was

quite shallow and can be seen on the 0000 UTC Skew-T for Fort Collins produced by RAMS for observed (versus forecast) data (Figure 5.2).

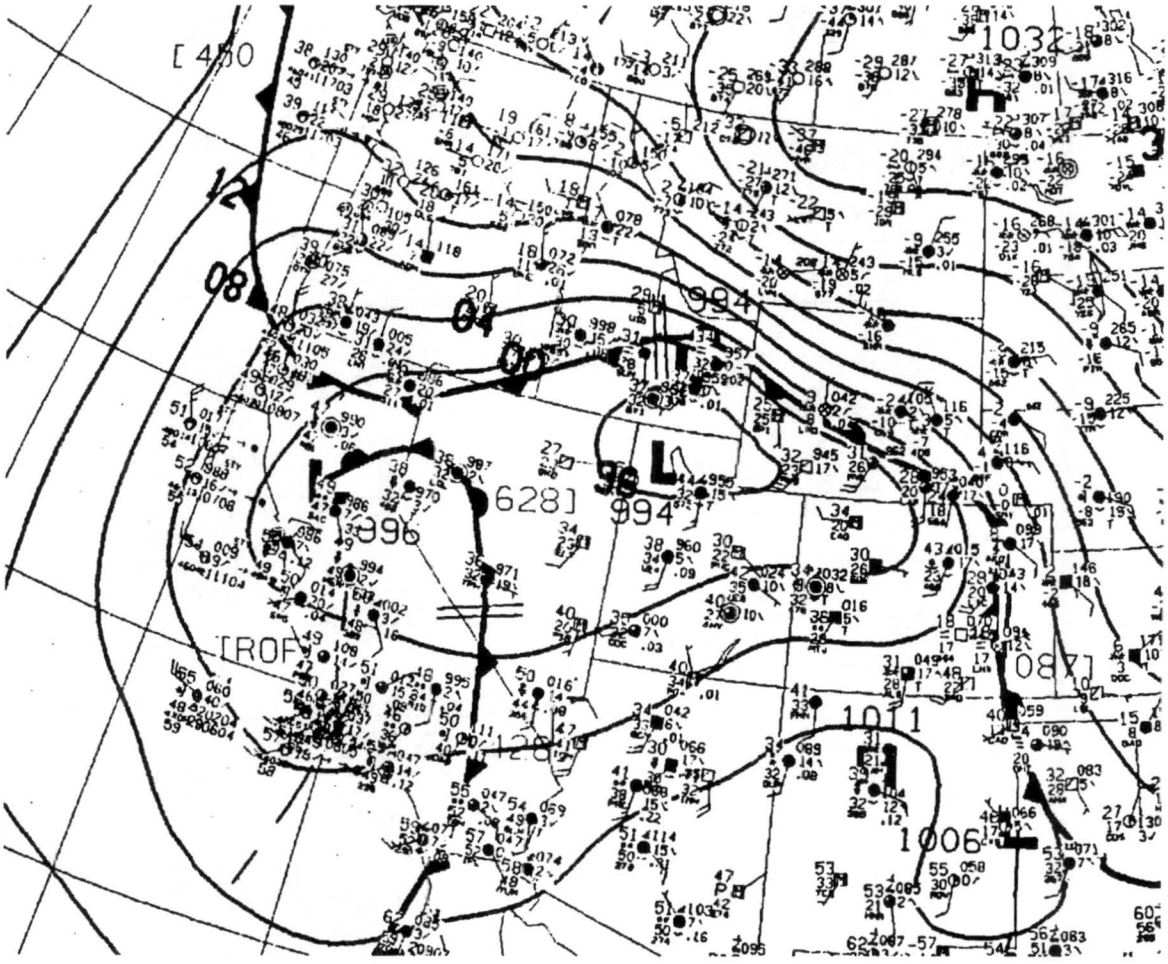


**Figure 5.1- Surface analysis for 0600 UTC on 8 February 1994**

While the surface low continued to move from Utah to Colorado, southerly flow in the southwestern part of the state began bringing in low-level moisture from Arizona and New Mexico. Figure 5.3 and Figure 5.4 compare the rapid increase in low-level moisture. Average relative humidities from the surface to 500 mb increased from 20-60% to 60-95% in 12 hours over the southwestern US. By 1500 UTC, moderate snow with southerly winds were being reported at Durango in the southwestern corner of the state.

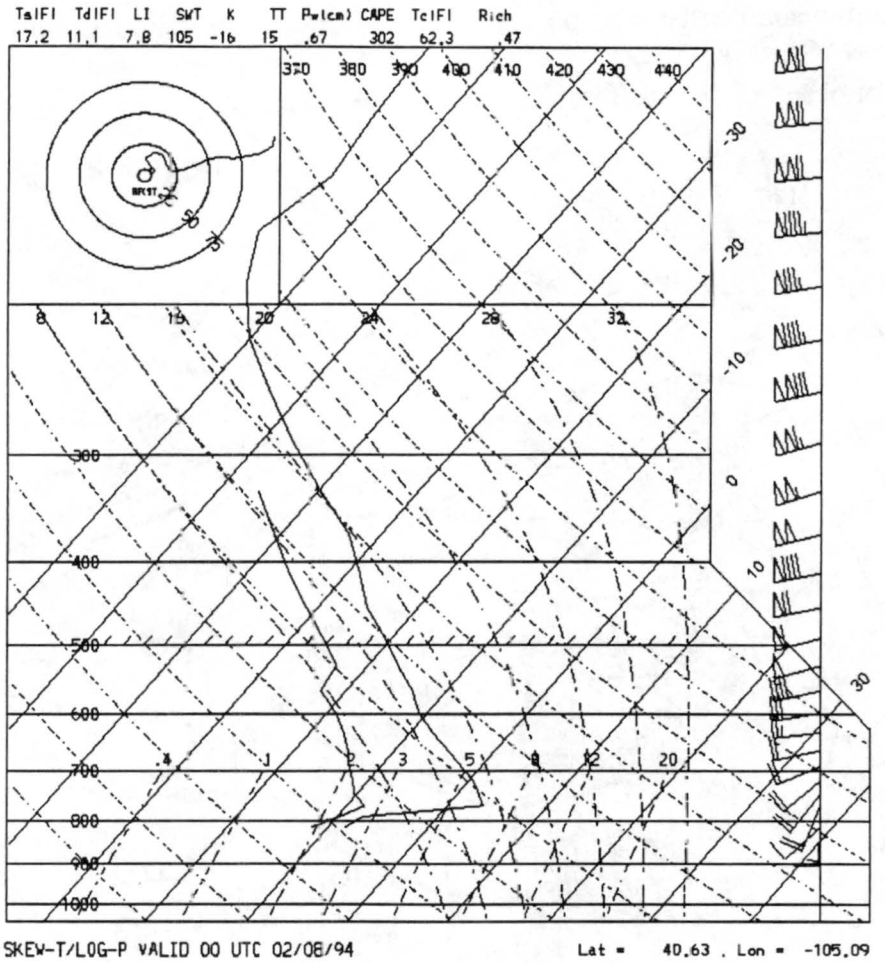


**Figure 5.2- 8 February 1994 0000 UTC Skew-T for Fort Collins**

In the eastern part of Colorado, the quasi-stationary front began to move westward as the arctic high dropped into South Dakota. The analyzed position of the front moved from the 104th meridian at 1200 UTC on the 8th (see Figure 5.6) to the 108th meridian at 0900 UTC on the 9th (see Figure 5.7). This caused the surface low to slowly move from the northwest corner of Colorado to the southwest corner during this same time period. With the shifting of the quasi-stationary front, the cold air over the Eastern Plains was pushed up the eastern slopes, causing upslope snow all along the Front Range. However, the maximum amounts of precipitation for the 24-hour period starting at 0000 UTC on the 8th were located in the western and southern mountains (Figure 5.5). The

totals found from the SNOTEL sites in Figure 5.5 should be considered only estimates because the SNOTEL measuring times were not at 0000 UTC for all sites.

## 5.3 Real-time setup results

### 5.3.1 Cold-air outbreak

The real-time forecasts produced by RAMS for the cold-air outbreak had areas of good and bad agreement. On the Eastern Plains, RAMS initially produced good results for the temperature gradient at the stationary front between Denver and Akron. However, as the simulation proceeds, the forecast gradient weakens (and reverses!) and all the temperatures are much higher than observed (Table 5.1). This is because the observed very cold air is quite shallow, and RAMS mixes this thin layer with the much warmer air between the surface layer and ~ 1 km. It is not until near the end of the 36-hour period does the entire surface layer mix in the shallow air and become cold and the forecast temperatures get closer to the observations. Since the cold air in most cold-air outbreaks in Colorado are very shallow, RAMS has had problems forecasting extreme lows. This is partly due to the lowest layer temperature is really for an elevation of 122 meters above the ground compared to observations measure at the surface.

The real-time version of RAMS is not the only model which has problems with shallow cold air. The NGM forecasts also missed the severity of the cold-air outbreak. Figure 5.8 shows the NGM minimum temperatures for the 8th. Although it properly forecast the extreme cold temperatures near the Canadian border (as did RAMS), it also missed the cold air near the stationary front.

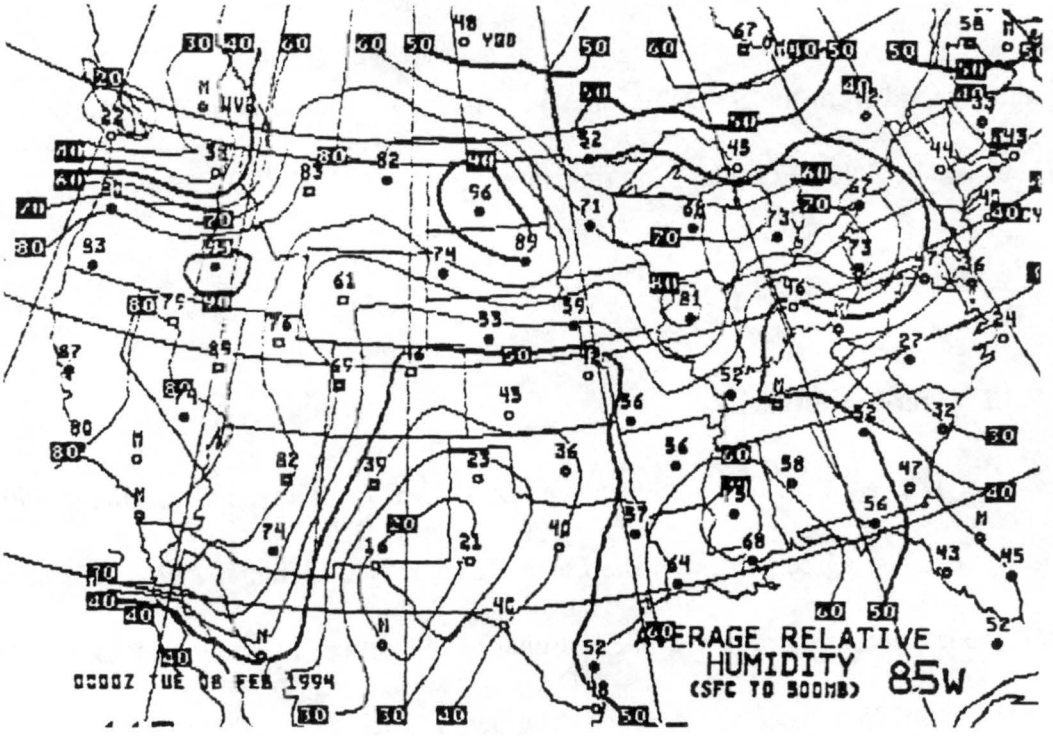


**Figure 5.3- 0000 UTC 8 February 1994 average relative humidity between the surface and 500 mb**

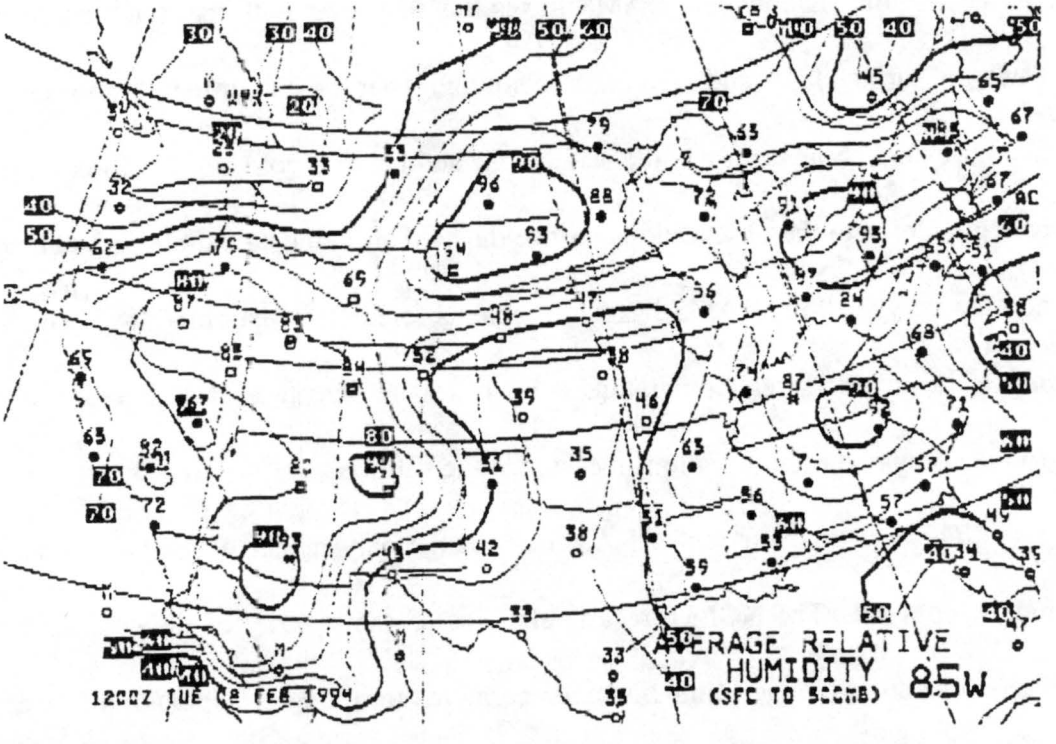


**Figure 5.4- 1200 UTC 8 February 1994 average relative humidity between the surface and 500 mb**

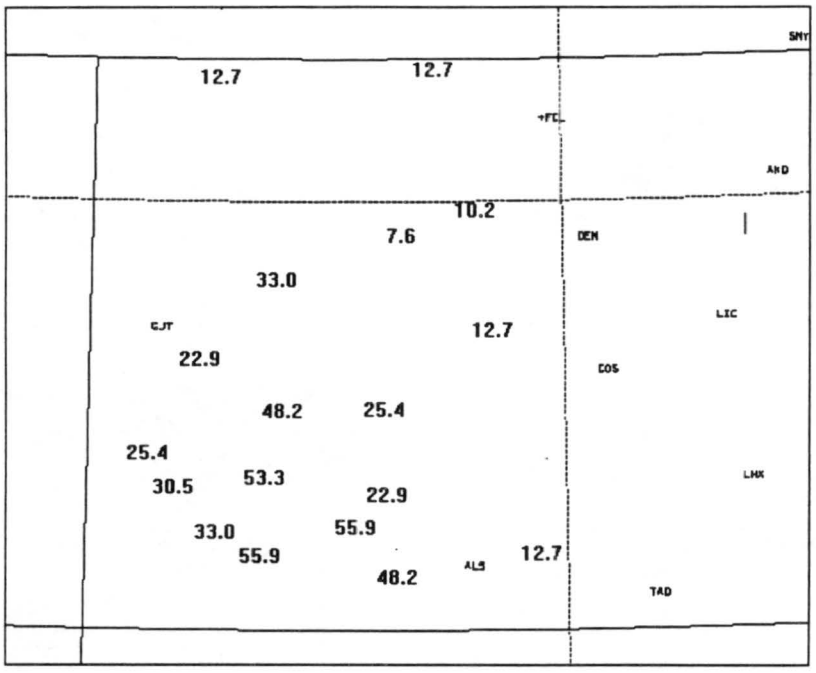


**Figure 5.5- 24-hour accumulated precipitation (in mm) as recorded at various SNOTEL sites**

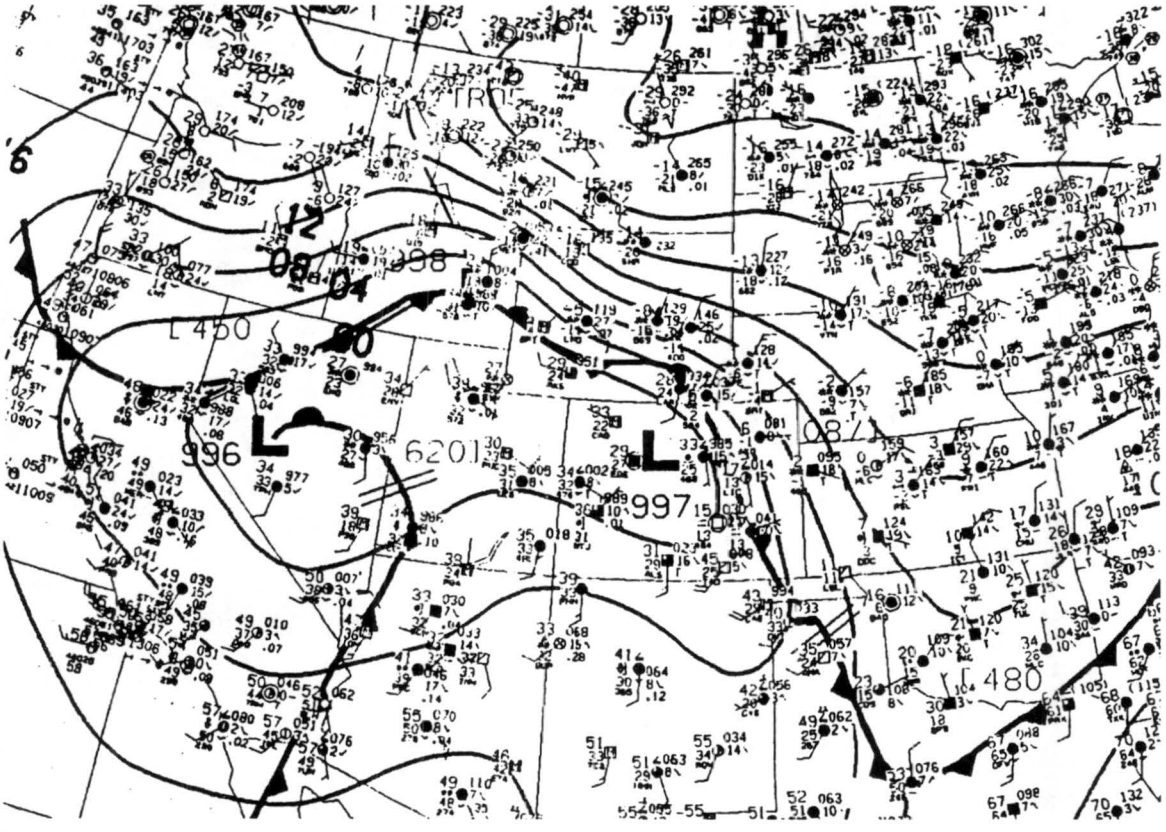


**Figure 5.6- Surface analysis for 1200 UTC 8 February 1994**

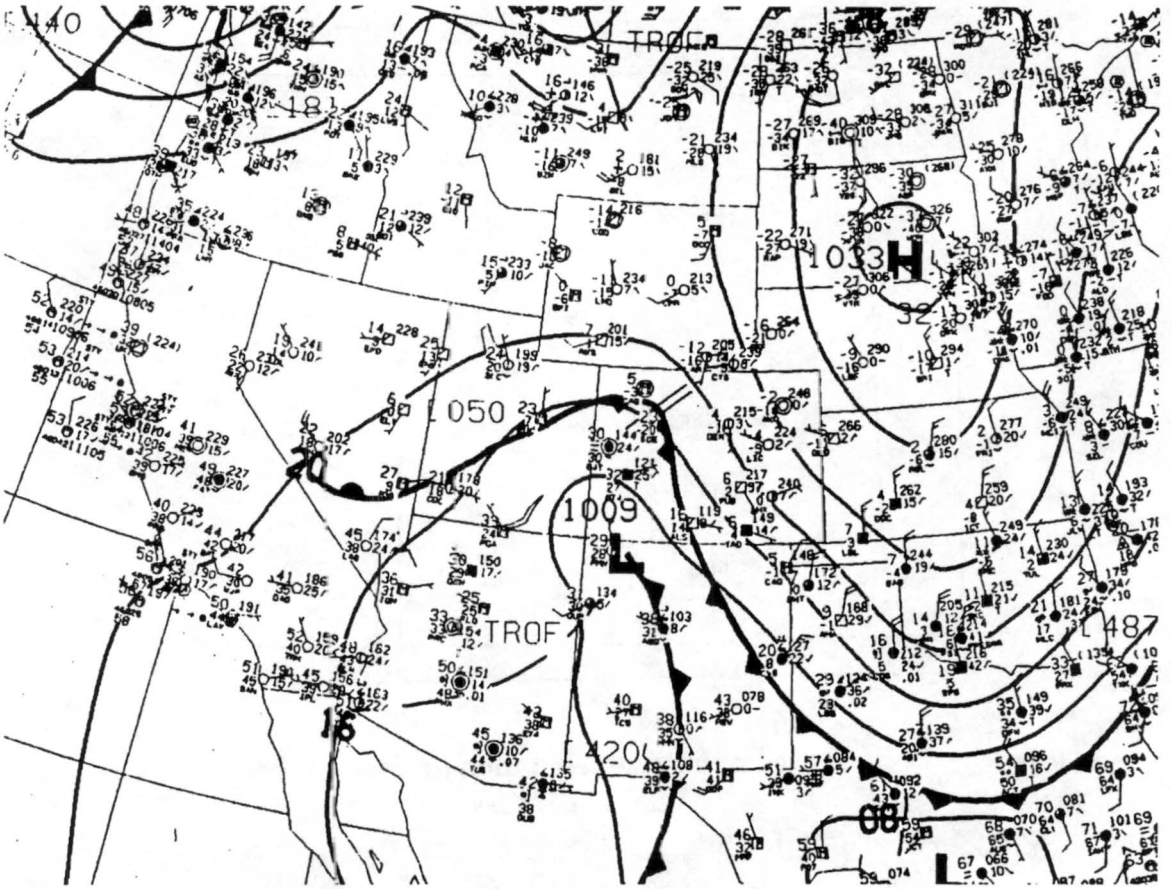


**Figure 5.7- Surface analysis for 0900 UTC 9 February 1994**

| | OBSERVED | | | FORECAST | | |
|---|---|---|---|---|---|---|
| **Time (UTC)** | **DEN** | **AKO** | **Difference** | **DEN** | **AKO** | **Difference** |
| **8th**, 0000 | 25 | 8 | 17 | 25 | 8 | 17 |
| 0300 | 23 | 5 | 18 | 38 | 6 | 32 |
| 0600 | 43 | 8 | 35 | 39 | 4 | 35 |
| 0900 | 32 | 6 | 26 | 39 | 11 | 28 |
| 1200 | 33 | 6 | 27 | 37 | 28 | 9 |
| 1500 | 9 | 0 | 9 | 36 | 37 | -1 |
| 1800 | 9 | 1 | 8 | 38 | 42 | -6 |
| 2100 | 11 | 4 | 7 | 39 | 46 | -7 |
| **9th**, 0000 | 9 | 2 | 7 | 38 | 46 | -8 |
| 0300 | 6 | 2 | 4 | 33 | 27 | 6 |
| 0600 | 4 | 0 | 4 | 32 | 12 | 30 |
| 0900 | 4 | -2 | 6 | 20 | 5 | 15 |
| 1200 | 4 | 1 | 3 | 15 | 4 | 11 |

**Table 5.1- Comparison between temperature observations at DEN (Denver) and AKO (Akron) and real-time RAMS forecasts during 8 - 9 February 1994 cold-air outbreak (in °F)**

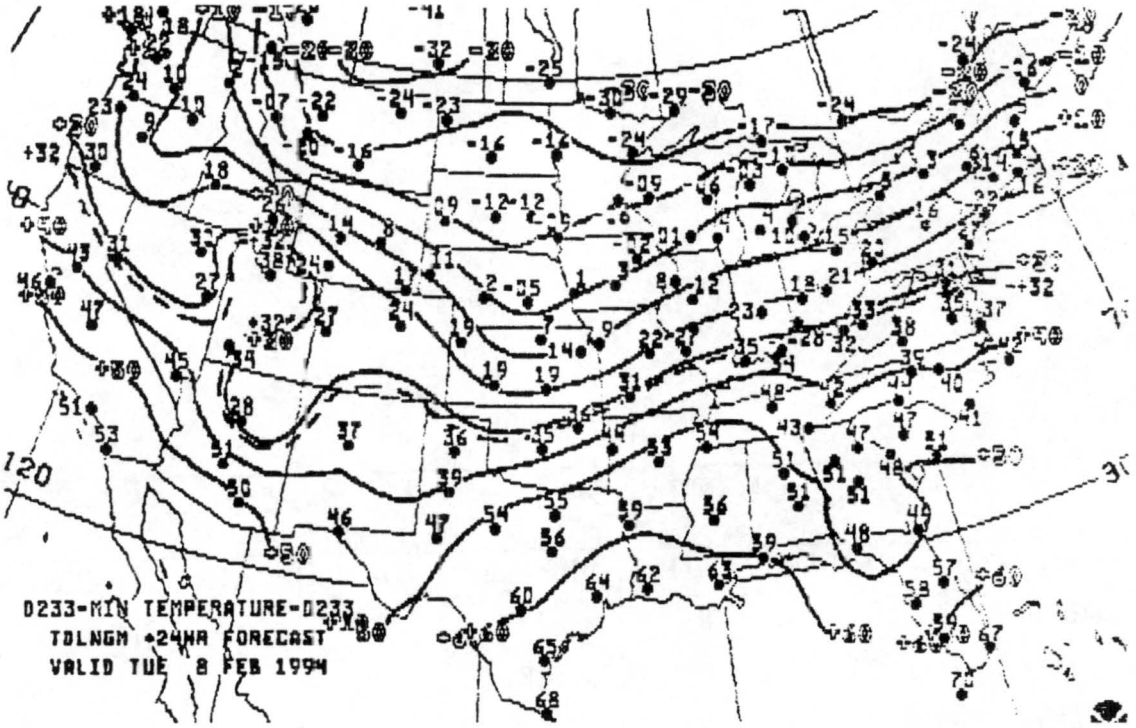


**Figure 5.8- NGM forecast of low temperatures, valid 8 February 1994**

### 5.3.2 Winter storm

The development of the storm by the real-time version of RAMS began well. As was observed in Figure 5.3 and Figure 5.4, RAMS picked up on the monsoonal flow and increased 700 mb relative humidity between 0000 UTC (see Figure 5.9) and 1200 UTC (see Figure 5.10). Also, the switch at 700 mb from WSW flow at 1200 UTC on the 8th to NW flow at 0000 UTC on the 9th can be seen (Figure 5.11 - Figure 5.14).

Figure 5.15 shows the accumulated total precipitation from 0000 UTC on the 8th to 0000 UTC on the 9th. The dump-bucket scheme used to forecast precipitation shows two maxima- one over the southwest corner of the state (near Durango) and one over the extreme western-central border (near Grand Junction). Although the maximum in the southwest exists in the observations, the total amounts forecast are generally much lower

than observed. The dump-bucket's precipitation efficiency scheme did poorly with this storm. This may be due to the convective nature of the precipitation; the few available radars in the region did show snow showers over the western slopes compared to light stratiform snow over the Front Range. Thompson (1993) also found that the precipitation efficiency scheme did poorly in the convective regions of the 8 - 9 March 1992 Front Range snowstorm. Therefore, in an effort to obtain more realistic results, the bulk microphysics version of RAMS was employed.

## 5.4 Bulk microphysics

### 5.4.1 Description

The bulk microphysics version of RAMS is fully described in Flatau et. al, 1989. This parameterization considers the complexities of the precipitation process versus the simplistic approach used by the dump-bucket scheme. Processes such as nucleation, latent heat release, and the separation of water into various species and just some of the added details obtained when using the bulk microphysics(see Cotton et al., 1986).

The different species available when using the bulk microphysics are rain, snow, pristine ice crystals, aggregates of ice crystals, and graupel. In the version of the microphysics used in this simulation, pristine ice crystal mixing ratios and concentrations were predicted. For the other species, mixing ratios were predicted while the concentrations were diagnosed.

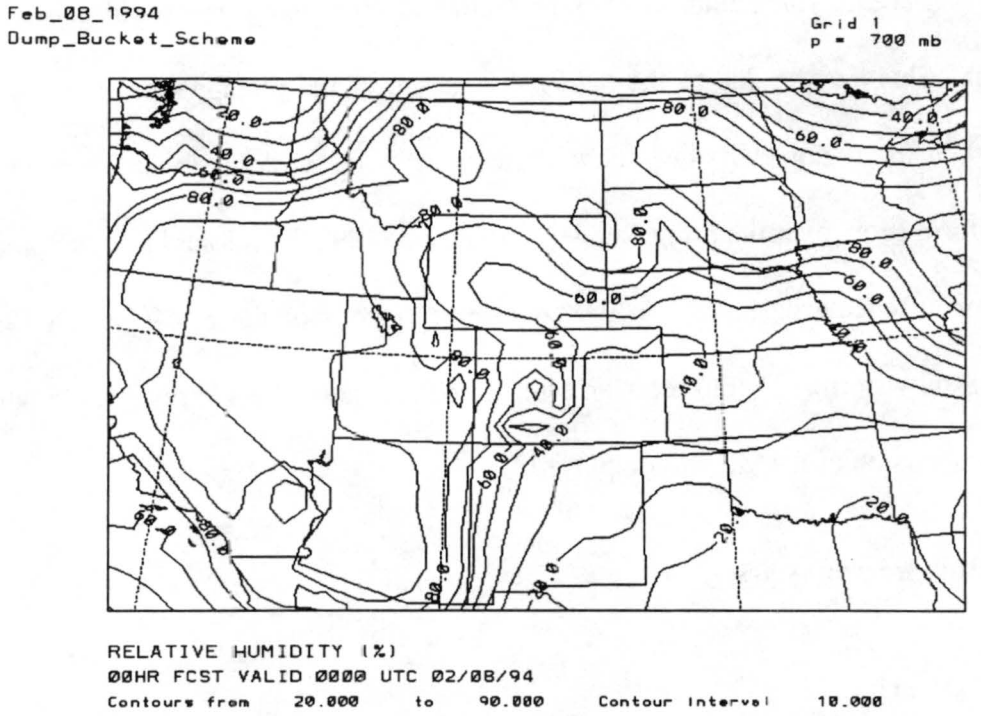


**Figure 5.9- Real-time RAMS 0000 UTC 8 February 1994 relative humidity analysis for 700 mb**

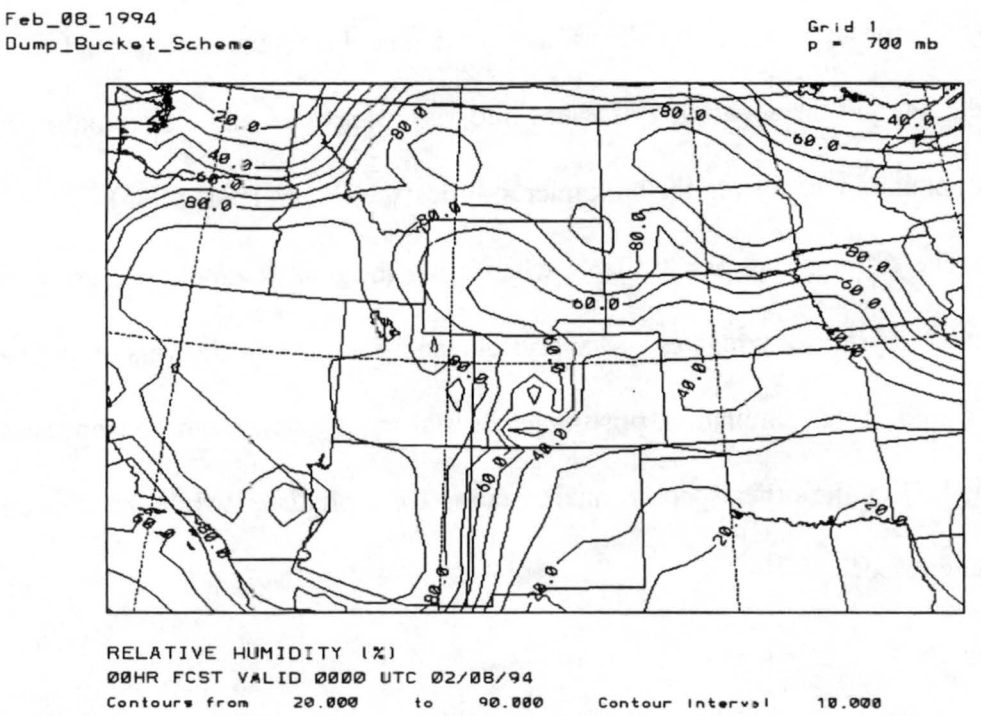


**Figure 5.10- Real-time RAMS 1200 UTC 8 February 1994 relative humidity analysis for 700 mb**

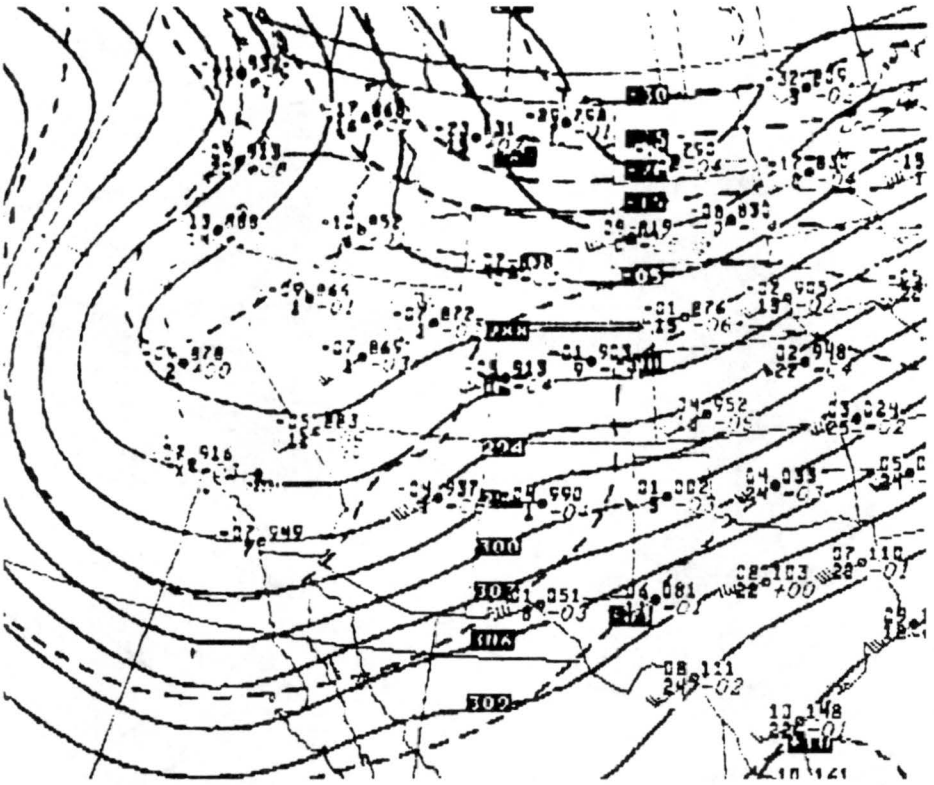

**Figure 5.11- 700 mb heights/temperature analysis for 1200 UTC 8 February 1994**

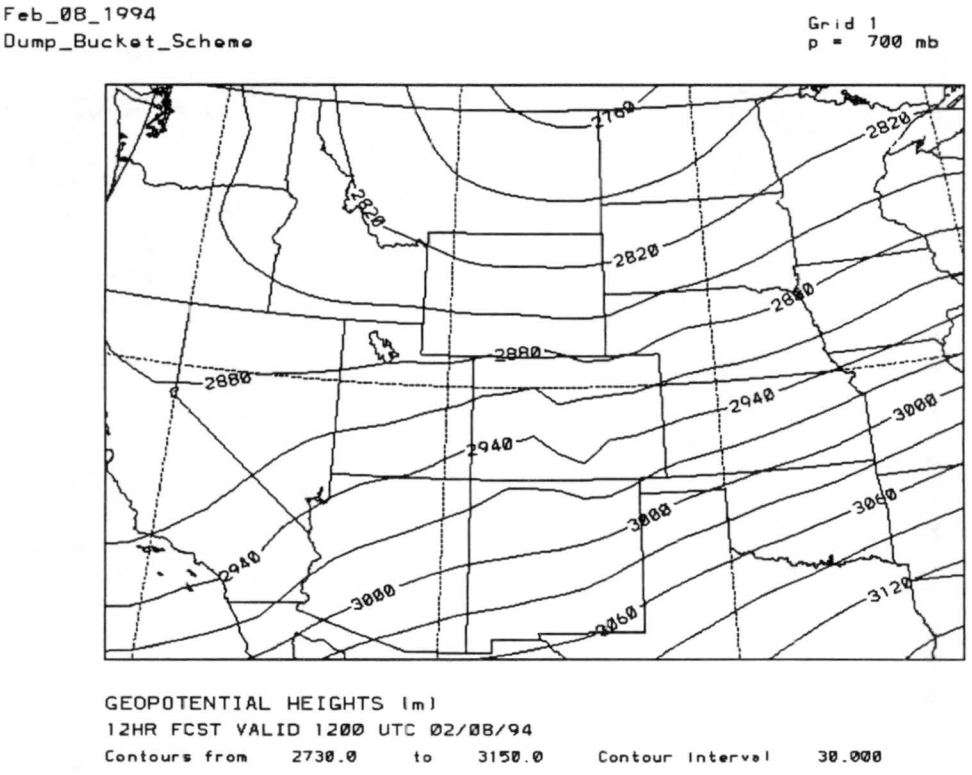


**Figure 5.12- Real-time RAMS 1200 UTC 8 February 1994 geopotential heights analysis for 700 mb**

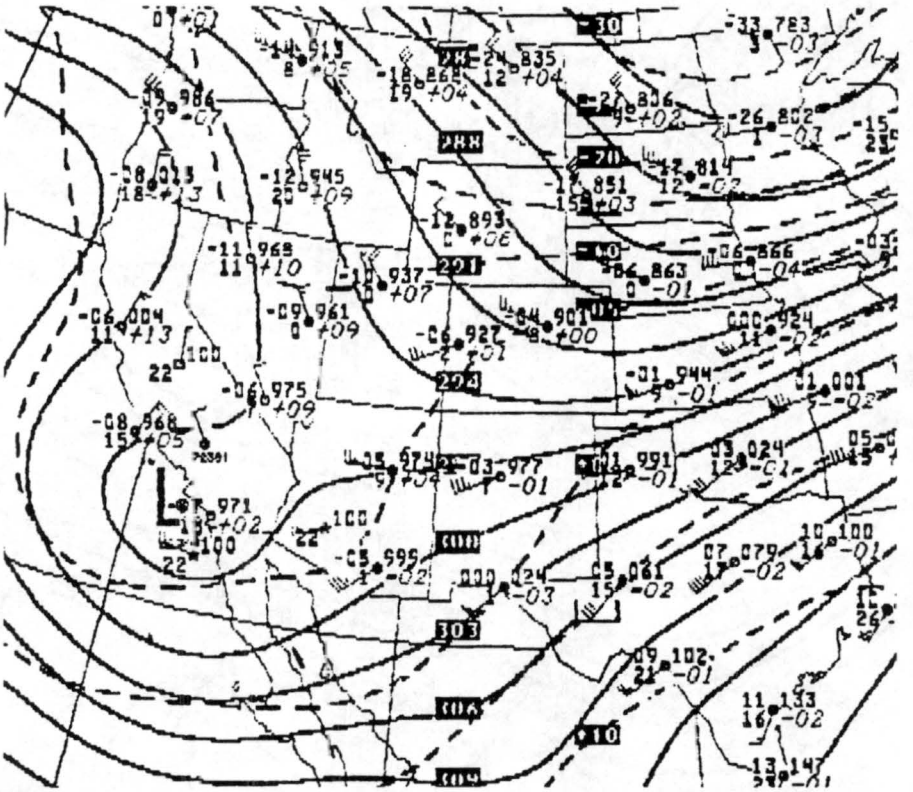

**Figure 5.13- 700 mb heights/temperature analysis for 0000 UTC 9 February 1994**

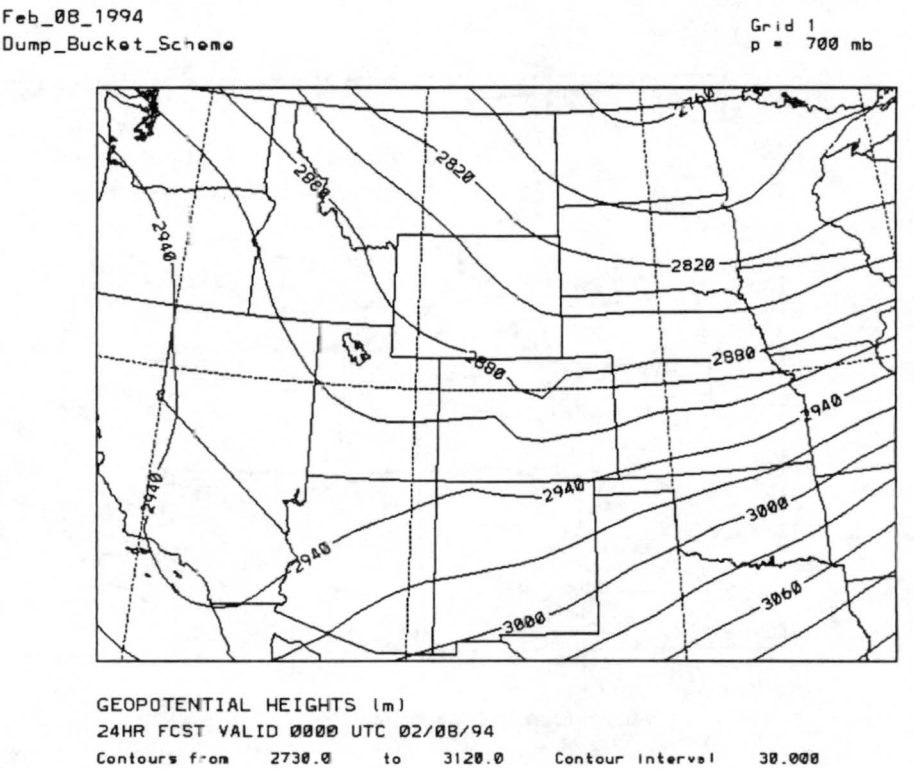


**Figure 5.14- Real-time RAMS 0000 UTC 9 February 1994 geopotential heights analysis for 700 mb**

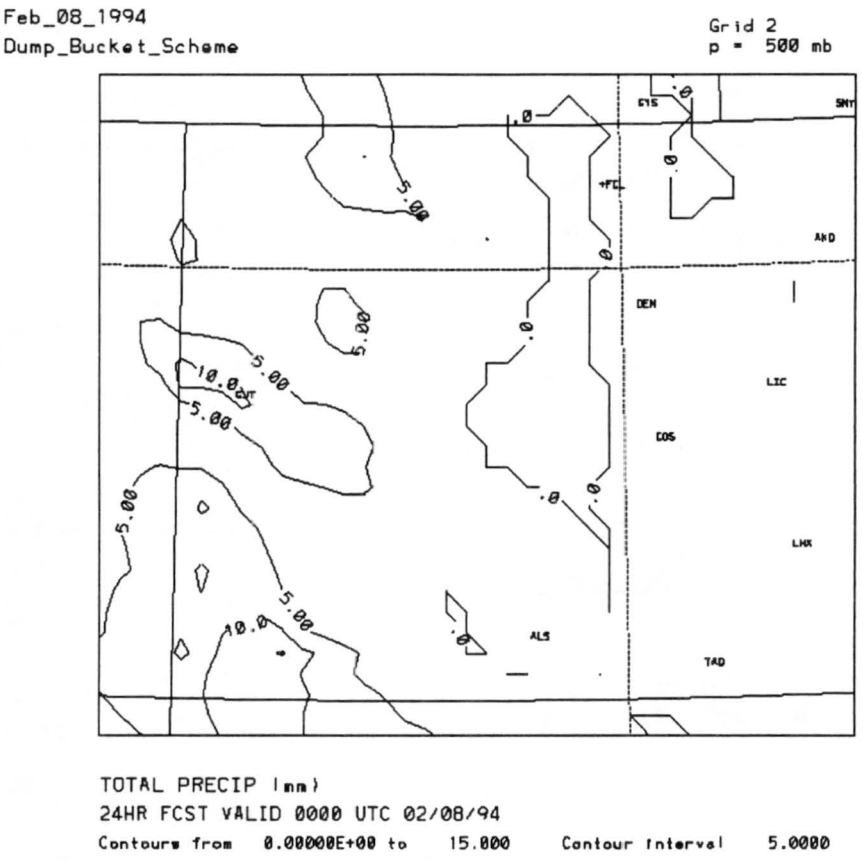


**Figure 5.15- Real-time RAMS 24-hour accumulated total precipitation valid 0000 UTC 9 February 1994**

### 5.4.2 Results

The addition of the bulk microphysics produced great improvements in the precipitation forecasts. Figure 5.16, Table 5.2, and Table 5.3 shows the 24-hour total accumulated precipitation for the period ending 0000 UTC on the 9th as forecast using the bulk microphysics. Compared to the dump-bucket scheme (Figure 5.15), the results shown match existing observations in both amounts and locations.

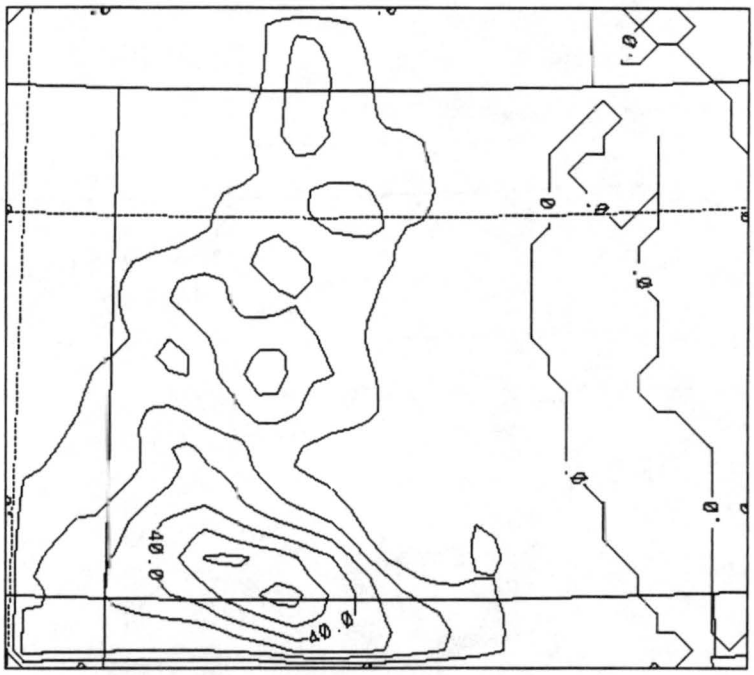


**Figure 5.16- Bulk microphysics RAMS 24-hour accumulated total precipitation valid 0000 UTC 9 February 1994. Contours in 10 mm increments**

The temperature forecast results obtained from the bulk microphysics for the cold-air outbreak in the eastern part of the state were not greatly improved. A sensitivity run with 50 meter vertical grid spacing was performed, but even with this improved vertical resolution, the cold-air outbreak was not well forecast. This implies that the initialization with the ETA data set did not pick up the shallow cold-air from the start of the simulation. Unfortunately, the MAPS data set with its finer vertical resolution was not available for this day for comparisons.

## 5.5 Summary

The bulk microphysics is a vast improvement over the simple dump-bucket scheme. In the simulation of the winter storm in the western part of Colorado, the bulk microphysics version of RAMS produced realistic results throughout the fine grid's do-

main. Most other fields (such as heights, temperatures, and winds) were little changed with the inclusion of the bulk microphysics.

| Site | Predicted | Observed |
|---|---|---|
| Arrow | 4 | 5 |
| Bear Lake | 7 | 10 |
| Beartown | 59 | 33 |
| Berthoud Summit | 6 | 8 |
| Bison Lake | 22 | 30 |
| Brumley | 13 | 18 |
| Burro Mountain | 18 | 18 |
| Butte | 22 | 36 |
| Cascade | 38 | 25 |
| Cascade 2 | 38 | 25 |
| Columbine | 13 | 10 |
| Columbine Pass | 22 | 23 |
| Copeland Lake | 7 | 13 |
| Copper Mountain | 10 | 10 |
| Crosho | 9 | 10 |
| Culebra | 10 | 10 |
| Cumbres Tressel | 35 | 43 |
| Dry Lake | 18 | 15 |
| El Diente Park | 39 | 30 |
| Elk River | 22 | 13 |
| Fremont Pass | 8 | 13 |
| Grizzly Peak | 6 | 18 |
| Hoosier Pass | 5 | 10 |
| Idarado | 38 | 20 |
| Independence Pass | 13 | 28 |
| Ivanhoe | 14 | 18 |
| Joe Wright | 12 | 15 |
| Kiln | 14 | 15 |
| Lake Irene | 14 | 13 |
| Lake Eldora | 0 | 3 |
| Lily Pond | 32 | 28 |

**Table 5.2- Part 1, predicted versus observed precipitation for all available SNOTEL sites using bulk microphysics. Precipitation in mm**

| Site | Predicted | Observed |
|---|---|---|
| Lizard Head Pass | 35 | 18 |
| Lone Cone | 35 | 18 |
| Lynx Pass | 7 | 5 |
| McClure Pass | 21 | 33 |
| Mesa Lake | 19 | 38 |
| Middle Creek | 23 | 28 |
| Mineral Creek | 28 | 23 |
| North Lost Trail | 26 | 36 |
| Nast Lake | 14 | 18 |
| Niwot | 1 | 8 |
| Overland Reservoir | 27 | 25 |
| Park Cone | 18 | 25 |
| Park Reservoir | 22 | 23 |
| Phantom Valley | 14 | 13 |
| Red Mountain Pass | 28 | 23 |
| Ripple Creek | 16 | 15 |
| Roach | 5 | 10 |
| Schofield Pass | 21 | 38 |
| Slumgullion | 10 | 10 |
| Spud Mountain | 31 | 41 |
| Stillwater Creek | 15 | 5 |
| Summit Ranch | 9 | 13 |
| Trinchera | 10 | 10 |
| Upper San Juan | 30 | 48 |
| Vail Mountain | 11 | 20 |
| Whiskey Creek | 10 | 13 |
| Willow Creek Pass | 16 | 13 |
| Willow Park | 5 | 15 |
| Wolf Creek Pass | 30 | 86 |

**Table 5.3- Part 2, predicted versus observed precipitation for all available SNOTEL sites using bulk microphysics. Precipitation in mm**

The down side of the bulk microphysics is its computational cost. For example, on the IBM RISC/6000 workstation used for these simulations, the time required to run the entire 36-hour forecast using 90-second timesteps was about 6.5 hours. For the same timestep using the bulk microphysics, the required time for completion was almost 16 hours. With greater computing speed and the optimization of the new bulk microphysics version of RAMS (see Walko et al., 1994), one can expect major improvements in snow-fall prediction in future winter seasons.

# 6. SEASONAL SNOWFALL STUDY

## 6.1 Introduction

The effects of Colorado snowfall go well beyond the recreation value and temporary driving problems. The seasonal snowfall and subsequent run-off is the main source of water for Colorado and most neighboring states. The ability to accurately forecast snowfall is the first step in understanding this complex hydrological cycle.

The original intent of the seasonal snowfall study was to use the newly developed bulk microphysics using a single moment prediction scheme (Walko et. al, 1994). During the time of the seasonal snowfall study, this scheme had not yet been optimized enough to use under the real-time criteria. Therefore, bulk microphysics was abandoned and a precipitation efficiency scheme developed by Rhea (1978) was used.

## 6.2 Rhea model description

One of the first studies of Colorado snowfall using a mesoscale model was done by J. Owen Rhea at Colorado State University in the late 1970's. Rhea (1978) used his model to determine if the distribution of snow could be predicted using the output from the twice-a-day normal rawinsondes launched from sites surrounding the Colorado Rockies. The sounding data were then interpolated to points along the model domain. The domain was bounded by the Colorado state borders to the west, north, and south, and by the 105th meridian to the east (Figure 6.1). The mean 700 mb wind was used to advect parcels over the domain of 10 km grid spacing with averaged terrain at each grid point. A comparison of model predicted precipitation with snowcourse water equivalent precipita-

tion and streamflow runoff showed favorable correlations (Rhea, 1978; Branson, 1991).

An important simplification Rhea used to obtain his results was a precipitation efficiency. Through empirical experiments, he determined that this efficiency is of the form $E = -kT_c$ , where $k$ is a positive constant and $T_c$ is the temperature (in °C) of the highest layer with ≥ 65% relative humidity, which can be considered cloudtop temperature. A reasonable value of $k$ that worked for Rhea throughout the Colorado Rockies was 0.01. For example, if the cloud top temperature is -20 °C, the efficiency will be (-0.01) ×(-20) = 20%. Other studies indicate this efficiency to be low. Chapell (1970) found efficiencies at Wolf Creek Pass to be near 100% at temperatures less than -20 °C and between 20% and 35% at warmer temperatures. Nonetheless, Rhea's efficiency was used by RAMS and is at the heart of the dump-bucket scheme used in the seasonal snowfall study.

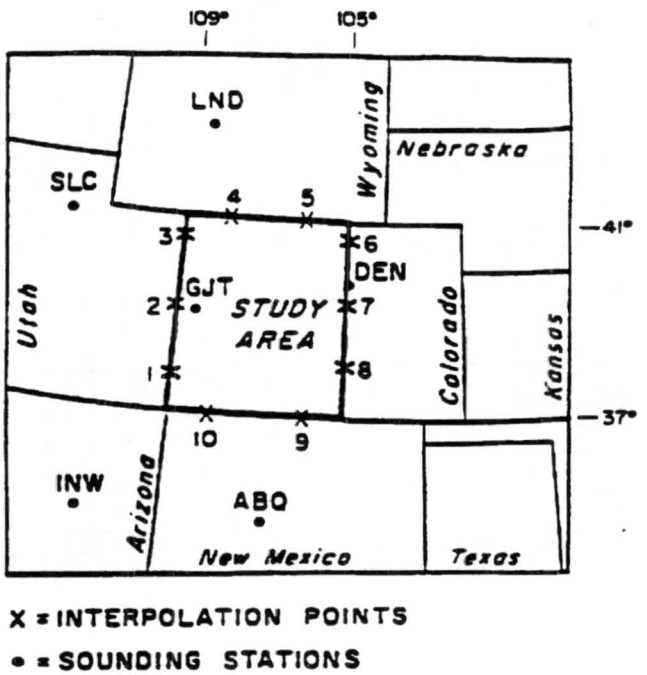


**Figure 6.1- CSU-Rhea model domain, border interpolation points and rawinsonde stations (from Rhea, 1978)**

## 6.3 Setup

A study of seasonal snowfall was conducted from 17 December 1993 to 14 April 1994 using precipitation data obtained from Grid #2. During this time, RAMS was successfully run 113 out of 119 days for a success rate of 95%. Because the only reliable measurements of snow data are made at SNOTEL sites, it was determined at which grid points on Grid #2 SNOTEL sites existed. Figure 6.2 shows a close-up of Grid #2 with grid points containing SNOTEL sites filled in.

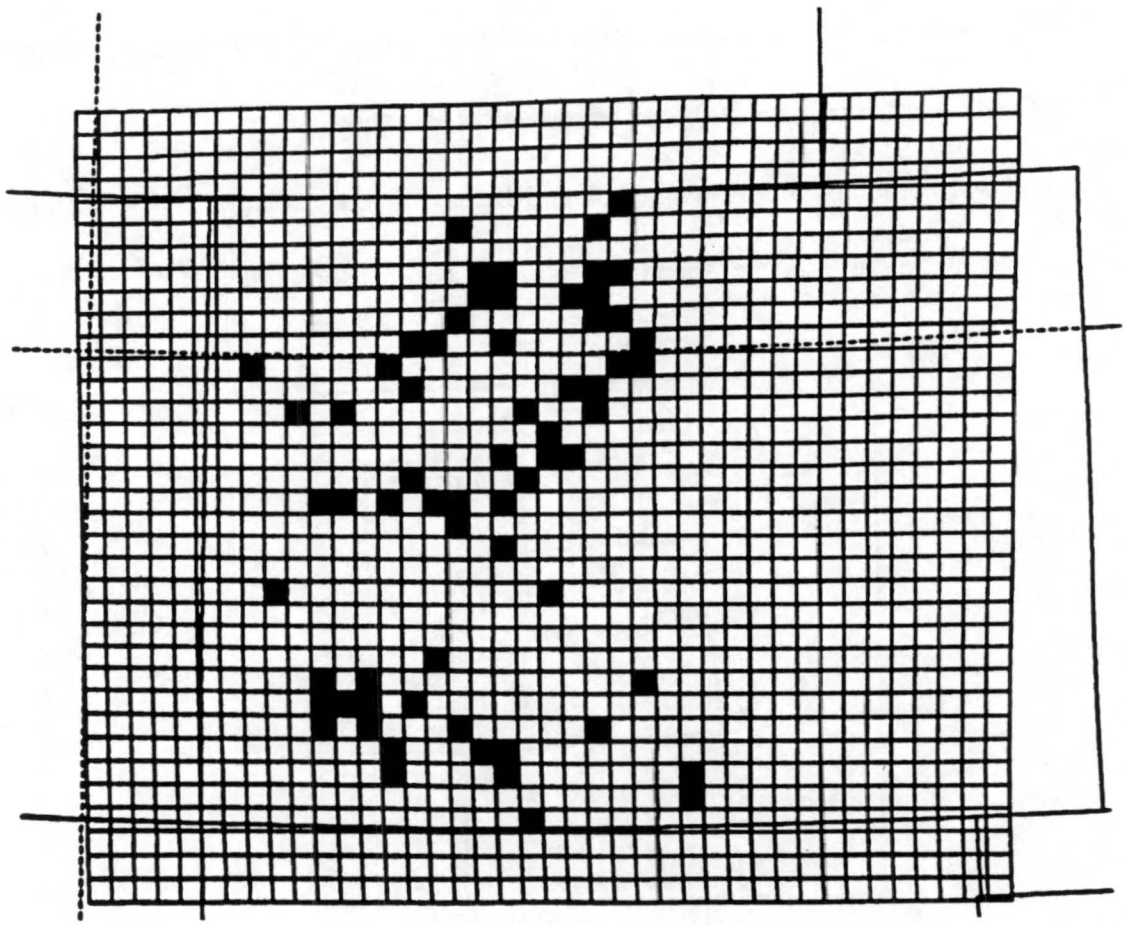

**Figure 6.2- Location of SNOTEL sites projected onto RAMS Grid #2**

Each day, the visualization package of RAMS (known as VAN) would produce a table of 24 hour predicted water equivalent precipitation. Table 6.1 shows a typical day's output. This table was then downloaded to a personal computer. For verification purposes, SNOTEL data were routinely obtained from the Centralized Database System at the Soil Conservation Service in Portland, Oregon and also downloaded to a personal computer (see example in Table 6.2). Both predicted and observed precipitation were combined by the personal computer into a Microsoft Excel ™ worksheet. At this time, the SNOTEL data were converted to millimeters (the unit used by RAMS), bad data were removed (see the third-from-bottom line in Table 6.2 for an example), data were reduced to one observation a day, and running totals were made (see example in Table 6.3). By the end of the season, 56 SNOTEL sites had reported observations consistently enough to use for comparisons.

### 6.4 Results

Overall, the RAMS predicted precipitation amounts were much smaller than those observed at the SNOTEL sites. Predicted values normally differed from observed values by a factor of between 2 and 30. However, the amount which the predictions varied from the observations was relatively consistent from month to month for each individual site. Table 6.4 shows a listing of some of the SNOTEL sites and the ratio of observed/predicted values.

| Site | Equiv. Water(mm) | 15-to-1 snow (in) | 20-to-1 snow (in) |
|---|---|---|---|
| Cath Bluffs | 2.50497 | 1.47793 | 1.97893 |
| Columbine Pass | .92014 | .54288 | .72691 |
| W Fork Parac | 1.41430 | .83444 | 1.11730 |
| Scotch Creek | 8.28955 | 4.89083 | 6.54874 |
| El Diente Pk | 4.99893 | 2.94937 | 3.94916 |
| Lone Cone | 4.26975 | 2.51915 | 3.37310 |
| Mesa Lake | 7.28012 | 4.29527 | 5.75130 |
| Lizard Hd Pass | 2.08335 | 1.22917 | 1.64584 |
| Park Reserv. | 5.29432 | 3.12365 | 4.18251 |
| Naval Oilshale | 2.00531 | 1.18313 | 1.58420 |
| Cas/Cas#2/Idar | 2.50337 | 1.47699 | 1.97766 |
| Molas Crk/Spud Mt | 1.44322 | .85150 | 1.14014 |
| Minl Ck/Red Mt Ps | 1.21140 | .71473 | .95701 |
| Beartown | 6.87732 | 4.05762 | 5.43308 |
| Vallecito | 2.19902 | 1.29742 | 1.73723 |
| Overland Res. | 4.35260 | 2.56804 | 3.43856 |
| Burro Mnt | 4.29660 | 2.53499 | 3.39432 |
| Up. Rio Grande | .33877 | .19987 | .26763 |
| McClure Pass | .95664 | .56442 | .75574 |
| Bison Lake | 3.68585 | 2.17465 | 2.91182 |
| Ripple Creek | .38513 | .22723 | .30426 |
| Slumgullion | .04797 | .02830 | .03790 |
| N. Lost Trail | 1.57840 | .93126 | 1.24694 |
| Trapper Lake | .01744 | .01029 | .01378 |
| Middle Creek | .25247 | .14896 | .19945 |
| Butte | 1.46640 | .86518 | 1.15846 |
| Schofield Ps | .37572 | .22168 | .29682 |
| Crosho | 1.03789 | .61235 | .81993 |
| Elk River | 2.99454 | 1.76678 | 2.36569 |
| U Sn Jn/Wlf Ck Ps | .49530 | .29223 | .39129 |
| Rabbit Ears | 5.03474 | 2.97049 | 3.97744 |
| Dry Lake | 4.96863 | 2.93149 | 3.92522 |
| Lily Pond | .35943 | .21206 | .28395 |
| Stump Lakes | .00023 | .00014 | .00018 |
| Park Cone | 1.18111 | .69685 | .93307 |
| Brum/Ind Ps | .13794 | .08139 | .10897 |
| Ivanh/Kiln/Nast Lk | .38238 | .22560 | .30208 |
| Lynx Pass | .95985 | .56631 | .75828 |
| Columbine | 4.70859 | 2.77807 | 3.71979 |
| Tower | 3.33377 | 1.96692 | 2.63368 |
| Cumbres Trs. | .35713 | .21071 | .28213 |
| Hagerman Tn. | .09686 | .05715 | .07652 |
| Vail Mnt | .38605 | .22777 | .30498 |
| Porphyry Crk | .05463 | .03223 | .04315 |
| Fremont Pass | .00000 | .00000 | .00000 |
| Copper Mnt. | .17168 | .10129 | .13563 |
| Hoosier Pass | .00000 | .00000 | .00000 |
| Summit Ranch | .11889 | .07015 | .09392 |
| Willow Ck Ps | 1.55821 | .91934 | 1.23098 |
| Roach | .00000 | .00000 | .00000 |
| Sangre School | .05440 | .03209 | .04297 |
| Griz Pk/Love Ps | .00000 | .00000 | .00000 |
| Berthoud Sum | .00000 | .00000 | .00000 |
| Stillwater Crk | .80814 | .47680 | .63843 |
| L Irene/Phant Vy | .24283 | .14327 | .19184 |
| Joe Wright | .06794 | .04008 | .05367 |
| Deadman Hill | .00000 | .00000 | .00000 |
| Arrow | .00000 | .00000 | .00000 |
| Bear/Cope Lake | .00000 | .00000 | .00000 |
| Willow Park | .00000 | .00000 | .00000 |
| South Colony | .17512 | .10332 | .13835 |
| Lake Eldora | .00000 | .00000 | .00000 |
| Niwot/Uni. Prk | .00000 | .00000 | .00000 |
| Cule/Trin/Whi Ck | .08217 | .04848 | .06491 |
| Apishapa | .10604 | .06256 | .08377 |
| Patterson Hol. | .05922 | .03494 | .04678 |

**Table 6.1- Typical daily precipitation forecast in tabular form**

United States Department of Agriculture — Soil Conservation Service — West National Technical Center, Water Supply Forecasting Staff, Portland, OR

D A T A  R E P O R T

** Provisional data, subject to revision **

03/18/94

| Site Name | MM/DD (PT) | Snow Water Equivalent | Precip (YTD) | AM Temp | Previous Days Max | Previous Days Min | Previous Days Avg |
|---|---|---|---|---|---|---|---|
| APISHAPA | 12/29 0300 | 2.8 | 6.5 | 9.3 | 37.5 | 13.6 | 22.4 |
| | 12/30 0000 | 2.8 | 6.6 | 25.3 | 37.9 | 8.7 | 22.4 |
| | 12/30 0300 | 2.7 | 6.5 | 19.4 | 37.9 | 8.7 | 22.4 |
| | 12/31 0000 | 2.8 | 6.6 | 31.1 | 47.4 | 14.1 | 29.4 |
| | 12/31 0300 | 2.6 | 6.7 | 34.1 | 47.4 | 14.1 | 29.4 |
| | 01/01 0000 | 2.8 | 6.6 | 19.7 | 40.8 | 17.6 | 29.6 |
| | 01/01 0300 | 2.6 | 6.4 | 22.6 | 40.8 | 17.6 | 29.6 |
| | 01/02 0000 | 2.8 | 6.6 | 29.1 | 39.3 | 19.5 | 29.4 |
| | 01/02 0300 | 2.6 | 6.6 | 22.2 | 39.3 | 19.5 | 29.4 |
| | 01/03 0000 | 2.8 | 6.6 | 20.8 | 30.9 | 15.4 | 22.2 |
| | 01/03 0300 | 2.6 | 6.4 | 24.0 | - 60.3 | 204.4- | 60.3 |
| | 01/04 0000 | 2.8 | 6.6 | 19.5 | 37.5 | 18.8 | 27.1 |
| | 01/04 0300 | 2.6 | 6.5 | 24.0 | 37.5 | 18.8 | 27.1 |

**Table 6.2- Example of downloaded SNOTEL data**

Microsoft Excel

File Edit Formula Format Data Options Macro Window Help

Normal

A1 | DATE

WOLFCRSM.XLS

| | A | B | C | D | E | F |
|---|---|---|---|---|---|---|
| 1 | DATE | TIME | Season Precip (in.) | Monthly Precip (mm) | RAMS Precip (mm) | |
| 2 | 17-Dec | 1800 | 12.5 | 0 | 0.07951 | |
| 3 | 18-Dec | 1600 | 12.6 | 2.54 | 0 | |
| 4 | 19-Dec | 1600 | 12.7 | 5.08 | 0.03525 | |
| 5 | 20-Dec | 1600 | 12.9 | 10.16 | 0.05225 | |
| 6 | 21-Dec | 1600 | 12.9 | 10.16 | 0 | |
| 7 | 22-Dec | 1800 | 12.9 | 10.16 | 0 | |
| 8 | 23-Dec | 1600 | 12.9 | 10.16 | 0.00217 | |
| 9 | 24-Dec | 1600 | 13.1 | 15.24 | 0.00434 | |
| 10 | 25-Dec | 1600 | 13.2 | 17.78 | 0 | |
| 11 | 26-Dec | 1600 | 13.2 | 17.78 | 0 | |
| 12 | 27-Dec | 1600 | 13.2 | 17.78 | 0 | |
| 13 | 28-Dec | 1600 | 13.3 | 20.32 | 0 | |
| 14 | 29-Dec | 1600 | 13.3 | 20.32 | 0.01494 | |
| 15 | 30-Dec | 1600 | 13.3 | 20.32 | 0 | |
| 16 | 31-Dec | 1600 | 13.3 | 20.32 | 0.02318 | |
| 17 | 1-Jan | 1600 | 13.3 | 20.32 | 0.01443 | |
| 18 | 2-Jan | 1600 | 13.3 | 20.32 | 0.06414 | |
| 19 | 3-Jan | 1600 | 13.4 | 22.86 | 0.00007 | |

**Table 6.3- Example of Microsoft Excel™ worksheet combining SNOTEL observations and RAMS output**

| | Dec | Jan | Feb | Mar | Average | Stand. Dev | StDev/Avg |
|---|---|---|---|---|---|---|---|
| Mesa Lake | 6.42 | 7.97 | 6.88 | 6.89 | 7.04 | 0.657621979 | 0.093412213 |
| Summit Ranch | 9.44 | 9.12 | 7.72 | 9.87 | 9.0375 | 0.930533001 | 0.102963541 |
| Vail Mountain | 13.15 | 12.37 | 9.86 | 11.27 | 11.6625 | 1.427850949 | 0.12243095 |
| Ripple Creek | 15.49 | 18.47 | 21.87 | 18.32 | 18.5375 | 2.610534747 | 0.140824531 |
| Red Mountain Pass | 28.07 | 20.04 | 28.59 | 23.8 | 25.125 | 4.012152373 | 0.159687657 |
| Niwot | 11.8 | 9.75 | 7.43 | 9.16 | 9.535 | 1.802599974 | 0.189050863 |
| Burro Mountain | 6.31 | 4.23 | 6.07 | 7.21 | 5.955 | 1.250319959 | 0.20996137 |
| Mineral Creek | 14.6 | 11.19 | 20.55 | 17.43 | 15.9425 | 3.992921862 | 0.250457699 |
| Ivanhoe | 10.49 | 11.35 | 10.56 | 17.3 | 12.425 | 3.273311269 | 0.263445575 |
| Roach | 18.74 | 19.45 | 28.12 | 14.64 | 20.2375 | 5.666523773 | 0.280001175 |
| Wolf Creek Summit | 68.34 | 73.88 | 59.45 | 33.84 | 58.8775 | 17.71833396 | 0.300935569 |
| Willow Creek Pass | 2.95 | 4.62 | 5.94 | 6.6 | 5.0275 | 1.611156417 | 0.320468706 |
| Nast Lake | 5.72 | 7.44 | 7.92 | 12.04 | 8.28 | 2.678706155 | 0.323515236 |
| Upper San Juan | 74.55 | 76.92 | 55.4 | 33.84 | 60.1775 | 20.02805095 | 0.332816268 |
| Lizard Head Pass | 14.25 | 6.94 | 17.14 | 13.16 | 12.8725 | 4.296753619 | 0.333793251 |
| N. Lost Trail | 5.55 | 12.46 | 14.34 | 11.27 | 10.905 | 3.787105315 | 0.347281551 |
| Middle Creek | 27.8 | 49.74 | 40.98 | 22.84 | 35.34 | 12.27831693 | 0.347433982 |
| Butte | 12.32 | 17.32 | 25.96 | 13.92 | 17.38 | 6.088108628 | 0.350293937 |
| Kiln | 5.72 | 7.05 | 8.58 | 12.97 | 8.58 | 3.151327762 | 0.367287618 |
| Overland Reservoir | 3.1 | 6.72 | 8.47 | 7.88 | 6.5425 | 2.407382742 | 0.367960679 |

**Table 6.4- Ratio of observed/predicted precipitation values for selected SNOTEL sites. Table includes average of four months, standard deviation, and a weighted standard deviation**

At first glance, it appears that there is poor correlation between the observations and predictions using the precipitation efficiency. Rhea himself called the precipitation efficiency "a complex, elusive factor to quantitatively determine...neither is it theoretically spatially constant."

## 6.5 Modifications

One of the factors that Rhea realized affected the precipitation efficiency was the topography downwind of the sites. He found that the maximum precipitation rates occurred about 50 km upwind of the highest topography in response to the greatest vertical displacement between grid points. In Figure 6.3, Rhea shows the precipitation rates com-

pared to the terrain profile he used in his study. For example, relatively flat topography between 170 km and 190 km fails to generate enough condensate to offset the depletion by upwind precipitation of the imported cloud water. Consequently, precipitation rates decrease.

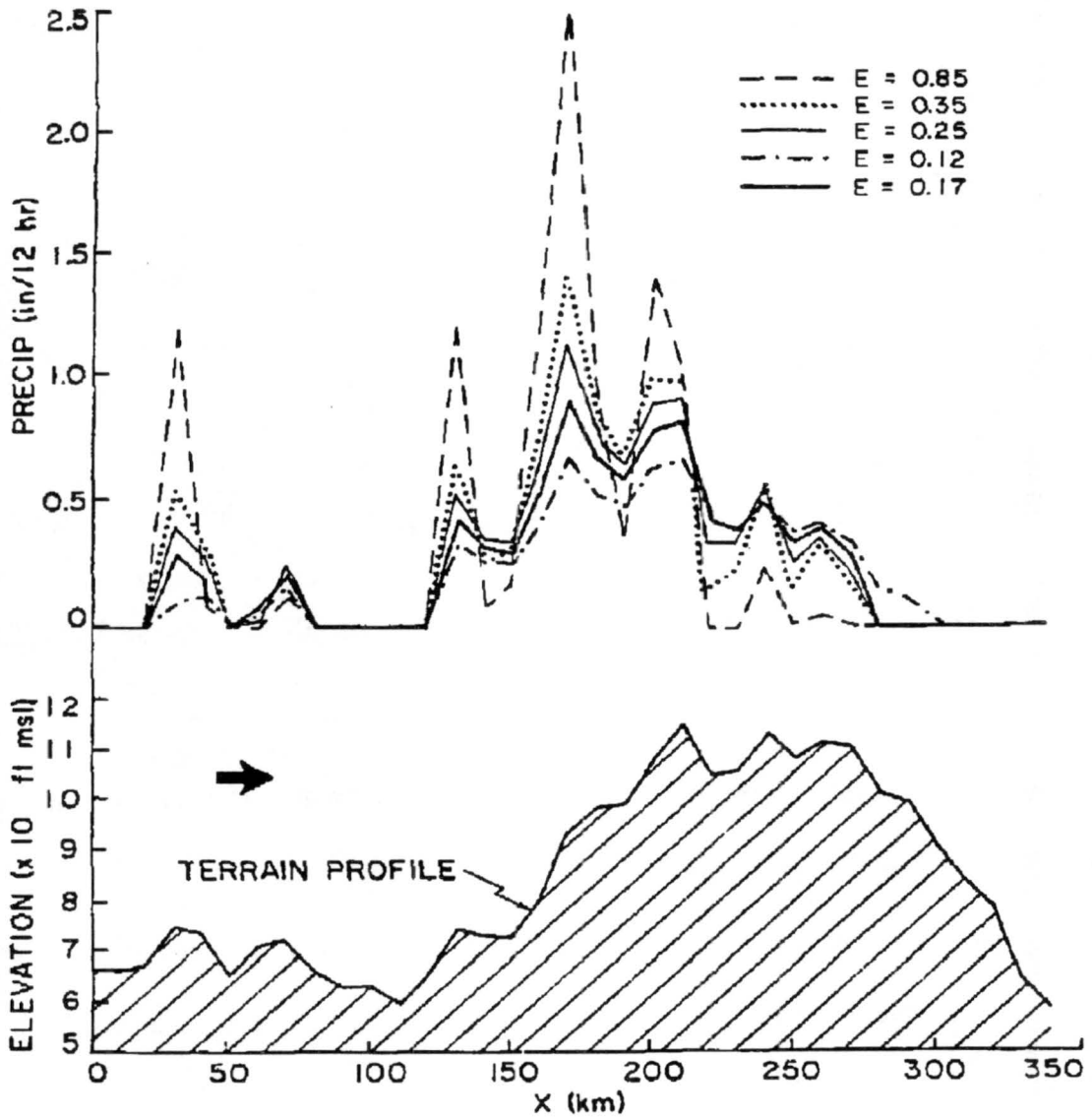


**Figure 6.3- Upslope effects in Rhea model for various precipitation efficiencies (from Rhea, 1978)**

Figure 6.4 shows the average ratio between observation/prediction compared to a upslope value. This upslope factor is the difference between the elevation 3 grid points to the west and 3 grid points to the east.

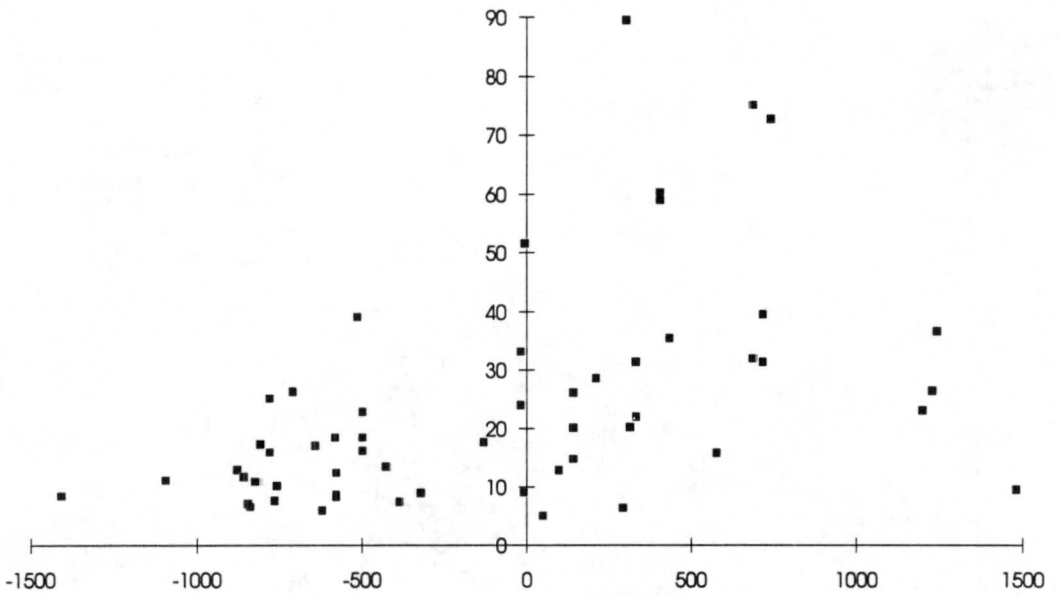


**Figure 6.4- Upslope factor versus ratio of observations/predictions for all SNOTEL sites (negative values imply a west-to-east upslope)**

Examining the results, we see a clustering of points between a ratio of 5 and 25 and an upslope of 500 to 1000 m over the six adjacent grid points. This line extends even into the 0 to 500 m downslope region.

The results are further clarified by dividing the SNOTEL sites into western and eastern sites. A site is considered "western" if it is located on the western side of the 106th meridian (approximately the location of the Continental Divide). Out of the 56 SNOTEL sites used in the comparison, 38 were "western" and 18 were "eastern". Figure 6.5 shows the linear dependence of ratio with upslope factor even clearer with the eastern points removed, although there are a few anomalous points. Figure 6.6 shows two

grouping of points. The first set of points is a region of strong west-to-east downslope with a slope of opposite sign compared to the western points. The second set of points correspond with relatively small ratios and little change in topography. The slope of this line is the same sign as the slope of the western points, but much steeper.

Using least-squares linear curve fitting, equations for each of these three regions can be obtained. Table 6.5 lists results of this curve fitting. Figure 6.7 compares these regions' equations to the plotted values.

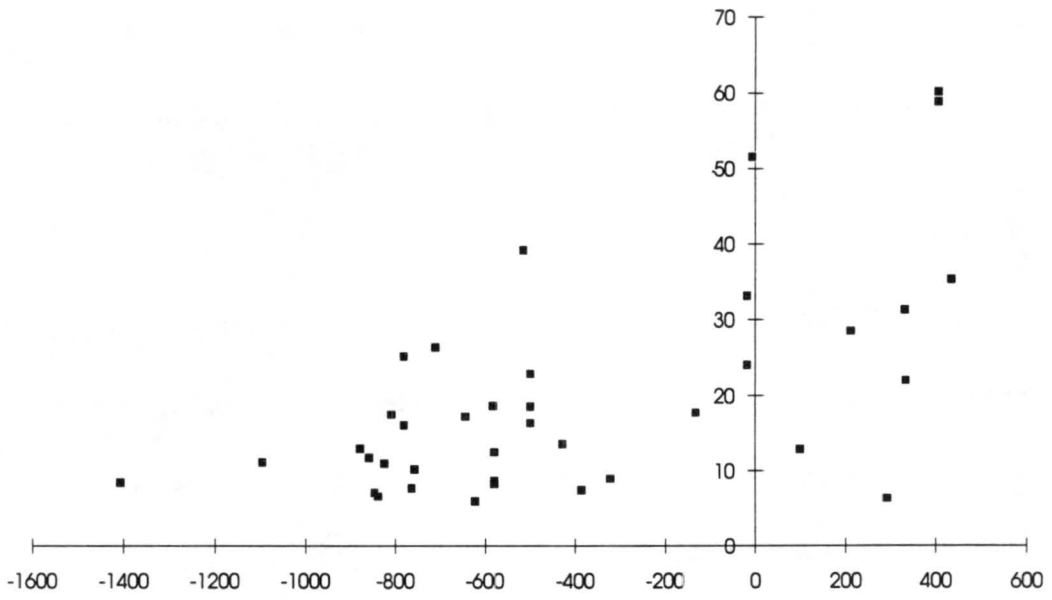


**Figure 6.5- Upslope factor versus ratio of observations/predictions for western SNOTEL sites (negative values imply a west-to-east upslope)**

| Region | Equation |
|---|---|
| West-to-East Upslope | y=0.0182x + 27.25 |
| East-to-West Upslope | y=-0.03082x + 64.72 |
| Eastern Mix | y=0.09404x + 6.12 |

**Table 6.5- Least-squares fit of ratio versus upslope factor for three distinct snow regions. x=upslope factor, y=ratio**

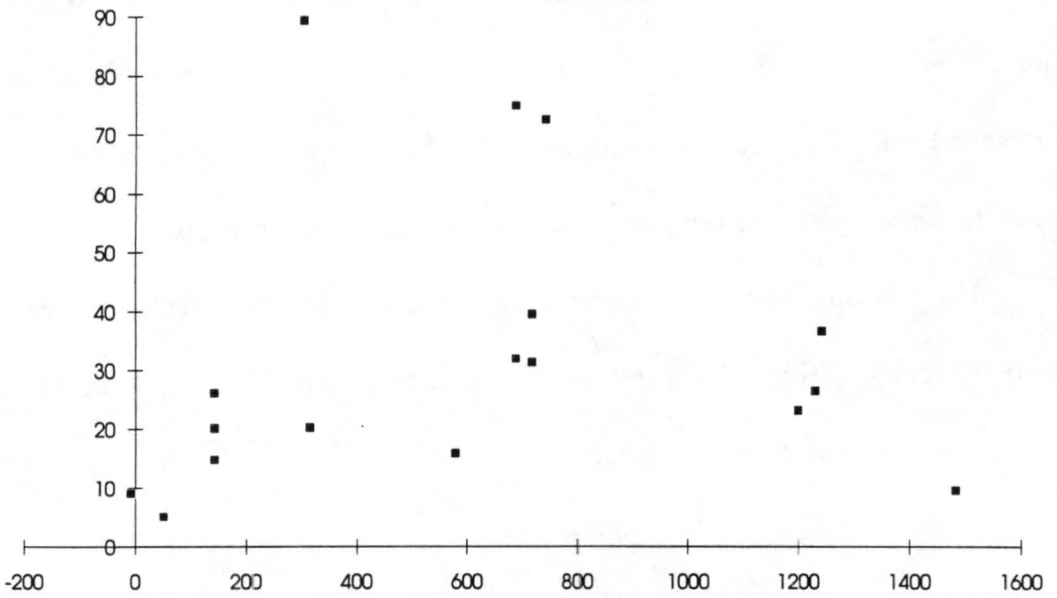


**Figure 6.6- Upslope factor versus ratio of observations/predictions for eastern SNOTEL sites (negative values imply a west-to-east upslope)**

## 6.6 Summary

Figure 6.8 shows the percentage error in the corrected precipitation calculations. The results indicate that 50% of stations have a predicted precipitation within ±40% of the measured value. These errors may be smaller when using many years worth of data as Rhea did; however, a source of these errors is the assumption of purely west-to-east and east-to-west upslope. At sites where the upslope feature is not due east or west (depending on the region), the simple corrected precipitation scheme will not detect it and incorrectly predict the precipitation.

Of all the defined regions, the "Eastern Mix" region has the worst correlations. This is because these areas receive precipitation from a wide variety of flow regimes; there is no predominant upslope feature, and the amount of snow is more dependent on the wind directions. Therefore, the simple prediction method fails. The region that does the

best is the "West-to-East Upslope" region in the western part of the state. The flow is almost always out of the west, making use of the eastern upslope feature more often.

As noted in Chapter 5, the best method of producing accurate results is the use of the bulk microphysics scheme in RAMS. This setup removes the need for bulk precipitation efficiency entirely and allows prediction of different precipitation types (such as rain, snow, graupel, etc.). Upslope effects are accounted for explicitly as hydrometeors settle and evaporate in the self-saturated leeward slopes. However, the amount of time required to use this scheme is not feasible on the single processor workstations available for this study. In the near future, when RAMS is configured on a cluster of workstations (see Cotton et al., 1994), use of bulk microphysics will likely produce forecasts that are both more accurate and available in an amount of time useable for forecasting.

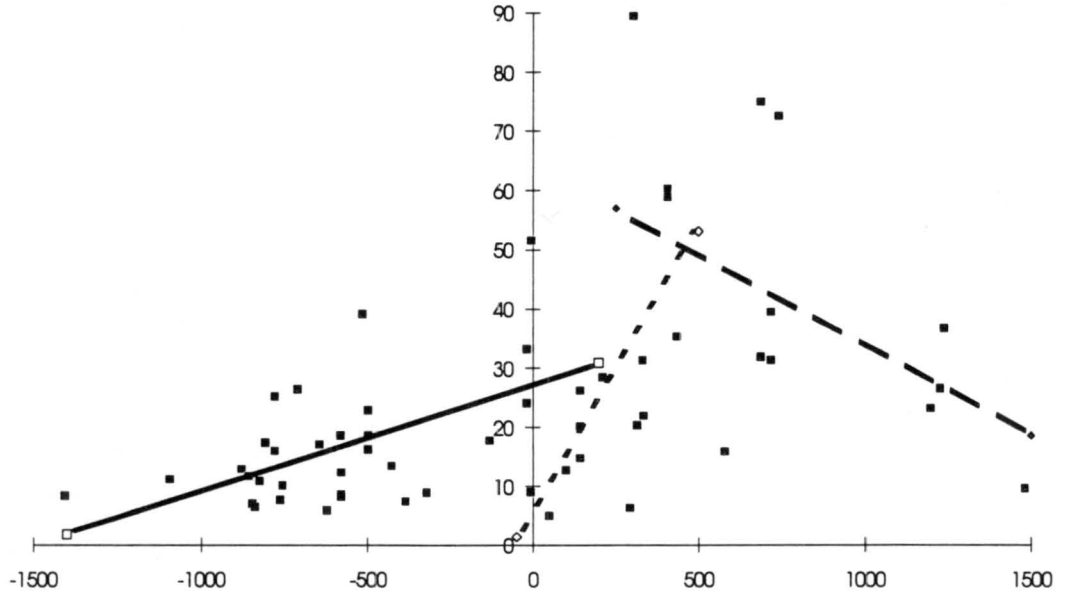


**Figure 6.7- Same as Figure 6.4 but with regional equations overlaid, where solid is the west-to-east upslope, dashed is the east-to-west upslope, and dotted is the eastern mix**

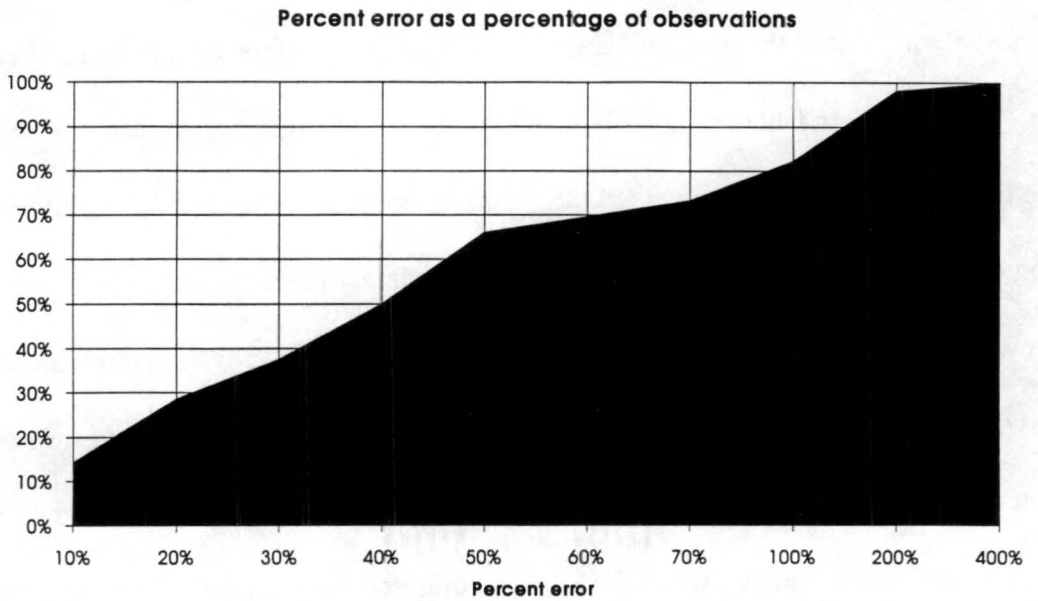


**Figure 6.8- Percentage error as a percentage of observations**

# 7. SUMMARY AND CONCLUSIONS

## 7.1 Summary

Throughout this study, the real-time version of the Regional Atmospheric Modeling System (RAMS) has shown its flexibility, speed and accuracy in most areas of forecasting. By having the ability to initialize with ETA or MAPS datasets, RAMS has shown its flexibility. Along with this, both these datasets have greatly improved vertical and horizontal resolutions, compared to standard NCAR-archived data normally used. The use of the time-varying boundary conditions also allows true forecasting throughout most of the domain compared to nudging toward non time-varying observations.

The modifications to the real-time version allows RAMS the ability to produce useable forecasts on most existing workstations within time periods suitable for forecasting. In this study, an 80 km course grid over the western US and a 16 km fine grid over Colorado produced 36-hour forecasts on an IBM RISC 6000/375 workstation normally within 9 hours of initialization time. This proved that a large supercomputer is not required to create fine resolution results in small amounts of time. The use of automation code (UNIX shell scripts) reduced the modeler's daily interaction and minimized the time between outside data availability and model execution.

Two case studies demonstrated the worth of the mesoscale setup. The investigation of the downslope windstorm of 3 July 1993 provided a sensitivity study of the different configurations of the model while pointing out the importance of balancing time and complexity when producing real-time results. The winter storm of 8 February 1994 case

study showed many meteorological fields are produced as accurately using the real-time setup as those produced using bulk microphysics.

The seasonal snowfall study provided an interesting look at the complexity of orographically-produced precipitation and assumptions that can and cannot be made when attempting to forecast it. Through use of a efficiency scheme based on cloud top temperature ("dump-bucket" scheme), real-time precipitation forecasts were made for the Colorado Rockies and compared to observations obtained from SNOTEL sites. Though not accurate when used alone, the dump-bucket scheme showed some dependence of a simple precipitation efficiency on upstream upsloping barriers.

### 7.2 Conclusions

Real-time RAMS has been proven to work in a variety of situations. Consistent results are produced with computer resources attainable by most researchers, WSO's or specialized forecast centers. Numerical forecasting has the opportunity to be in the hands of those who issue local forecasts and can modify the model, compared to inferring results of synoptic-scale models produced at one central location.

The two major problems with the real-time setup both have their roots in computer speed and resources. The simple dump-bucket scheme had only limited usefulness in producing accurate orographic precipitation forecasts. Though it did well in forecasting its maximum precipitation in areas where the maximum precipitation actually occurred, the amounts were often off by an order of magnitude. Interpolation between these values and those measured for totals in the seasonal snowfall study did fairly well; however the accuracy of this interpolation had a limited success rate for individual daily events. Studies

showed that use of the bulk microphysics provided much better results, but real-time constraints did not allow for its regular use with the workstations available for this project.

In the downslope windstorm case study, it was pointed out that although the 16 km grid spacing was much smaller than any operational forecast model currently in use, it was still not small enough to predict certain events. A finer resolution is required, but this, in turn, is not within the real-time constraints. Also, a combination of bulk microphysics and finer grid spacing increases accuracy more that the total of each of these individual improvements.

### 7.3 Future Research

In the near future, there will be no need for a separate real-time version of RAMS. RAMS code is now being tested to run in parallel on a group of linked workstations. This will allow real-time use of bulk microphysics even at grid spacing smaller than the 16 km used in this study (Cotton, et al., 1994). Using the new microphysics, a month's worth of forecasts used for the seasonal snowfall study could be re-run and the results could be compared to the SNOTEL data already collected. The month of February would be a good choice since snowfall that was both convective and stratiform in nature occured at this time. Also, comparison runs using MAPS data and ETA data could be made, especially during a cold-air outbreaks and orographically-produced snow events.

An improvement in the basic way RAMS forecasts are performed is an area of future research which should be considered. By altering RAMS to interpret its own results and perform a particular course of action would allow for some real-time studies and improved forecasts of potential events. For example, the criteria used by certain "expert

systems", such as Weaver's downslope windstorm prediction criteria (Lee et. al, 1989) could be coded into RAMS model-output data files. If the criteria is met, a third grid could be spawned in the region of potentially strong winds. This type of RAMS operation could be used to spawn grids in areas of high CAPE (for thunderstorm prediction), for convergence zones in Colorado for non-supercell tornado studies (Wakimoto and Wilson, 1989) or hailstorm prediction.

# REFERENCES


Barnes, L.L., 1973: Mesoscale objective map analysis using weighted time series observations. NOAA Tech. Memo. ERL NSSL-62, 60pp. [NTIS COM-73-10781]

Benjamin, S.G., K.A. Brewster, R. Brummer, B.F. Jewett, T.W. Schlatter, T.L. Smith, and P.A. Stamus, 1991: An isentropic three-hourly data assimilation system using ACARS aircraft observations. *Mon. Wea. Rev.*, **119**, 888-906.

Benjamin, S.G., T.L. Smith, P.A. Miller, D. Kim, T.W. Schlatter, and R. Bleck, 1991: Recent improvements in the MAPS isentropic-sigma data assimilation system. Preprint volume of the Ninth Conference on Numerical Weather Prediction, October 1991, AMS, Denver, CO, 118-121.

Benjamin, S.G., 1989: An isentropic mesoalpha-scale analysis system and its sensitivity to aircraft and surface observations. *Mon. Wea. Rev.*, **117**, 1586-1603.

Branson, M.D., 1991: An historical evaluation of a winter orographic precipitation model. Masters thesis, Atmos. Sci. Paper No. 505, Colorado State University, Dept. of Atmos. Sci., Fort Collins, CO, 116 pp.

Chappell, C.F., 1970: Modification of cold orographic clouds. PhD dissertation, Atmos. Sci. Paper No. 173, Colorado State University, Dept. of Atmos. Sci., Fort Collins, CO, 196 pp.

Cotton, W.R, G. Thompson, P.W. Mielke, 1994: Real-time mesoscale prediction on workstations. *Bull. Amer. Meteor. Soc.*, **75**, 349-362.

Cotton, W.R., G.J. Tripoli, R.M. Rauber, and E.A. Mulvihill, 1986: Numerical simulation of the effects of varying ice crystal nucleation rates and aggregation processes on orographic snowfall. *J. Climate Appl. Meteor.*, **25**, 1658-1680.

Cotton, W.R., M.A. Stephens, T. Nehrkorn, and G.J. Tripoli, 1982: The Colorado State University three-dimensional cloud/mesoscale model - 1982, Part II: an ice parameterization. *J. Rech. Atmos.*, **16**, 295-320.

Cram, J.M., 1990: Numerical simulation and analysis of the propagation of a prefrontal squall line. PhD dissertation, Atmos. Sci. Paper No. 471, Colorado State University, Dept. of Atmos. Sci., Fort Collins, CO, 332 pp.

Davies, H.C., 1983: Limitations of some common lateral boundary schemes used in regional NWP models. *Mon. Wea. Rev.*, **111**, 1002-1012.

Doesken, N.J., 1987: The contribution of SNOTEL precipitation measurements to climate analysis, monitoring and research in Colorado. Preprints, *Western Snow Conference*, Vancouver, BC, Canada, 20-30.

Doyle, J.D. and T.T. Warner, 1993: A numerical investigation of coastal frontogenesis and mesoscale cyclogenesis during GALE IOP 2. *Mon. Wea. Rev.*, **121**, 1048-1077.

Durran, D.R., and J.B. Klemp, 1983: A compressible model for the simulation of moist mountain waves. *Mon. Wea. Rev.*, **111**, 363-371.

Flatau, P.J., G.J. Tripoli, J. Verlinde, and W.R. Cotton, 1989: The CSU-RAMS cloud microphysics model: General theory and code documentation. Atmos. Sci. Paper

No. 451, Colorado State University, Dept. of Atmos. Sci., Fort Collins, CO, 88 pp.

Grant, L.O. and A.M. Kahan, 1974: Weather modification for augmenting orographic precipitation. *Weather and Climate Modification*, W.N. Hess, Ed., John Wiley and Sons, 282-317.

Heckman, S.T., 1991: Numerical simulation of cirrus clouds - FIRE case study and sensitivity analysis. Masters thesis, Atmos. Sci. Paper No. 483, Colorado State University, Dept. of Atmos. Sci., Fort Collins, CO, 132 pp.

Lee, T.J., R.A. Pielke, R.C. Kessler, and J. Weaver, 1989: Influence of cold pools downstream of mountain barriers on downslope winds and flushing. *Mon. Wea. Rev.*, **117**, 2041-2057.

Lilly, D.K. and E.J. Zipser, 1972: The Front Range windstorm of 11 January 1972-a meteorological narrative. *Weatherwise*, April 72, 56-63.

Maddox, R.A., 1980: Mesoscale convective complexes. *Bull. Amer. Meteor. Soc.*, **61**, 1374-1387.

Mahrer, Y. and R.A. Pielke, 1977: A numerical study of airflow over irregular terrain. *Beitr. Phys. Atmos.*, **50**, 98-113.

Mesinger, F., T.L. Black, D.W. Plummer, and J.H. Ward, 1990: Eta model precipitation forecasts for a period including tropical storm Allison. *Wea. and Forecasting*, **5**, 483-493.

Mesinger, F., Z.I. Janjic, S. Nickovic, and D. Gavrilov, 988: The step mountain coordinate: Model description and performance for cases of Alpine lee cyclogenesis and for a case of an Appalachian redevelopment. *Mon. Wea. Rev.*, **116**, 1493-1518.

Meyers, M.P., 1990: An evaluation of the factors affecting wintertime quantitative precipitation forecasts in an explicit cloud model over mountainous terrain. Masters thesis, Atmos. Sci. Paper No. 450, Colorado State University, Dept. of Atmos. Sci., Fort Collins, CO, 127 pp.

Nicholls, M.E., R.A. Pielke, J.L. Eastman, C.A. Finley, W.A. Lyons, C.J. Tremback, R.L. Walko, and W.R. Cotton, 1993: Applications of the numerical model to dispersion over urban areas. *The effect of urbanization on wind fields, air pollution spreading, and wind forces.*, NATO Advance Study Institute.

Pielke, R.A., W.R. Cotton, R.L. Walko, C.J. Tremback, W.A. Lyons, L.D. Grasso, M.E. Nicholls, M.D. Moran, D.A. Wesley, T.J. Lee, and J.H. Copeland, 1992: A comprehensive meteorological modeling system - RAMS. *Meteorol. Atmos. Phys.*, **49**, 69-91.

Rhea, J.O., 1978: Orographic precipitation model for hydrometeorological use. PhD dissertation, Atmos. Sci. Paper No. 287, Colorado State University, Dept. of Atmos. Sci., Fort Collins, CO, 199 pp.

Rhea, J.O. and L.O. Grant, 1974: Topographic influences on snowfall patterns in mountainous terrain, Advanced Concepts and Techniques in the Study of Snow and Ice Resources, Nat'l Academy of Sci., Washington, DC, 182-192.

Sousounis, P.J., 1993: A numerical investigation of wind speed effects on lake-effect storms. *Bound. Lay. Meteor.*, **64**, 261-290.

Talagrand, O. and P. Courtier, 1987: Variational assimilation of meteorological observations with the adjoint vorticity equation. I: Theory. *Quart. J. Roy. Meteor. Soc.*, **113**, 1311-1328.

Thompson, G., 1993: Prototype real-time mesoscale prediction during 1991-92 winter season and statistical verification of model data. Master's thesis. Atmos. Sci., Paper No. 521, Colorado State University, Dept. of Atmos. Sci., Fort Collins, CO, 105 pp.

Tripoli, G.J., 1986: A numerical investigation of an orogenic mesoscale convective system. PhD dissertation, Atmos. Sci. Paper No. 401, Colorado State University, Dept. of Atmos. Sci., Fort Collins, CO, 290 pp.

Tripoli, G.J. and W.R. Cotton, 1982: The Colorado State University three-dimensional cloud/mesoscale model - 1982. Part I: General theoretical framework and sensitivity expericments. *J. Rech. Atmos.*, **16**, 185-220.

Tremback, C.J., 1990: Numerical simulation of a mesoscale convective complex: model developement and numerical results. PhD dissertation, Atmos. Sci. Paper No. 465, Colorado State University, Dept. of Atmos. Sci., Fort Collins, CO, 274 pp.

Tremback, C.J., G.J. Tripoli, and W.R. Cotton, 1985: A regional scale atmospheric numerical model including explicit moist physics and a hydrostatic time-split scheme. Preprint Volume of the Seventh Conference on Numerical Weather Prediction, June 1985, AMS, Montreal, Canada, 355-358.

Tyler, D., 1992: *The last water hole in the west: the Colorado-Big Thompson Project and the Northern Colorado Water Conservancy District.* University Press of Colorado. 613 pp.

Wakimoto, R.M. and J.W. Wilson, 1989: Non-supercell tornadoes, *Mon. Wea. Rev.*, **117**, 1113-1140.

Walko, R.L., W.R. Cotton, J.L. Harrington, and M.P. Meyers, 1994: New RAMS cloud microphysics parameterization. Part I: The single-moment scheme. Submitted to *Atmos. Research.*

Walko, R.L., C.J. Tremback, and R.F.A. Hertenstein, 1993: RAMS - The Regional Atmospheric Modeling System Version 3a: User's guide. Published by ASTeR, Inc., P.O. Box 466, Fort Collins, Colorado, 104 pp.

Warner, T.T. and N.L. Seaman, 1990: A real-time mesoscale numerical weather-prediction system for research, teaching, and public service at Pennsylvania State University. *Bull. Amer. Meteor. Soc.*, **71**, 792-805.